5-2011

THE INTERPLAY BETWEEN SYMMETRY AND STATIC DIPOLES WITH ADSORPTION ON MOLECULAR SUBSTRATES

Zhengzheng Zhang
University of Nebraska-Lincoln, grobray@huskers.unl.edu

THE INTERPLAY BETWEEN SYMMETRY AND STATIC DIPOLES WITH ADSORPTION ON MOLECULAR SUBSTRATES

by

Zhengzheng Zhang

A DISSERTATION

Presented to the Faculty of

The Graduate College at the University of Nebraska

In Partial Fulfillment of Requirements

For the Degree of Doctor of Philosophy

Major: Physics and Astronomy

Under the Supervision of Professor Peter A. Dowben

Lincoln, Nebraska

May, 2011

THE INTERPLAY BETWEEN SYMMETRY AND STATIC DIPOLES WITH ADSORPTION ON MOLECULAR SUBSTRATES

Zhengzheng Zhang, Ph.D.

University of Nebraska, 2011

Advisor: Peter A. Dowben

This thesis presents evidence of preferential adsorption and the associated dipole-dipole interactions that can occur at molecule to molecule interfaces. The results are discussed in the context of the possibility of interactions caused by strong intrinsic dipoles when adsorbed on electrostatically biased substrates. Key is the discovery of lock and key adsorption chemistry by comparing the reversible absorption of the three isomers of di-iodobenzene (1,2-di-iodobenzene, 1,3-di-iodobenzene, and 1,4-di-iodobenzene) on molecular films of a quinonoid zwitterion. There is unequivocal evidence that the molecular adsorption and absorption of 1, 3-diiodobenzene is strongly favored at 150 K over the other isomers of di-iodobenzene. Our experiments also demonstrate that reversible isomer-selective adsorption chemistry of small molecules is indeed possible, with a preferential adsorption mechanism illustrating that symmetry does matter.

Evidence of selective adsorption on specific ferroelectric domains of the molecular ferroelectric, copolymers of polyvinylidene fluoride with trifluoroethylene (PVDF-TrFE) is presented. The adsorption of di-iodobenzene depends not only on the dipole orientation of the PVDF-TrFE ferroelectric domains, but also the di-iodobenzene isomer.

Foundational to this work is the investigation of the interaction and orientation of a strongly dipolar zwitterionic p-benzoquinonemonoimine-type molecule, with a large intrinsic dipole of 10 Debye, on both conducting (gold) and on polar insulating substrates (lithium niobate). I have studied surface electronic spectroscopic properties and the preferential absorption pattern of these unusual zwitterionic molecules $C_6H_2(\cdots NHR)_2(\cdots O)_2$, where R = H, *n*-$C_4H_9$, C_3H_6-S-CH_3, C_3H_6-O-CH_3, CH_2-C_6H_5 on gold and demonstrated the selective deposition of molecules onto specific ferroelectric domains for a spatially periodically poled ferroelectric surface (lithium niobate).

ACKNOWLEDGMENTS

The first person I would like to show my great gratitude to is my academic advisor Professor Peter A. Dowben. He is a respectable professor who really "advise" student and promote student. His insight in physics, excitement for the work, patience and frequent encouragement give me deep impression and influence. Five years ago, I was totally a layman in the field of UHV and surface science, but Peter recruited me anyway, and has been guiding and tutoring me ever since. The stage I have grown to today is mostly attributed to my advisor Prof. Peter A. Dowben. Without his guidance and help, I may have encountered many detours in pursuing my PhD and wouldn't have so many publications and academic fruit. I am thereby sincerely grateful to him for his help, patience and kindness.

I also would like to thank my colleagues and peers, Ihor Ketsman, Luis Rosa, Danqin Feng, Jie Xiao, Ning Wu, Jing Liu, Juan Colon-Santana, Keisuke Fukutani, Lingmei Kong, Xin Zhang, who gave me a lot of help in their own way, facilitating the practice of my experiments.

And I am very thankful to scientists who work in Louisiana State University and Center for Advanced Microstructures and Devices (CAMD), especially Dr. Orhan Kizilkaya and Dr. Yaroslav Losovyj. I have learnt many valuable experimental skills from them, and without their help, my synchrotron experiments are not able to complete smoothly.

My beloved mother and father, my relatives, my aunt Xinghua, my friends all stand behind me all the way, encouraging me, believing in me and giving me unselfish, spiritual supports. Without their love and eternal support, I am not able to successfully complete my five years' Ph.D. study, they are all my most precious treasures in my life.

CONTENTS

Chapter 1 **Introduction**……....1

Introduction……...1

References…….…. 10

Chapter 2 **Experimental Methods**……..15

2.1 Ultraviolet Photoemission Spectroscopy (UPS)……...15

2.1.1 Theory……15

2.1.2 The Photoemission Experiment ……21

2.2 X-ray Photoemission Spectroscopy (XPS)……...24

2.3 Inverse Photoemission Spectroscopy (IPES) ……..26

2.4 Infrared Micro-Spectroscopy (IR)……28

2.5 Non-contact Ferroelectric Poling……..29

2.6 Spatially Resolved X-ray Absorption near Edge Spectroscopy (μ-XANES)……...30

2.7 Sample Preparation……...31

2.7.1 Au (111) Substrate….....31

2.7.2 Periodically Poled Lithium Niobate Substrate (PPLN).....32

2.7.3 PVDF-TrFE Substrate……..35

2.7.4 *P*-benzoquinonemonoimine Zwitterionic Compounds……....37

2.7.4.1 General……..38

2.7.4.2 Synthesis of Zwitterion 3……..39

2.7.4.3 Synthesis of Zwitterion 4……..40

2.7.4.4 Functionalization of Gold Surfaces……..…41

2.7.5 D-Cysteine…….41

2.7.6 MEH-PPV Dopped with PbSe and PCBM……....42

References……...43

Chapter 3 Altering the Static Dipole on Surfaces though Chemistry: *p*-benzoquinonemonoimine Zwitterionic Compounds …….49

3.1 Introduction …….....49

3.2 The Characterization of *p*-benzoquinonemonoimine Zwitterionic Compounds……51

3.3 Adsorption of *p*-benzoquinonemonoimine Zwitterionic Compounds on Surfaces……54

3.4 Bonding to the Au Substrate……..57

3.5 Electronic Properties …….59

3.6 Conclusion…….66

References……...68

Chapter 4 The Interface Bonding and Orientation of a Butyl Pendant Groups Zwitterion……..73

4.1 Introduction…….....73

4.2 Modeling Procedure……..76

4.3 The Bonding and Orientation of a Zwitterion, with Pendant Alkyl Chains, Adsorbed on Gold……...77

4.4 Franck–Condon Scattering from a P-benzoquinonemonoimine Zwitterion on Gold……...89

4.5 Conclusion……....93

References……...95

Chapter 5 Band Mapping and Electron Pockets at the Fermi Level for *p*-benzoquinonemonoimine Zwitterion…….104

5.1 Introduction…….104

5.2 Electron Pockets at the Fermi Level and Band Structure……....106

5.2.1 Theoretical Approaches……....106

5.2.2 Band Structure of the (6Z)-4-(benzylamino)-6 -(benzylliminio)-3-oxocyclohexa-1,4-dien-1-olate Zwitterion……..107

5.2.3 Electron Pockets at the Fermi Level of the (6Z) -4-(benzylamino)-6-(benzylliminio)-3-oxocyclohexa-1,4 -dien-1-olate Zwitterion…….....111

5.3 Conclusion……115

References…….116

Chapter 6 Di-idobenzene Isomers Adsorptions on Molecule films of Quinonoid Zwitterion and PVDF…….122

6.1 Di-idobenzene Isomers Adsorbed on Quinonoid Zwitterion: Lock and Key Adsorption Chemistry……122

6.1.1 Adsorption of Di-iodobenzene on p-benzoquinonemonoimine Zwitterion Molecular Films……126

6.1.2 Isomeric Dependence of the Di-iodobenzene Adsorption on p-Benzoquinonemonoimine Zwitterion Molecular Films…..130

6.1.3 Summary…….139

6.2 Di-idobenzene Isomers Adsorbed on PVDF: Dipole Orientation Mediated Chemistry at Polymer Surfaces…….140

6.2.1 The Adsorption of Di-iodobenzene on Ferroelectric Films of the Copolymer 70% Vinylidene Fluoride with 30% Trifluoroethylene, P(VDF-TrFE 70:30)…….141

6.2.2 The Influence of Ferroelectric Poling on Di-iodobenzene Adsorption on Ferroelectric Films of the Copolymer 70% Vinylidene Fluoride with 30% Trifluoroethylene, P(VDF-TrFE 70:30)…….147

6.2.3 Summary……....151

References……..153

Chapter 7 Spatially Selective Deposition of Zwitterionic D-Cysteine and a *p*-benzoquinonemonoimine Molecular System on Periodically Poled Lithium Niobate……161

7.1 Selective Deposition of the *P*-benzoquinonemonoimine Zwitterion on Periodically Poled Lithium Niobate…….163

7.2 Selective Deposition of Zwitterionic D-Cysteine on Periodically Poled Lithium Niobate……....170

References……..179

Chapter 8 Applications…….182

8.1 The Electrical Transport Properties of Ultra-thin Films of Zwitterions……..183

8.2 Doping Poly[2-methoxy-5-(2'-ethylhexyloxy)-1,4-phenylenevinylene] with PbSe nanoparticles or PCBM fullerenes…….186

References……..195

Chapter 1 Introduction

This dissertation describes my research work mainly directed at the investigation of preferential adsorption and the associated dipole-dipole interactions of molecules with an intrinsic strong dipole on electrostatically biased substrates. If electrostatic dipolar interactions can lead to preferential adsorption on electrostatically biased substrates, then the large-dipole molecules can be used for chemical testing, possibly even for chemical signatures (protein specific) disease markers. This would be sort of like the standard 'gel electrophorisis' but on a solid state chip.

The interactions of adsorbate molecules on a ferroelectric substrate can harken back to the problem of the cavity field introduced by Lars Onsager [1], who considered the effective internal electric field in polar liquids. The cavity field can orient molecules in the ferroelectric phase, and the molecules then polarize the neighbor molecules. This in turn generates an opposite reaction field. With adsorption on a ferroelectric, there are some significant differences from Onsager's cavity field concept as there is an effective external field provided by the ferroelectric substrate acting on the adsorbate molecules with a strong dipole, but the reaction field concept is retained. The substrate–molecule dipolar interactions may include a number of complexities due to the interplay between interface dipoles and interface chemistry. Dipole contributions from the chemical bonds formed with the substrate, the local field induced by the substrate and image dipoles within the substrate, may all contribute to the total interface dipole between a conducting substrate and a dipolar adsorbate molecule.

Interfacial dipole interactions have long been implicated as important in surface adsorption and surface catalysis [38-41] (Figure 1.3 shows the origins of various interfacial

dipoles). The investigation of surface dipole interactions are, unfortunately, often complicated by the influence of the substrate (including band structure effects [42]) and strong perturbations due to surface charges that induce large surface dipoles on metal surfaces [43]. Ferroelectric materials provide a great opportunity to investigate dipole interactions with adsorbates [44-55], particularly as the surface electric dipoles are "reversible" [44-45, 48-55].

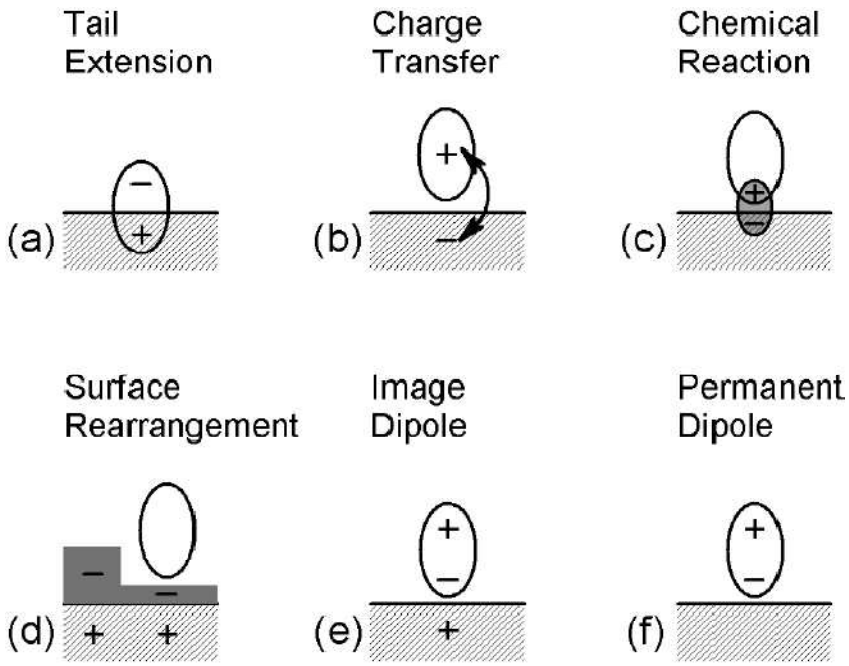

Figure 1.3 Various origins for interfacial dipole. (a) electronic orbital tailing into the vacuum and leaving vacancy (hole) behind, (b) charge transfer between adsorbate and substrate, (c) chemical reaction occurs between adsorbate and substrate. (d) metal surface dipole layer, as shown in (a), disturbed by non-polar adsorbed molecule causing surface charge rearrangement, (e) image charge induced by polar molecule approaching metal surface, (f) interfacial dipole caused by adsorbed molecule with permanent dipole [56].

In this dissertation, the ferroelectric materials employed as electrostatically biased substrates to study preferential adsorption and the associated dipole-dipole interactions mainly include periodically poled lithium niobate(PPLN) and poly(vinylidene fluoride (PVDF)-trifluoroethylene (TrFE)) copolymers.

In a properly oriented ferroelectric sample, such as lithium niobate ($LiNbO_3$) crystalline thin film, the polarization can be aligned perpendicular to the surface in the positive or negative direction to form antiparallel ferroelectric domains. A domain wall separates these two domain states. The distinctly oriented domains differ in the sign of key non-vanishing components of the piezoelectric, electro-optic, and nonlinear optical tensor. In this case, the abrupt change in the normal component of the spontaneous polarization on the surface results in the appearance of a bound polarization charge, which in ambient conditions is compensated by the accumulation of ionic species or dipole molecules and through redistribution of mobile carriers in the bulk [57]. This screening significantly affects the surface charge distribution and the surface potential and results in band bending [58]. Similarly, charged surface states can pin the surface Fermi level resulting in a change in both the surface charge, the surface potential, and the molecular band offsets [59]. It has been recently shown that these electrically switchable properties of the ferroelectrics can be used to tailor surface reactivity.

Besides, molecules possessing a strong intrinsic dipole are keys for testing if electrostatic dipolar interactions can lead to preferential adsorption on electrostatically biased substrates [2-16]. Both the magnitude of the molecular electrostatic dipole and the frontier orbital symmetry play a dominant role in the adsorption process. Even when intermolecular interactions do not involve any irreversible chemical reaction between the

molecular species, there is a balance between the chemical interactions and the electrostatic dipolar interactions [2, 3, 10-16].

Insight into these problems can be gained by comparing the adsorption of different isomers of a simple molecule. The investigation of molecular isomeric effects in surface science is documented [17-27], with most of the emphasis involving chiral surfaces [17-24] or chiral molecules. Isomer-specific surface chemistry has generally not been an emphasis in the study of molecular adsorbates on molecular substrates. Electrostatic interactions have often been implicated as the origin of the isomer-dependent chemistry [25-27] and while the surface structures tend to depend on the isomer (often a chiral isomer), the adsorption process itself has not been conclusively demonstrated to be isomer-dependent.

The molecules we chose to emphasize in these studies are the three isomers of di-iodobenzene (1, 2-di-iodobenzene, 1, 3-di-iodobenzene, and 1, 4-di-iodobenzene). Such small molecules provide a clear test of preferential isomeric adsorption, particularly because their intrinsic dipole depends on the isomer. By using photoemission and inverse photoemission spectroscopy, we investigate di-iodobenzene adsorption/absorption on films made of several different dipolar molecular systems. One such substrate were the small, highly dipolar molecules, from the family of p-benzoquinonemonoimine zwitterions with rather high symmetry properties. We find that there is a lock and key adsorption chemistry evident by comparing the reversible absorption of the three isomers. Our experiments also show the unequivocal evidence that the molecular adsorption and absorption of 1, 3-diiodobenzene is strongly favored at 150 K over the other isomers of di-iodobenzene and we are able to demonstrate that reversible isomer-selective adsorption chemistry of small

molecules is indeed possible, with a preferential adsorption mechanism illustrating that symmetry does matter.

One of the molecular substrate in the di-iodobenzene adsorption studies is from the family of p-benzoquinonemonoimine zwitterions. The quinonoid zwitterions (as figure 1.1 shows), although electrically neutral as a whole, carry positive and negative charges on different parts of the molecules. The positive charge is delocalized between the amino groups over 4 bonds involving 6π electrons, while the negative charge is spread likewise between the oxygen atoms [28-30]. The result is a large electric dipole of typically 10 Debye that is formed across the "benzene" like plane of the benzoquinonemonoimine "core"; this makes these zwitterionic compounds fascinating candidates for the study of the electronic structure. These molecules not only have a very strong local dipole, but the delocalized benzene π molecule of the zwitterion "core" loses aromatic character due to the large charge separation.

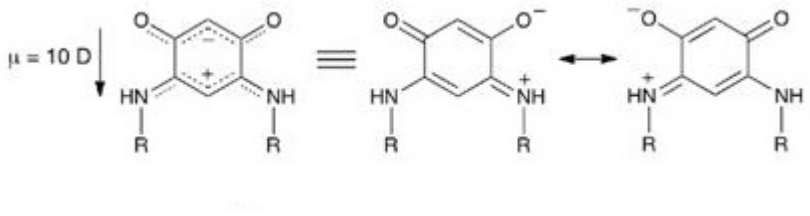

Figure 1.1 Representation of the family of the zwitterion studied.

More specifically, we investigate surface electronic spectroscopic properties of zwitterionic compounds of the *p*-benzoquinonemonoimine type $(C_6H_2(\cdots NHR)_2(\cdots O)_2$,

where R = H, *n*-C_4H_9, C_3H_6-S-CH_3, C_3H_6-O-CH_3, CH_2-C_6H_5, etc.) (as shown in figure 1.2), adsorbed on Au.

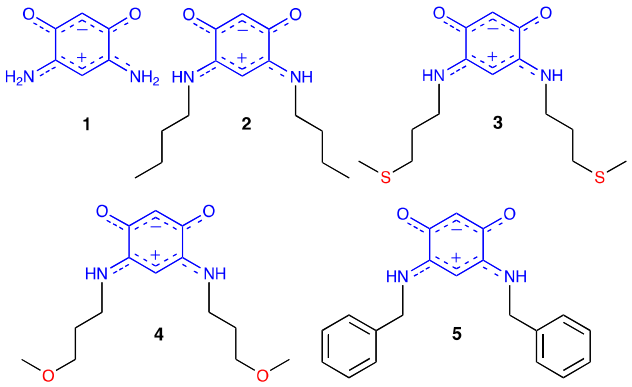

Figure 1.2 Zwitterionic compounds with different pendant groups studied.

We show that ultra-thin films of *p*-benzoquinonemonoimine compounds of good coverage can be readily formed on Au, and exhibit properties tunable by the choice of the pendant R groups. These molecules exhibit very efficient interface dipole screening, thus the *p*-benzoquinonemonoimine type zwitterionic compounds may become organic materials of interest for their interfacial electronics properties. We also show that organized films, exhibiting crystallinity, can be closely packed on substrates, and may be n-type conductors. This new type of self-assembled molecular film is therefore a powerful tool for engineering metal-organic interfaces for electronics applications.

An investigation of the electronic structure of molecules on ferroelectric surfaces can also provide additional information regarding the polarization effect on molecular adsorption. In this dissertation, we investigate the polarization effect on adsorption of quinonoid zwitterion molecules $C_6H_2(\cdots NHR)_2(\cdots O)_2$, where R=*n*-$C_4H_9$, d-cysteine

molecules [a chiral isomer of *l*-cysteine (chemical formula $C_3H_7NO_2S$)], folate acid and fibroblast cells on ferroelectric substrates using a combination of infrared spectramicroscopy and spatially resolved x-ray absorption near edge spectroscopy (XANES).

We have shown that although experiments were performed in the absence of any external electronic excitation (optical or thermal), the adsorption was still affected by polarization with preferential deposition occurring on the positive domains. This observation allows us to exclude selective molecular adsorption due to the surface charge resulting from, for example, the pyroelectric effect, restricting the possible surface interactions to polarization-dependent surface chemistry and dipole-dipole interaction between polar molecules and ferroelectric polarization dipoles.

In recent years, there is a rich literature of cysteine adsorption chemistry and the characteristics of cysteine adsorption molecules on polar surfaces could be of interest in differentiating amino acid molecules. Our work could be widely applicable in other fields outside physics.

The reason we choose polymer ferroelectric materials as substrate is because of their surprising simplicity compared to the complex surfaces formed with the inorganic ferroelectric materials. The complexities associated with inorganic ferroelectrics include surface compositional instabilities, an abundance of lattice defects (point defects, steps and grain boundaries), and considerable difficulty in preparing a stable reproducible surface with well-ordered dipoles oriented along the surface normal. And the best way to study the dipole interaction and the band offsets at the interface is to use a switchable ferroelectric material at one side. The organic ferroelectric polymer polyvinylidene fluoride with

trifluoroethylene [P(VDF-TrFE, 70%:30%)] becomes our preference due to its highly ordered, controllable surface.

Evidence of selective adsorption on specific ferroelectric domains of the molecular ferroelectric, copolymers of polyvinylidene fluoride with trifluoroethylene (PVDF-TrFE), and the inorganic ferroelectric lithium niobate is also presented in this thesis. The adsorption of di-iodobenzene depends not only on the dipole orientation of the PVDF-TrFE ferroelectric domains, but also the di-iodobenzene isomer.

Organic materials are commonly regarded as electrical insulator with a large range of application in electronics, biomedical and pharmaceutical purposes. This is largely true even today when we observed man made organic materials in our surroundings. However, electrical conduction on organic materials began to draw attention of scientists. Even today questions such as underlying mechanism of electron mobility, synthesis of materials with determine conductivity properties, which electronic state promotes conduction, are current subject of research for scientist in materials and nanotechnology research.

Electronic properties at organic interfaces are of crucial importance for characterizing and understanding carriers injection and transport in organic electronics [60, 61], especially for the purpose of improving device properties [62, 63]. The HOMO and LUMO energy levels of free molecules are generally shifted when the molecules are brought into contact with a conducting substrate, and simple arguments based on vacuum levels alignment fail [64]. The fundamental reason is that the energy level alignment is dependent on the interfacial electronic structure and on interfacial dipole layer [61, 65, 66]. In most cases the Fermi level of the substrate should lie in the middle of molecular adlayer HOMO-LUMO bandgap, consistent with the intrinsic dielectric properties of the bulk

molecular material. With an interface dipole and charge transfer across the interface molecular band offsets will occur, however, and these can then be exploited for better molecular electronic device performance. The chemical bonding at the interface, the adsorbate molecular orientation [67], the adsorbate dipole [68, 69], and their interplay [70, 71] all play a role in establishing the interface dipole. This result is an interface potential barrier due to an offset between the conduction band minimum (lowest unoccupied molecular orbital) or the valence band maximum (the highest occupied molecular orbital) and the electyrode Fermi level leading to a charge injection barrier at the metal-molecules [65, 66]. If the molecular species have an intrinsic significant dipole, one can expect an efficient screening of the ubiquitous metal-vacuum interface dipole, so that there may be a suppression of the changes of molecular-type energy level alignments when decreasing the thickness of molecular adlayers [65, 72].

In the last chapter of this dissertation, we will discuss relating applications. We will show the conductivity property of the *p*-benzoquinonemonoimine molecules and the study of the shifts of positions of the molecular orbitals of the conjugated semiconducting polymer, poly[2-methoxy-5-(2'-ethylhexyloxy)-1,4-phenylenevinylene] (MEH-PPV) when lead selenide (PbSe) quantum dots or the fullerene based molecule [(6)]-1-(3-(methoxycarbonyl)propyl)-[(5)]-1-phenyl-[5,6]-C61, known as PCBM, are dispersed in the polymer host. We demonstrate that MEH-PPV doped with a large-*Z* semiconducting material, such as PbSe nanocrystal quantum dots, is a candidate for use as a good gamma radiation detector.

References

[1] L. Onsager, J. Am. Chem. Soc., 58, 1486, (1936).

[2] V. S. Lvov, R. Naaman, V. Tiberkevich, Z. Vage, Chem. Phys. Lett. 381, 650–653, (2003).

[3] D. Cahen, R. Naaman, Z. Vager, Adv. Funct. Mater. 15, 1571–1578, (2005).

[4] C. G. Duan, W. N. Mei, W. G.Yin, J. J. Liu, J. R.Hardy, S. Ducharme, P. A. Dowben, Phys. Rev. B 69, 235106, (2004).

[5] M. Kuehn, H. Kliem, Phys. Status Solidi B 245, 213–223, (2008).

[6] W. Guo, S. X. Du, Y. Y. Zhang, W. A. Hofer, C. Seidel, L. F. Chi, H. Fuchs, H.-J. Gao, Surf. Sci., 603, 2815–2819, (2009).

[7] M. Feng, L. Gao, Z. Deng, W. Ji, X. Guo, S. Du, D. Shi, D. Zhang, D. Zhu, H. Gao, J. Am. Chem. Soc. 129, 2204–2205,(2007).

[8] P. A. Lewis, C. E. Inman, F. Maya, J. M. Tour, J. E. Hutchison, P. S. Weiss, J. Am. Chem. Soc. 127, 17421–17426,(2005).

[9] H. J. Gao, K. Sohlberg, Z. Q. Xue, H. Y. Chen, S. M. Hou, L. P. Ma, X. W. Fang, S. J. Pang, S. Pennycook, J. Phys. Rev. Lett. 84, 1780–1783, (2000).

[10] P. A. Dowben, L. G. Rosa, C. C. Ilie, J. Xiao, J. Electron Spectrosc. Relat. Phenom. 174, 10–21, (2009).

[11] J. Xiao, P. A. Dowben, J. Mater. Chem. 19, 2172–2178, (2009).

[12] J. Xiao, A. Sokolov, P. A. Dowben, Appl. Phys. Lett. 90, 242907, (2007).

[13] L.G. Rosa, J. Xiao, Ya. B. Losovyj, Y. Gao, I.N. Yakovkin, X. C. Zeng, P.A. Dowben, P.A. J. Am. Chem. Soc. 127, 17261–17265, (2005).

[14] L. G. Rosa, P. A. Jacobson, P. A. Dowben, J. Phys. Chem. B 110, 7944–7950, (2006).

[15] Dowben, P. A.; Rosa, L. G.; Ilie, C. C. Z. Phys. Chem. 222, 755–778, (2008).

[16] N. L. Levshin, S. G. Yudin, A. P. Diankina, Moscow Univ. Phys. Bull. 52,71-74, (1997).

[17] A. Ahmadi, G. Attard, J. Feliu, A. Rodes, Langmuir 15, 2420–2424, (1999).

[18] A. J. Gellman, ACS Nano 4, 5–10, (2010).

[19] G. A. Attard, J. Phys. Chem. B 105, 3158–3167, (2001).

[20] D. S. Sholl, A. J. Gellman, AIChE J. 55, 2484–2490, (2009).

[21] G. Held, M. J. Gladys, Top. in Catal. 48, 128–136, (2008) .

[22] J. N. James, D. S. Sholl, Curr. Opin. Colloid Interface Sci. 13, 60–64, (2008).

[23] T. Greber, Z. Sljivancanin, R. Schillinger, J. Wider, B. Hammer, Phys. Rev. Lett., 96, 056103, (2006).

[24] A. Kiihnle, T. R. Linderoth, F. Besenbacher, J. Am. Chem. Soc. 128, 1076–1077, (2006).

[25] S. Blankenburg, W. G. Schmidt, Phys. Rev. Lett. 99, 196107, (2007).

[26] Q. Chen, N. V. Richardson, Nat. Mater. 2, 324–328, (2003).

[27] A. Kiihnle, T. R. Linderoth, B. Hammer, F. Besenbacher., Nature 415, 891–893, (2002).

[28] O. Siri, P. Braunstein, Chem. Commun. 208-209, (2002).

[29] P. Braunstein, O. Siri, J. Taquet, M. Rohmer, M. Bénard, R. Welter, J. Am. Chem.Soc. 125, 12246-12256, (2003).

[30] Q.Z. Yang, O. Siri, P. Braunstein, Chem. Commun. 2660–2662, (2005).

[31] P. Braunstein, O. Siri, J.-P. Taquet, M.-M. Rohmer, M. Bénard, R. Welter, J. Am. Chem. Soc. 125, 12246–12256, (2003); P. Braunstein, O. Siri, P. Steffanut, M. Winter, Q.-

Z. Yang, C. R. Chimie, 9, 1493-1499, (2006); P. Braunstein, O. Siri, J.-p. Taquet, Q.-Z. Yang, Angew. Chem., Int. Ed., 45, 1393-1397, (2006); J.-p. Taquet, O. Siri, P. Braunstein, R. Welter, Inorg. Chem., 43, 6944-6953, (2004); Q.-Z. Yang, A. Kermagoret, M. Agostinho, O. Siri, P. Braunstein, Organometallics, 25, 5518-5527, (2006).

[32] O. Siri, P. Braunstein, Chem. Commun., 208-209, (2002).

[33] Q.-Z. Yang, O. Siri, P. Braunstein, Chem. Eur. J., 11, 7237-7246, (2005).

[34] Q.-Z. Yang, O. Siri, P. Braunstein, Chem. Commun., 2660-2662, (2005); Q.-Z. Yang, O. Siri, H. Brisset, P. Braunstein, Tetrahedron Lett., 47, 5727-5731, (2006).

[35] S. Kera, Y, Yabuuchi, H. Yamane, H. Setoyama, K. K. Okudaira, A. Kahn, N. Ueno, Phys. Rev. B, 70, 085304, (2004).

[36] S. Balaz, A. N. Caruso, N. P. Platt, D. I. Dimov, N. M. Boag, J. I. Brand, Y. B. Losovyj, P. A. Dowben, J. Phys. Chem. B, 111, 7009-7016, (2007).

[37] X. Lu, K. W. Hipps, X. D. Wang, U. Mazur, J. Am. Chem. Soc., 118, 7197-7202, (1996); J. Xiao, P. A. Dowben, J. Materials Chem., 19, 2172-2178, (2009); P.A. Dowben, J. Xiao, B. Xu, A. Sokolov, B. Doudin, Appl. Surf. Sci., 254, 4238-424, (2008).

[38] L.J. Whitman, C.E. Bartosch, W. Ho, G. Strasser, M. Grunze, Phys. Rev. Lett. 56, 1984, (1986).

[39] L.J. Whitman, C.E. Bartosch, W. Ho, J. Chem. Phys. 85, 3688, (1986).

[40] G. Ertl, S.B. Lee, M. Weiss, Surf. Sci. 114, 527, (1982).

[41] M. Kiskinova, D.W. Goodman, Surf. Sci. 108 64 (1981).

[42] P.A. Dowben, A. Miller, H.-J. Ruppender, M. Grunze, Surf. Sci. 193, 336, (1988).

[43] J.K. Nørskov, S. Holloway, N.D. Lang, Surf. Sci. 137, 65, (1984).

[44] A.L. Cabrera, G. Tarrach, P. Lagos, G.B. Cabrera, Ferroelectrics 281, 53, (2002).

[45] E. Ramos-Moore, J.A. Baier-Saip, A.L. Cabrera, Surf. Sci. 600, 3472, (2006).

[46] A.L. Cabrera, F. Vargas, R.A. Zarate, G.B. Cabrera, J. Espinosa-Gangas, J. Phys. Chem. of Solids 62, 927, (2001).

[47] R.F. Goncalves, N.L.V. Carreno, M.T. Escote, K.P. Lopes, A. Valentini, E.R. Leite, E. Longo, M.A. Machado, Quimica Nova 27, 862, (2004).

[48] J.L. Giocondi, G.S. Rohrer, Chem. Materials 13, 241, (2001).

[49] Y. Yun, L. Kampschulte, M. Li, D. Liao, E.I. Altman, J. Phys. Chem. C 111, 13951, (2007).

[50] Yang Yun, Eric I. Altman, J. Am. Chem. Soc. 129, 15684, (2007).

[51] D. Li, M.H. Zhao, J. Garra, A. M. Kolpak, A. M. Rappe, D. A. Bonnell, J. M. Vohs, Nature Materials 7, 473, (2008).

[52] A.S. Castela, A.M. Simões, Corrosion Science 45, 1647, (2003).

[53] N.L. Levshin, S.G. Yudin, Polymer Sci. B 46, 348, (2004); translated from Vysokomolekulyaniye Svedineniya, Ser. B 46, 1981, (2004).

[54] N.L. Levshin, S.G. Yudin, A.P. Diankina, Moscow University Physics Bulletin 52, 71, (1997); translated from Vestnik Moskovskogo Universiteta Fizika, UDC 541.183.03.

[55] N.L. Levshin, S.G. Yudin, Moscow University Physics Bulletin 54, 34, (1999).

[56] J. Xiao, Ph.D. thesis, 2009, University of Nebraska-Lincoln.

[57] V. M. Fridkin, Ferroelectric semiconductors (Consultants Bureau, New York, 1980).

[58] W.-C. Yang, B. J. Rodriguez, A. Gruverman, and R. J. Nemanich, Appl. Phys. Lett. 85, 2316, (2004).

[59] J. Xiao, A. Sokolov, and P. A. Dowben, Appl. Phys. Lett. 90, 242907, (2007).

[60] S. Braun, W. R. Salaneck, M. Fahlman, Adv. Mater. 21, 1450–1472 (2009).

[61] S. Karthäuser, J. Phys. Cond. Matter 23, 013001, (2011).

[62] Y. Yuan, T. J. Reece, P. Sharma, S. Poddar, S. Ducharme, A. Gruverman, Y. Yang, J. Huang, Nature Materials, 13 FEBRUARY 2011 | DOI: 10.1038/NMAT2951.

[63] H. Ma, H.-L. Yip, F. Huang, A. K.-Y. Jen, Adv. Funct. Mater. 20, 1371–1388, (2010).

[64] I. G. Hill, A. Rajagopal, A. Kahn, Y. Hu, Appl. Phys. Lett. 73, 662-664, (1998).

[65] H. Ishii, K. Sugiyama, E. Ito, K. Seki, Adv. Mater. 11, 605-625, (1999).

[66] X. Y. Zhu, Surf. Sci. Rept. 56, 1-83, (2004).

[67] N. Koch, N. Elschner, J. Schwartz, A. Kahn, Appl. Phys. Lett. 82, 2281-2883, (2003).

[68] S. Kera, Y, Yabuuchi, H. Yamane, H. Setoyama, K. K. Okudaira, A. Kahn, N. Ueno, Phys. Rev. B, 70, 085304, (2004).

[69] P.A. Dowben, L.G. Rosa, C.C. Ilie, J. Xiao, J. Electron Spectroscopy and Related Phenomena, 174, 10–21, (2009).

[70] V.S. L'vov, R. Naaman, V. Tiberkevich, Z. Vager, Chem. Phys. Lett., 381, 650-653, (2003).

[71] D. Cahen, R. Naaman, Z. Vager, Adv. Funct. Mater., 15, 1571-1578, (2005).

[72] S. Balaz, A. N. Caruso, N. P. Platt, D. I. Dimov, N. M. Boag, J. I. Brand, Y. B. Losovyj, P. A. Dowben, J. Phys. Chem. B, 111, 7009-7016, (2007).

Chapter 2 Experimental Methods

In this Chapter, I will briefly introduce the experimental techniques and sample preparation methods used in the research work described in this dissertation.

In our experiment, ultraviolet photoemission spectroscopy (UPS) and inverse photoemission spectroscopy (IPES) are two major microscopic techniques to study the electronic structures of the sample surface and the interface between two different films, which gives the most direct picture of the energy level alignment at the interface. The surface sensitivity of the techniques originates from the very limited mean free path of the photoelectrons [1, 2] (usually less than 10 nm for almost all the materials). Ultraviolet photoemission spectroscopy investigates the occupied electronic states, while inverse photoemission spectroscopy investigates unoccupied electronic states. In the following, I will introduce them respectively. The spectroscopy experiments are usually performed in ultra-high vacuum (UHV) with a base pressure in the region of 10^{-10} Torr. The vacuum was maintained using turbomolecular and ion pumps.

2.1 Ultraviolet Photoemission Spectroscopy (UPS)

2.1.1 Theory

Photoemission spectroscopy (PES) or photoelectron spectroscopy, is a standard method in condensed matter physics to probe surface electronic structures of materials. This technique utilizes photo-ionization and analysis of the kinetic energy distribution of the emitted photoelectrons to study the composition and electronic state of the surface region of a sample. The physics behind the PES technique is an application of the photoelectric effect: a photon impinges on sample surface and the excited electrons are escaped out of the

surface and then collected and analyzed by an energy analyzer. The escape depth of electrons is only a few Å in metals [3-6], and in some insulators and semiconductors, the mean free path could be very large [7] and the bulk electronic structure can also be measured. This advantage makes photoemission technique suitable for investigating electronic structures near the sample surface. Thus it is a surface sensitive technique.

Depending on the variety of incident photo energies, photoemission spectroscopy can be referred to several techniques. Ultraviolet photoemission spectroscopy (UPS) uses ultraviolet photon (photon energy region below 200 eV) to study valence energy levels and chemical bonding; especially the bonding character of molecular orbitals. A photon of energy $h\nu$ is incident on surface, and is absorbed by an atom resulting in the ejection of an electron with binding energy E_B as shown in figure 2.1.

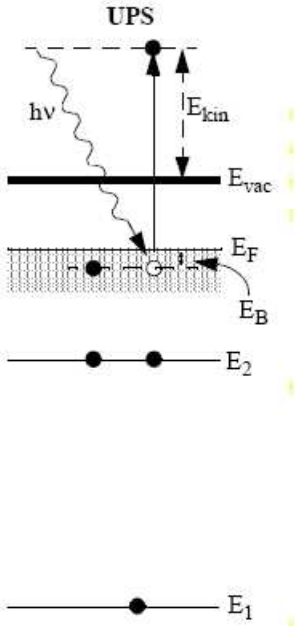

Figure 2.1 Schematic view of ultraviolet photoemission spectroscopy [8].

This electron is emitted into the vacuum with a kinetic energy E_{kin}, which follows equation 2.1:

$$E_{kin} = h\nu - E_B - (E_{vac} - E_{Fermi}), or\ E_{kin} = h\nu - E_B - \varphi \qquad 2.1$$

where φ is a parameter that depends on the work function of the spectrometer rather than that of the sample itself (i.e. the contact potential difference between the sample and the spectrometer).

The photoemission process involves a transition from an initial state i of wave function ψ_i to a final state f of wave function ψ_f. This transition is induced by the photon field with the associated vector potential $\vec{A}$. The transition probability or partial cross section σ of a photoelectric event occurring for an excitation may be calculated by use of Fermi's golden rule [8, 9, 10]:

$$\sigma(\omega)=4\pi^2\alpha\hbar\omega \sum_{f,i}\left|\langle\psi_f|E.U_{ext}(x)|\psi_i\rangle\right|^2\delta(h\omega - E_f - E_i) \qquad 2.2$$

where E and ψ are electronic energy and wave function for initial (i) and final (f) states separately, $E.U_{ext}$ is the interaction potential proportional to $\vec{A}.\vec{P} + \vec{P}.\vec{A}$ and $\vec{A}$ is the vector potential of the incident electromagnetic field, $\vec{P}$ is the momentum operator of the electron.

The photoemission process is very rapid (on a time scale of 10^{-16} s), the excited state of the system usually has no time to relax into an equilibrium state. In this case, the process can use simple "the frozen orbital approximation", where the transition matrix element contains only two-electron wave functions:

$$\langle\psi_f|E.U_{ext}(x)|\psi_i\rangle = \langle\varphi_{f,E_{kin}}|E.U_{ext}(x)|\varphi_{i,u}\rangle \qquad 2.3$$

where we assume final state wave function ψ_f as a product of $\varphi_{f,E_{kin}}$ which is free

electron of kinetic energy E_{kin} and $\psi_{f,R}^{u}(N-1)$ which represent the N-1 remaining electrons (and the index u indicates the electron u is not included). In a similar way, the initial state wave function is a product of orbital $\varphi_{i,u}$ of the excited electron and $\psi_{i,R}^{u}(N-1)$ of N-1 remaining electrons. The photoemission experiment then measures the Hartree-Fock energy of the orbital u: $E_{B,u} = -\varepsilon_u$, which is the Koopmans' binding energy.

When we take into account relaxation, by assuming the final state of N-1 electrons has m excited states and corresponding wave function: $\psi_{f,m}^{u}$ (N-1), the transition matrix elements becomes:

$$\langle \psi_f | E.U_{ext}(x) | \psi_i \rangle = \langle \varphi_{f,E_{kin}} | E.U_{ext}(x) | \varphi_{i,u} \rangle . \sum_m c_m \qquad 2.4$$

where $|c_m|^2$ is the probability that the removal of an electron in orbital φ_u of the N-electron ground state leaves the system in the excited state m of the N-1 electron system, and c_m is given by:

$$c_m = \langle \psi_{f,m}^{u}(N-1) | \psi_{i,R}^{u}(N-1) \rangle \qquad 2.5$$

for a strongly correlated system, many of c_m are nonzero, we observe "satellite" peaks, and for $m = u$, we obtain the "main" photoemission peak.

In the UPS experiment (the schematics of photoemission experiment is shown in figure 2.2 (a)), we can use either an analyzer with a large acceptance angle to get information integrated over large parts of the reciprocal space, i.e. we get the densities of occupied electronic states. Or we can use an analyzer which accept only electron in a small solid angle in order to measure the emission angle of the electrons to do angle resolved UPS, and investigate the dispersion of electronic bands $E(k_\perp)$ and $E(k_\parallel)$ for bulk and surface states [8, 11-17]. A movable electron energy analyzer is usually used when recording angle resolved spectra, and we need to extract information about the electron

wave vector from the geometry of the experiment. For typical experimental geometrical parameters as shown in figure 2.2(b), different photoelectron emission angles θ correspond to the different parallel wave vector k and thus a different point in the surface Brillouin zone. Photoelectrons emitted along the surface normal have no parallel wave vector and are representative of the surface Brillouin zone center($\bar{\Gamma}$).

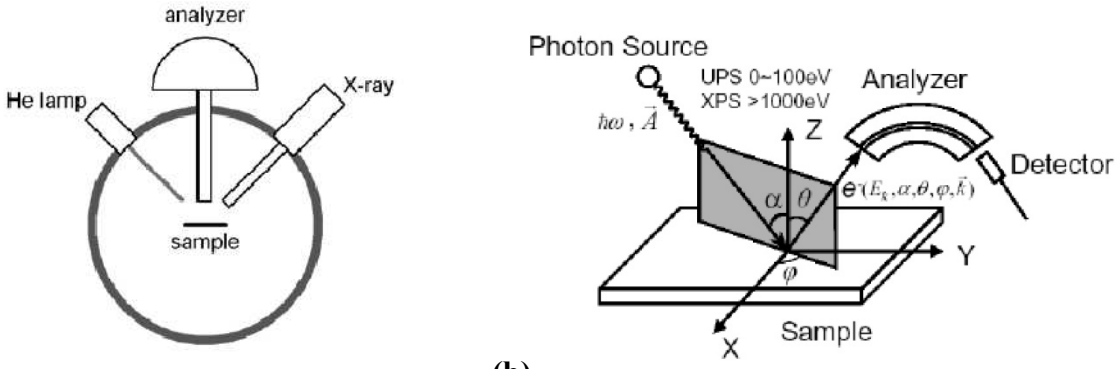

(a) **(b)**

Figure 2.2 (a) Top view schematics of experimental setup of photoemission. The big grey circle is the cross section of vacuum chamber body [18]. (b) Schematic of photoemission spectroscopy experiments process [10].

In photoemission process, the energy and momentum must be conserved. An electron in a valence band of a solid (a periodic array of atoms) does not belong to a single atom. We are observing state sharp in k -space and "fuzzy" in real space. We can define the spacing between each repeat atom as real space value a, and define the reduced momentum or wavevector $k = 2\pi/a$ in the reciprocal space. Thus, the same state of the electron is reproduced by adding a reciprocal lattice vector G. The perpendicular component of the wavevector of the electron $k_{\perp}$ is not conserved due to the broken symmetry at the surface (a potential step exists at the surface). The conservation laws then becomes:

$$E_f - E_i = h\nu$$

$$k_{\|}(f) = k_{\|}(i) + G_s \quad 2.6$$

where G_s is a surface reciprocal lattice vector, and k is the component of the wavevector parallel to the surface.

When we fix the photon energy and rotate the electron energy analyzer to collect photoelectrons that are ejected as a function of angle θ off the surface normal, we can probe a finite $k_{\|}$ value. This idea is represented mathematically in reduced zone by:

$$k_{\|}(f) = \sqrt{\frac{2m}{\hbar^2}E_{kin}}sin\theta = k_{\|}(i) \quad 2.7$$

This means we can sample different surface plane electron wave vectors by rotating the analyzer to obtain different collection angles θ for the emitted photoelectrons. When the binding energy of a state (the energy position of a photoemission peak) varies as a function of wave vector (analyzer angle) this is called dispersion. Thus we can use angle resolved UPS to map out band dispersion of electronic bands.

The perpendicular component of the wave vector in the initial state $k_{\perp}(i)$ is directly related to the information of final state $E_f(k)$. For photon energies above about 30 eV, the photoelectron may be generally assumed to be free-electron-like, as a reasonable approximation. For a free electron, we have:

$$E_{kin} = \frac{\hbar^2}{2m}k^2 - V_0 \quad 2.8$$

where V_0 defines inner constant potential as a sum of the work function φ and the Fermi energy E_F: $V_0 = \varphi + E_F$. When combined with Equation 2.7, the perpendicular component of the wave vector in the initial state$k_{\perp}(i)$ is given by:

$$k_{\perp}(i) = \sqrt{\frac{2m}{\hbar^2}(E_{kin}cos^2\theta + V_0)} \quad 2.9$$

This means we can vary the incident photon energy (fix the angle of emission photoelectrons) to map out the perpendicular wave vector to the surface.

2.1.2 The Photoemission Experiment

Compared to other photoemission spectroscopy, such as XPS (we will discuss it latter in this chapter), UPS has greater surface sensitivity due to the smaller mean free path of resulting photoelectron (on the order of 5 ~10 Å). For the UPS experiments in this dissertation, the light sources used are helium lamp ultraviolet (UV) light and synchrotron light. The UV light in laboratory was generated by a helium gas-discharge lamp, denoted as a "He lamp" in short. Photons with two different energies can be emitted from a He lamp: He I 21.2 eV and He II 40.8 eV depending on the gas pressure inside the lamp. He II light is more difficult to achieve than He I. The efficient generation of He II requires a lower gas pressure inside the lamp and emits light with much lower intensity. Gas pressure is a key to get a good monochromatic light with reasonable intensity. Lower pressure usually gives lower light intensity, but better monochromaticity. Too low pressure, however, will shut the lamp off. So gas pressure need be fine-tuned inside the lamp.

The UPS experiments in this dissertation were carried out using a helium lamp at $h\nu$ = 21.2 eV (He I) and a PHI hemispherical electron analyzer with an angular acceptance of $\pm 10^0$ or more, as described in detail elsewhere [19-25].

The angle-resolved photoemission spectroscopy (ARPES) measurements employed plane-polarized synchrotron radiation dispersed by a 3 m toroidal grating monochromator

[26, 27], at the Center for Advanced Microstructures and Devices (CAMD) [28]. The measurements were made in a UHV chamber employing a hemispherical electron analyzer with an angular acceptance of $\pm 1^0$, as described elsewhere [26, 27]. The combined resolution of the electron energy analyzer and monochromator was 120–150 meV for high kinetic photon energies (50–120 eV). The photoemission experiments were undertaken as a function of light incidence angle (as shown in figure 2.3), with respect to the surface normal, and with the photoelectrons collected along the surface normal, to preserve the highest point group symmetry and eliminate any wave vector component parallel with the surface.

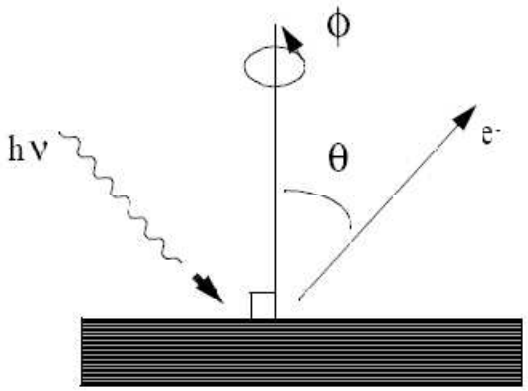

Figure 2.3 Schematic view of angle resolved photoelectron spectroscopy [8].

The high resolution photoemission studies in this dissertation were carried out on the 3 m normal incidence monochromator (NIM) beamline, also at the Center for Advanced Microstructures and Devices (CAMD) [29], as described elsewhere [30, 31]. This normal incidence monochromator is combined with a high resolution electron energy analyzer (Scienta SES-200 electron energy analyzer) [25, 30] endstation. The combined resolution (including beamline and analyzer) is 9 to 15 meV [30].

The light polarization dependent ultraviolet photoemission spectroscopies are also carried out using synchrotron light, dispersed by a 3 m toroidal grating monochromator, at CAMD, as described in detail elsewhere [32-34]. The measurements were performed employing a hemispherical electron energy analyzer with an angular acceptance of $\pm 1^0$. Synchrotron radiation has a unique advantage that other light sources cannot compete: highly linear polarization of the light. The peak intensity of photoemission spectrum can be enhanced by synchrotron light if the corresponding initial electronic state shares the symmetry with the light polarization (or suppressed if the symmetry of the electronic state is orthogonal to that of synchrotron light) according to Equation (3.0):

$$\langle \psi_i | (\vec{A} \,.\, \vec{P} + \vec{P}.\vec{A}) | \psi_f \rangle \qquad 3.0$$

The photoelectrons are collected along the sample surface normal throughout our experiments, so the final states are always fully symmetric along the surface normal. We change the incident angle (with respect to sample surface normal) of synchrotron light to alter the cross section between the incident photon and the excited (initial) electronic state. Except for the band structure measurements the photoelectrons were usually collected along the surface normal to keep the highest point group symmetry (Γ point) of the final state: the symmetry selection rules are thus at their most "selective". There are three commonly used schemes: (a) s-polarized light (small incident angle, say 30°, with respect to the surface normal) with more polarization (vector potential $\vec{A}$) lying parallel with surface; (b) p-polarized light (big incident angle, say 70°) with more polarization lying perpendicular to sample surface; (c) s+p polarized light (45° incident angle) with equal weight of the total polarization along the surface and surface normal.

2.2 X-ray Photoemission Spectroscopy (XPS)

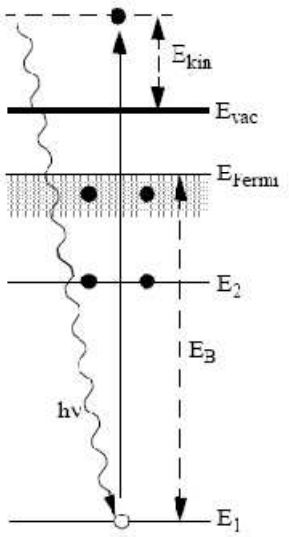

Figure 2.4 Schematic view of XPS [8].

X-ray photoemission spectroscopy (XPS) is often used as a chemical analysis technique to provide information on the atomic composition of a sample as well on the chemical states of the observed atoms. The XPS process is quite similar to the UPS process except the incident photons have much higher energy than for UPS and XPS interact with core levels of the atom, leading to ionization by removal of the core level electrons (as shown in figure 2.4). The electron emitted into the vacuum with a kinetic energy E_{kin} also follows the Equation 2.1, and the experimental setup is shown in figure 2.2(a).

In this dissertation, the core level X-ray photoemission spectra were performed with a PHI hemispherical electron analyzer with an angular acceptance of $\pm 10^0$and a SPECS X-ray source with a Mg anode ($h\nu$ = 1253.6 eV) or performed with a VG-Fisons X-ray source with a Mg anode ($h\nu$ = 1253.6 eV), and a VG 100 hemispherical analyzer, but data

collection times and the X-ray flux were specifically limited to avoid X-ray induced molecular fragmentation.

We can use angle-resolved X-ray photoemission spectroscopy (ARXPS) for non-destructive depth-profiling. Many of excited photoelectrons undergo inelastic scattering during propagation towards the surface, and can only travel a certain distance in the solid, characterized by the electron mean free path λ [4]. The effective probing depth is given by

$$\lambda_{eff} = \lambda \cos(\theta) \qquad 3.0$$

where θ is the emission angle with respect to the surface normal. The theoretical values of λ have been tabulated in reference [4], as a function of the core level kinetic energy.

According to the Beer-Lambert law, the photoelectron intensity from atom at depth *d*, for a material with uniform chemical composition, can be expressed as

$$I_d = I_0 e^{(-d/\lambda \cos(\theta))} \qquad 3.1$$

where I_0 is the intensity from the surface atoms. Thus information, of the sample composition as a function of depth from the surface, can be gained by changing the emission angle, and comparing the XPS intensities. The measured XPS intensities for each different elemental core levels must be normalized by taking into account the efficiency of the particular electron energy analyzer for passing and detecting the photoelectrons at the kinetic energies characteristic of the elements in the sample, the photoemission cross sections, and the photoemission geometry. Consider alloy with two elements in the sample surface region: A and B [9], the normalized intensity ratio is then given by

$$R(\theta) = \left[\frac{I_A(\theta)/\sigma_A}{I_B(\theta)/\sigma_B}\right]\left[\frac{E_{kin}^P(A)-C}{E_{kin}^P(B)-C}\right] \qquad 3.2$$

where σ_A, σ_B are the cross sections for elements A and B respectively, and we use the cross sections calculated by Scofield [10]. $E_{kin}^{P}(A,B) - C$ is the transmission factors of electron energy analyzer, and we set p=0.5 and C=0 for our type of analyzer [35].

2.3 Inverse Photoemission Spectroscopy (IPES)

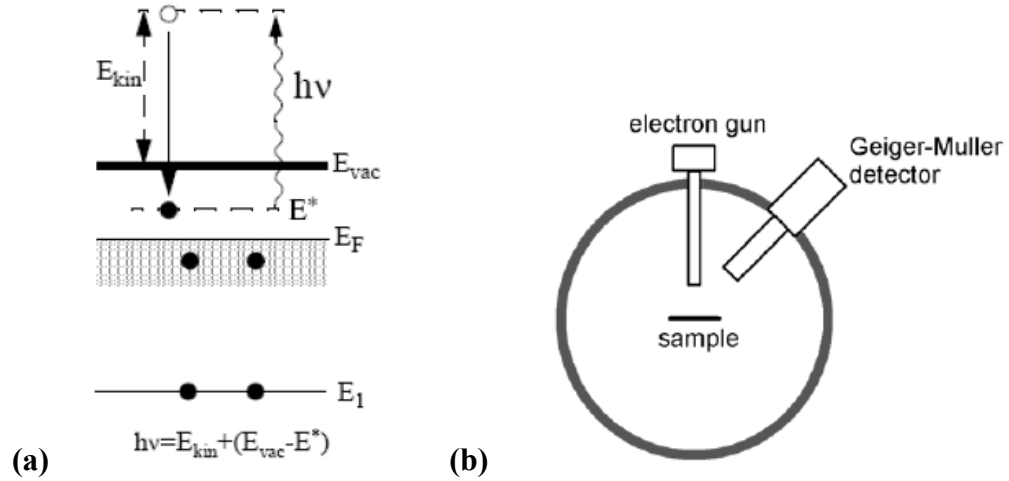

Figure 2.5 (a) Schematic of inverse photoemission spectroscopy [8]. (b) Top view schematics of experimental setup of inverse photoemission spectroscopy. The big grey circle is the cross section of vacuum chamber body [18].

Inverse photoemission spectroscopy investigates unoccupied electronic states above the Fermi Level. The inverse photoemission process can be regarded as the time reversed photoemission process [8, 36]. An incident electron to the sample surface results in the emission of a photon due to decay of this incident electron from the state above the vacuum level into an unoccupied state below the vacuum level and above the Fermi level, the schematics and experimental setup are shown in figure 2.5. Thus, an investigation of

unfilled electronic states, typically between the Fermi level and the vacuum level is possible. The energy of the unoccupied final state is given by the energy of the incident electron E_{kin} minus the detected photon energy $h\nu$.

The process of inverse photoemission is not exactly the inverse process of photoemission, the difference between inverse photoemission and photoemission is discussed in greater detail in reference [8]. The details of the dipole and symmetry selection rules which can be used for the interpretation of inverse photoemission are given in several reviews [12-13, 36-37].

Inverse photoemission studies in the vacuum ultraviolet photon energy range of a few volts to 30 eV since it's much easier to take advantage of conservation of the parallel component k of the wave vector. At these low energies, mapping of the unoccupied electronic states near E_F , as function of wave-vector k (unoccupied band) can be successfully taken experimentally, since one can probe only one k -point in the Brillouin zone for each incidence angle in IPES. Moreover, IPES has strength that it is very surface sensitive.

In our lab, the energy of the incident electrons is tuned by the electron gun and the emitted UV photons are detected by the vacuum compatible Geiger-müller detector at fixed energy. The principle of operation of the Geiger-müller detector is similar to that of a band pass filter. The detector is sealed with CaF_2 windows and filled with He (12 Torr< P < 18 Torr) and some iodine crystals (P=0.17 Torr). The Geiger-Müller (GM) photon detector uses the ionization of iodine gas to detect photons. The UV photons come into GM detector through a CaF_2 window which has the high-energy transmission threshold at 10.08 eV [38]. The incoming photons then ionize iodine gas with the ionization potential 9.28 eV [39]. The freed

electrons will be collected by electronics device simulating a pulse as a photon. The detectable photons lie in the range between 9.28 eV to 10.08 eV. The window and the iodine gas combined act as a band pass filter, so this GM detector only takes photons at a fixed energy 9.68 ± 0.4 eV. The different unoccupied states (with binding energy E_B) above the Fermi level are detected by incident electrons with different kinetic energies E_k. Note that the kinetic energy E_k is measured from the vacuum level E_V, while binding energy E_B is referenced with respect to the Fermi level E_F. So the energy relationships between these quantities are still the same as Equation (2.1) except E_B is positive here, instead of negative for occupied states (UPS).

2.4 Infrared Micro-Spectroscopy

The infrared microspectroscopy experiments in this dissertation were performed at the J. Bennett Johnston, Sr. Center for Advanced Microstructures and Devices (CAMD) in Baton Rouge, LA. Synchrotron IR radiation was directed from a Thermo Nicolet Nexus 670 FT-IR spectrometer into a Thermo Nicolet Continuum microscope after being extracted from a bending magnet port to a diamond window and subsequently collimated with a series of mirrors [40, 41]. The spectrometer is equipped with two beamsplitters, two detectors and a globar source. The user can switch between the globar source and the external radiation when using the microscope, one that uses Schwarzchild optics, two objectives (15× and 32×) and one condenser (15×). A liquid nitrogen-cooled mercury cadmium telluride (MCT-A) detector covers the required mid-IR spectral range of 4000 to 650 cm^{-1}, and chemical imaging (infrared mapping) is performed with a computer-controlled XY-stage of the microscope. The aperture size for mapping can be selected,

depending on different samples and situations. For example, in our experiments, the aperture size of $50\times20\mu m^2$ was employed for d-Cysteine and $40\times40\mu m^2$ for LR2 for the mapping, respectively [40, 41]. A clean gold substrate was used for a background spectrum and 15X Schwarzchild objective was chosen to focus the infrared beam onto the sample stage.

The software package responsible for microscope-to-computer imaging and infrared mapping is Omnic. For signal averaging, 256 scans with a resolution of 4 cm^{-1} were recorded. The subsequent spectra were all baseline corrected.

Any peak height differences due to concentration were normalized via peak area normalization. The maps were constructed by selecting a step size, i.e., spectra were taken at a "spot" separated by some step size.

2.5 Non-contact Ferroelectric Poling

In this dissertation, the complete polarization of P(VDF-TrFE, 70:30) films studied in Chapter 6, Section 6.2 was ensured by "Non-contact Ferroelectric Poling". The poling technique is performed in a single ultrahigh vacuum chamber with pressure of 1×10^{-10} Torr at room temperature. As the experiment schematics shown in figure 2.6, the polarization of PVDF was achieved by applying an appropriate DC bias voltage between a sharp micron sized electrode tip and the sample surface which is usually grounded. The applied voltage varies by different samples and experiments. In our experiment, we use -200 V to ensure the film poled up and 400 V to ensure the film poled down. The tip should be well positioned before each poling, and usually 0.05-0.1mm perpendicular above the sample surfaces. In the poling process, the tip is scanned from the top to the bottom along the

vertical line (~ 1 cm) of the PVDF surface each time and then gradually moved across the whole sample surface. In our experiment, we use the manipulator in the UHV chamber to move the PVDF sample so that the tip can be moved across the sample relatively. The scanning rate of the tip is 1min per vertical line and the moving step is 0.1 mm in the horizontal direction. Confirmation of complete ferroelectric poling was confirmed by piezoresponse force microscopy (figure 2.11).

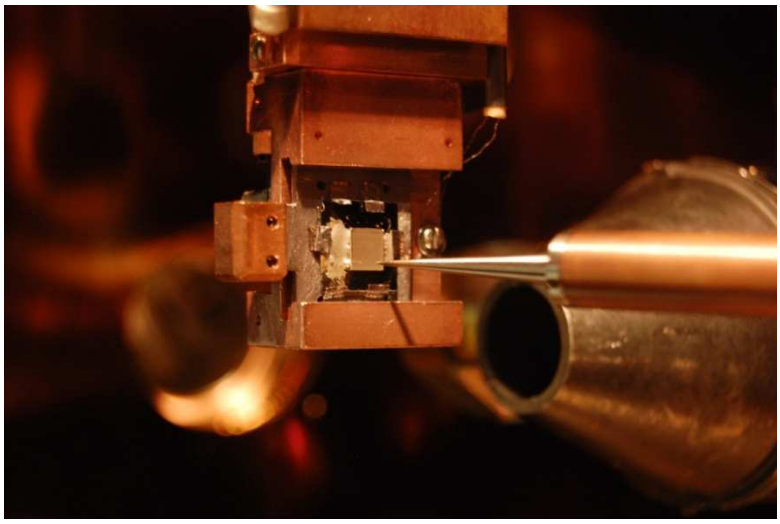

Figure 2.6 The view of the experimental set-up of non-contact ferroelectric poling.

2.6 Spatially Resolved X-ray Absorption near Edge Spectroscopy (μ-XANES)

Spatially resolved x-ray absorption near edge spectroscopy (μ-XANES) experiments were performed at the microXAS beamline (X05, Swiss Light Source, Switzerland). A microfocused x-ray beam of 2×2 μm^2 and a solid-state Sidetector was utilized in order to record the μ-XANES spectra. The energy of the incident x-ray beam was set using a fixed-

exit Si (111) double-crystal monochromator, with an energy resolution of about 2 eV at 19 keV.

2.7 Sample Preparation

2.7.1 Au (111) Substrate

In our experiments, Au (111) substrates were cleaned by Ar^+ ion sputtering every time before molecule adsorptions. Its photoemission and inverse photoemission spectra are taken as a reference for molecule coverage dependant measurements and Fermi level alignment. A clean Au(111) surface will show clear Fermi edge in UPS and image state in IPES (Au Fermi edge and image state at [111] direction are both surface states which require a clean surface to be observed), as shown in figure 2.7 and 2.8.

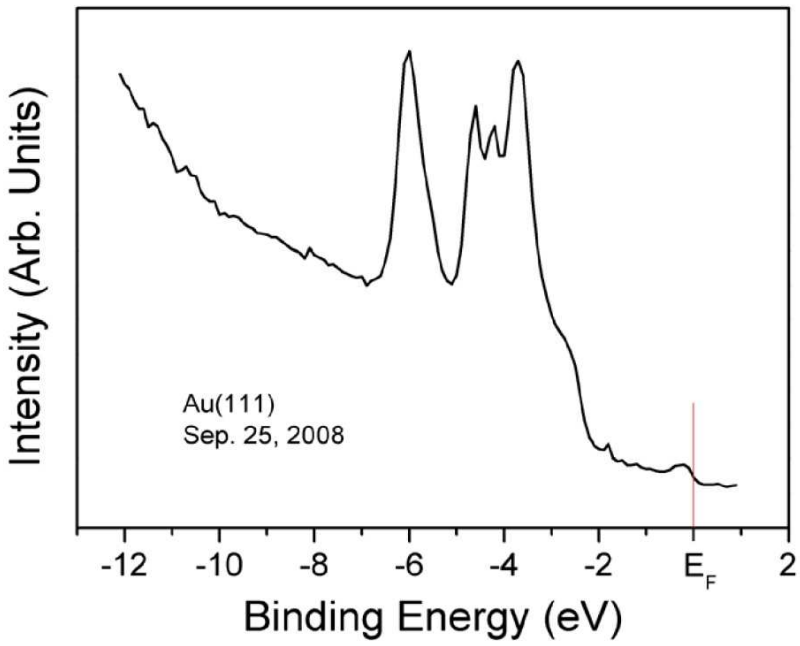

Figure 2.7 Ultraviolet photoemission spectrum (UPS) of Au(111) surface taken by He I (21.2 eV) light source at room temperature. The Fermi edge is clearly seen, as indicated by a red vertical bar [18].

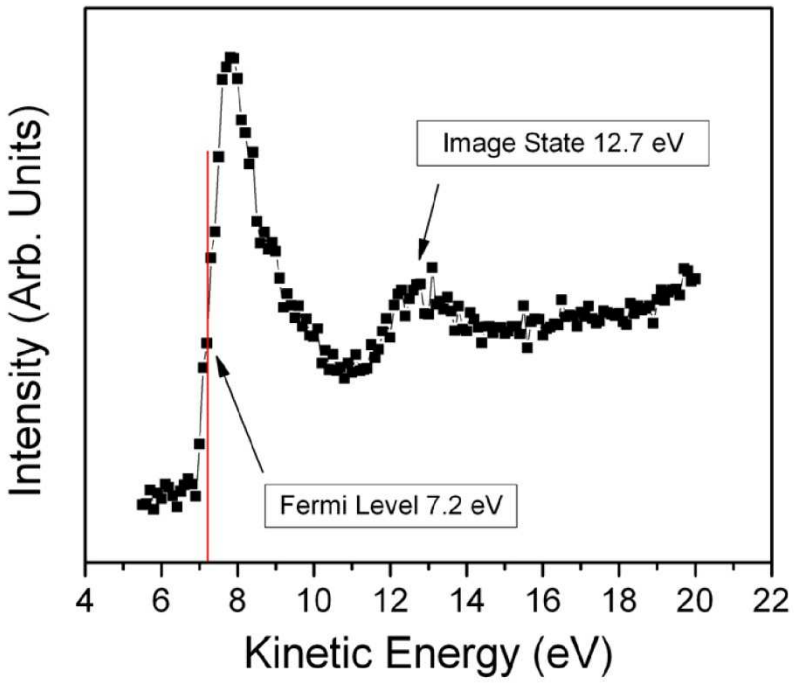

Figure 2.8 Inverse photoemission spectrum of Au (111) surface. Fermi level is at 7.2 eV kinetic energy, and the image state is clearly seen, as indicated in the figure [18].

2.7.2 Periodically Poled Lithium Niobate (PPLN)

The preparation of periodically poled lithium niobate substrate was briefly described here but was undertaken by Dr. Alexei Gruverman's group in physics department UNL.

In our experiment, periodically poled lithium niobate (PPLN) substrates of congruent composition (Crystal Technologies) have been used as ferroelectric templates. At room temperature, lithium niobate exhibits a hexagonal symmetry with polarization along the *c* axis (polar axis) which allows only two possible domain orientations. The samples used in this study were 5 x 5 x 0.5 mm^3 plane-parallel plates cut normal to the polar axis. A periodic domain pattern (period of ~28 μm) was been fabricated by depositing a photoresist mask on the +*c* sample face and applying a voltage of 10 kV through a fixture with an

electrolyte solution. The mask was been removed after poling the lithium niobate by means of chemical-mechanical polishing, leaving behind a bare ferroelectric surface of lithium niobate. As a result, periodic domain patterns containing stripes of antiparallel 180^0 domains, with their dipoles oriented either positive or negative along the surface normal have been produced (figure 2.9 (a)). These domain patterns have been observed in ambient environment by means of piezoresponse force microscopy (PFM) [42]. The imaging of ferroelectric domains using this technique exploits the fact that ferroelectric behavior implies piezoelectricity, and consequently mapping the piezoelectric response of a material provides a direct image of its ferroelectric domain structure. Imaging has been performed by applying an ac voltage of 2 V at 12 kHz to the sample surface through a conductive tip (NSC-14 MikroMasch, k= 5 N/m) and by detecting surface displacement using the same tip. From the atomic force microscopy (AFM) topographical mode images, the resulting surfaces are smooth with no features that can be associated with the ferroelectric domain stripes (figure 2.9 (b)).

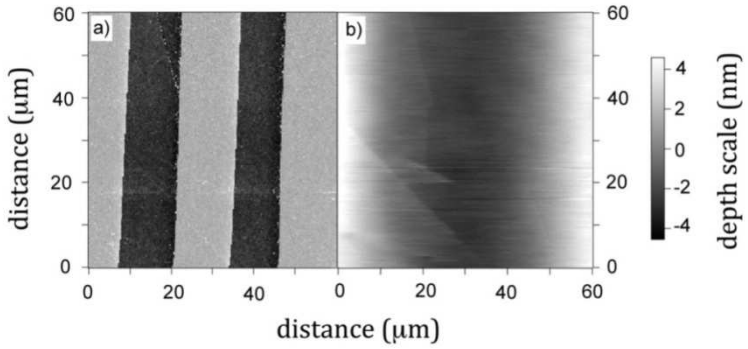

Figure 2.9 (a) piezoresponse force microscopy (PFM) phase image of the polar surface of the periodically poled lithium niobate sample showing antiparallel 180° domains; (b) atomic force microscopy (AFM) topographic image of the same area. The dipole direction is along the surface normal, either positive or negative with respect to the surface.

Spatially resolved X-ray adsorption near edge spectroscopy (μ-XANES) experiments were performed at the microXAS beamline (X05, Swiss light Source, Switzerland). A micro-focused X-ray beam of 2 × 2 μm^2 and a solid-state Si-detector was utilized in order to record the μ-XANES spectra. The energy of the incident X-ray beam was set using a fixed-exit Si(111) double-crystal monochromator, with an energy resolution of about 2 eV at 19 keV. The spectra were collected in fluorescence mode, with the sample placed at an angle of 45° relative to the incoming X-ray beam, in order to minimize scattering contributions to the fluorescence spectra. The sample was mounted on a 3 axis-motion manipulator which allows an accurate positioning (~ 50 nm) of the sample with respect to the photon beam. The Athena software (part of the Ifeffit program) has been used to normalize the raw data [43].

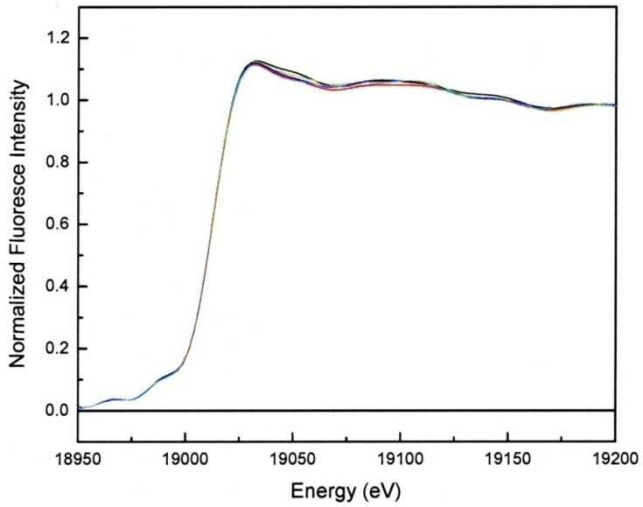

Figure 2.10 Spatially resolved near edge X-ray adsorption fine structure (XANES) spectra taken at the Nb K-edge at a number of different positions (denoted by five different colors) and spaced by roughly 10 μm in both vertical and horizontal directions. The fluorescence yields are plotted against photon energy. The Nb K-shell edge is at 18.986 keV.

As seen in figure 2.10, little variation was observed in the μ-XANES spectra taken at the niobium K-edge (18.986 keV), with changing sample position, across the periodically poled lithium niobate. The absence of spectral variations in the μ-XANES spectra indicate that the lithium niobate ($LiNbO_3$) is compositionally uniform and the bulk composition is not altered by the ferroelectric poling.

2.7.3 The PVDF-TrFE Substrate

The PVDF-TrFE substrate in this dissertation was prepared by Dr. Luis G. Rosa's group in department of physics and electronics, University of Puerto Rico-Humacao.

Ultrathin ferroelectric films of the copolymer 70% vinylidene fluoride with 30% trifluoroethylene, P(VDF-TrFE 70:30) were fabricated by Langmuir Blodgett (LB) deposition techniques on graphite substrates from the water subphase and dimethylsulphoxide (DMSO) [44, 45, 47-67]. The P(VDF-TrFE 70:30) films, nominally 9 molecular layers thick (roughly 30 Å thick, as determined by atomic force microscopy studies) were further prepared in ultrahigh vacuum by annealing at 110º C, which has proven to be an effective recipe in prior studies[44, 45, 47-66] and has been demonstrated to results in a surface free from impurities (including water) [67]. Poly(vinylidene fluoride) [PVDF, $-(CH_2-CF_2)_n-$] copolymers with trifluoroethylene [TrFE, $-(CHF-CF_2)-$] can form highly ordered crystalline ferroelectric polymer ultrathin films as has been demonstrated by X-ray and neutron scattering [46, 47, 50, 51, 59-60], scanning tunneling microscopy [45, 47-49, 56-59, 62, 65, 66], low energy electron diffraction [58, 59] and band mapping [45, 58, 59, 66]. Although not always evident in scanning tunneling microscopy, the band structure shows a characteristic super-periodicity dominated by $-(CH_2-CF_2)_2-$ or $-(CH_2-$

CF_2)-(CHF-CF_2)- “dimer” pairs[58, 59, 66] in the ferroelectric phase. The copolymer P(VDF-TrFE, 70:30), in spite of the low overall symmetry, does show all the characteristics of high local symmetry and symmetry selection rules, with the dipoles aligned along the surface normal at lower temperatures (especially below 150 K) [63, 64, 68].

The ferroelectric poling process of PVDF has been described in Section 2.5 and the ferroelectric domain orientations and hysteresis were determined and imaged in ambient environment by means of piezoresponse force microscopy [42]. As grown, the copolymer P(VDF-TrFE, 70:30) films have the dipoles generally oriented up and the ferroelectric coercivity is small, as seen in figure 2.11 where we plot the hysteresis loop of an as grown films. Some of the adsorption studies were carried out on the as grown films, and these P(VDF-TrFE) Langmuir Blodgett films should be regarded as at least partially poled as typically occurs during the deposition process. Complete polarization of these P(VDF-TrFE, 70:30) films was ensured by applying a voltage to a tip scanned 1-2 mm above the surface (non-contact poling), across the entire surface, with -200 V to ensure the film is poled up and 400 V applied to ensure the film is poled down. Confirmation of complete ferroelectric poling was confirmed by piezoresponse force microscopy.

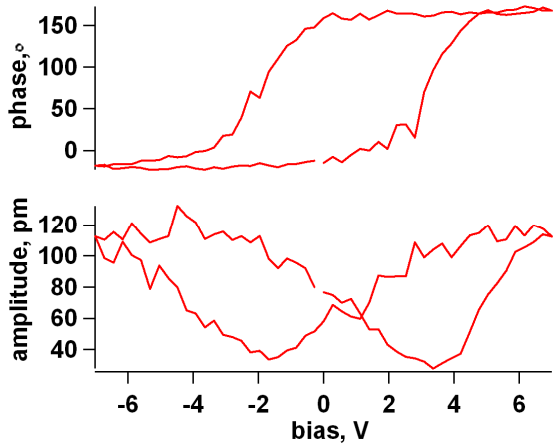

Figure 2.11 The piezoresponse force microscopy (PFM) amplitude and phase, as a function of applied voltage of a roughly 30 Å thick P(VDF-TrFE, 70:30) film.

2.7.4 *P*-benzoquinonemonoimine Zwitterionic Compounds

In this dissertation, we investigate thin films made of a series of small quinonoid zwitterion molecules with a large intrinsic dipole and significant flexibility in their design. These zwitterionic compounds of the *p*-benzoquinonemonoimine type include ($C_6H_2(\cdots NHR)_2(\cdots O)_2$, where R = H, *n*-$C_4H_9$, C_3H_6-S-CH_3, C_3H_6-O-CH_3, CH_2-C_6H_5, etc.) (as shown in figure 1.2), adsorbed on Au. These quinonoid zwitterions are prepared by Dr. Lucie Routaboul and Dr. Pierre Braunstein's group in Laboratoire de Chimie de Coordination, Institut de Chimie (UMR 7177 CNRS), Université de Strasbourg, 4 rue Blaise Pascal, 67083 Strasbourg, France, and Dr. Gero Decher Institut Charles Sadron (UPR 22 CNRS), Université de Strasbourg, 23 rue du Loess B.P. 84047, 67034 Strasbourg, France. I briefly introduce the synthesis processes here.

2.7.4.1 General

Commercial 4, 6-diaminoresorcinol dihydrochloride and functional amines were used directly without further purification. Solvents were freshly distilled under argon prior to use. ^{1}H NMR spectra were recorded in $CDCl_3$ on a Bruker AC300 instrument, operating at 75 MHz for ^{13}C spectra and 300 MHz for ^{1}H spectra. Chemical shifts were found in δ units, in parts per million (ppm) relative to the singlet at δ = 7.26 for $CHCl_3$. Elemental analyses were performed by the "Service de Microanalyse de l'Institut de Chimie" (Strasbourg, France).

The zwitterions **1**, **2** and **5** ($C_6H_2(\cdots NHR)_2(\cdots O)_2$, where R = H, *n*-$C_4H_9$, CH_2-C_6H_5, respectively) were synthesized according to established procedures [69]. Zwitterions **3** and **4** can be synthesized using two methods: (A) the "one pot synthesis", in which addition of amine to a suspension of diaminoresorcinol dihydrochloride in ethanol yielded smoothly the zwitterions; or (B) reaction of an amine with the "parent zwitterion" **1.** The yields in both reactions are good to excellent and the zwitterions were easily isolated as pure compounds. Method (A) allows the use of commercially available reagents and is easily scaled up. In method (B), the stable "parent zwitterion" **1,** which is also available in multi-gram quantities, can be quantitatively converted to the desired products within 2 h by using stoichiometric amounts of amine, which is advantageous if the latter is expensive.These two methods are described in detail in the following.

2.7.4.2 Synthesis of Zwitterion 3

Method A: 4, 6-Diaminoresorcinol dihydrochloride (0.300 g, 1.41 mmol) was dissolved in a mixture of water and ethanol (5 mL / 15 mL) and then 3-(methylthio)propylamine (1.1 mL, 9.81 mmol) was added to this solution. Immediately the color of the solution turned violet, and the solution was stirred for 2 h at room temperature in the presence of air. After concentration of the solution under reduced pressure, the residue was taken up in dichloromethane. The organic phase was dried over magnesium sulfate, and filtered through Celite. The solution was concentrated under reduced pressure and addition of pentane yielded the zwitterion **3** as a violet solid (0.410 g, 92%).

Method B: To a suspension of the parent zwitterion **1** (0.200 g, 1.45 mmol) in ethanol (10 mL) was added 3-(methylthio)propylamine (0.330 mL, 2.94 mmol). The mixture was refluxed for 2 h. After cooling to room temperature, the solution was filtered and evaporated to dryness under reduced pressure. The residue was taken up in dichloromethane and pentane was added to this solution to precipitate the product. After filtration the zwitterion **3** was obtained as a violet solid (0.430 g, 94%).

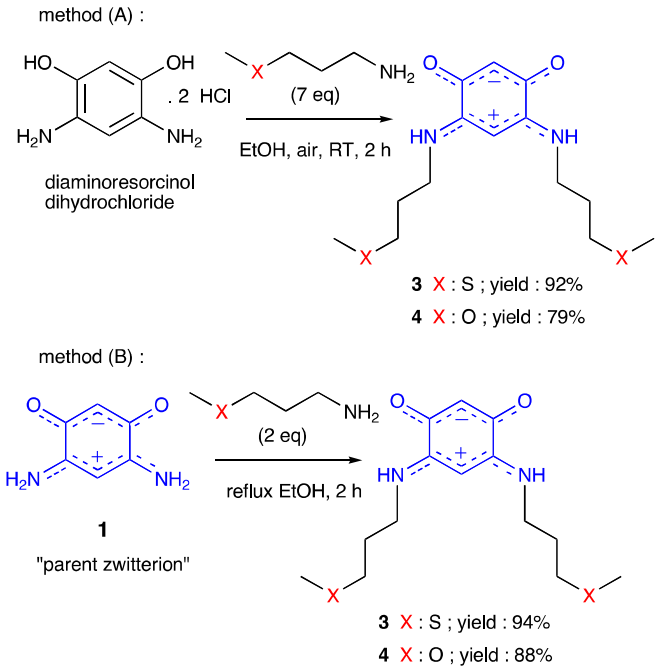

Figure 2.12 Synthetic methods leading to zwitterions **3** and **4**.

2.7.4.3 Synthesis of Zwitterion 4

Method A: 3-Methoxypropylamine (3.4 mL, 33.3 mmol) was added to a solution of 4, 6-diaminoresorcinol dihydrochloride (1.00 g, 4.69 mmol) in water (10 mL). Within a few minutes the color of the solution changed from brown to violet. After the reaction mixture was stirred for 2 h at room temperature in the presence of air, the product was extracted with dichloromethane. The organic layer was dried over magnesium sulfate, and filtered through Celite. The solution was concentrated under reduced pressure and addition of pentane precipitated the zwitterion **4** as a violet solid (1.05 g, 79%).

Method B: To a suspension of the parent zwitterion **1** (0.300 g, 2.17 mmol) in ethanol (15 mL) was added 3-methoxypropylamine (0.450 mL, 4.4 mmol). The solution was heated at 80 °C for 2 h. After cooling to room temperature, the solution was filtered and

evaporated to dryness under reduced pressure. The residue was taken up in dichloromethane and pentane was added to this solution to precipitate the product. After filtration the zwitterion **4** was obtained as a violet solid (0.541 g, 88%).

2.7.4.4 Functionalization of Gold Surfaces

These zwitterions were deposited on clean gold substrates from a CH_2Cl_2 solution. A typical overnight exposure to a 0.8 mmol solution (0.2 g/l) was followed by extensive washing by ethanol to remove the excess molecules not bonded to the Au substrate. The samples were dried and kept under nitrogen atmosphere. Our measurements established that this "washing" procedure left a very thin, 0.5-1 nm thick, adsorbed molecular film covering the whole substrate (i.e., no pinholes). The film thickness was estimated from the attenuation of the substrate gold core level signal and independently confirmed by atomic force microscopy and quartz crystal microbalance (QCM) experiments. Films 2-3 nm thick were obtained by dipping the substrates into a more concentrated solution of the molecules, or by ethanol washing of the surface for much shorter times (ca. 1 min). Both methods provided similar pinhole-free molecular films, as described elsewhere [70].

2.7.5 D-Cysteine

The d-cysteine powder ($\geq$ 99%, RT) with molecular weight 121.16 $g.mol^{-1}$ used in our experiments is bought from Sigma Aldrich. Deposition of d-cysteine molecules on PPLN has been carried out by immersing the PPLN substrate in aqueous 1*M* d-cysteine solution for 24 h. Following immersion, the samples were washed in a weak 1*M* NaOH alcohol-water solution to remove excess molecules followed by rinsing in ethanol using the

previously described cleaning process [71] and dried. Deposition was carried out in isothermal conditions at room temperature without illumination.

2.7.6 MEH-PPV Dopped with PbSe and PCBM

Powdered MEH-PPV (Sigma Aldrich) from a single batch with the average molecular weight 86 000 $g.mol^{-1}$ was dissolved in chlorobenzene. These solutions were heated to 80^0C and stirred for 8 h, then filtered and spincast onto coated glass substrates for the pristine MEH-PPV sample. The substrate was indium tin oxide (ITO) coated glass with sheet resistance of ~10 Ω/□ (150 nm thick ITO) obtained from Delta Technologies.

For the nanocrystal bearing films, PbSe nanocrystals in solution (obtained from Evident Technologies) were added to MEH-PPV solutions prepared as described above in appropriate volume to obtain the desired weight ratios. These PbSe crystals were 5–8 nm in diameter and suspended in hexane. PCBM bearing films were prepared from the same base MEH-PPV solution described above by adding powdered PCBM (Sigma Aldrich) in amounts needed to achieve the given weight ratios. These samples were dried, *in vacuo*, for 8 h at room temperature. Film thicknesses were measured to be 90 nm with good uniformity (±10%).

These samples were prepared by Dr. D. K. Chambers and Dr. S. Zivanovic. Selmic's group in Institute for Micromanufacturing, Louisiana Tech University, 911 Hergot Avenue, Ruston, LA 71270, USA.

References

[1] S. Hüfner, Photoelectron Spectroscopy, 3rd ed., Springer, (2003).

[2] J. Electron Spectrosc. Relat. Phenom. Vol. 100 (1999).

[3] C.J. Powell, Surf. Sci. 44 29 (1974).

[4] D.R. Penn, J. Electron Spectrosc. Relat. Phenom. 9, 29 (1976).

[5] S. Tamura, C.J. Powell, Surf. Interface Anal. 17, 911, (1991).

[6] S. Tamura, C.J. Powell, Surf. Interface Anal. 21, 165, (1994).

[7] C.J. Powell, Surf. Sci., 44, 29, (1974).

[8] Steinar Raaen, http://www.phys.ntnu.no/~sraaen/dif4903/elspec.pdf "Electron Spectroscopy".

[9] J.H. Scofield, J. Electron Spectr. Relat. Phenom. 8, 129 (1976).

[10] X. Bo, Ph.D thesis, 2002, University of Nebraska-Lincoln.

[11] E.W. Plummer and W. Eberhardt, Adv. Chem. Phys. 49, 533 (1982)

[12] H.-P. Steinrück, Vacuum 45, 715 (1994); H.-P. Steinrück, J. Phys. Condensed Matt. 8, 6465 (1996)

[13] N.V. Richardson and A.M. Bradshaw, Electron Spectroscopy: Theory, Techniques and Applications, Edited by C.R. Brundle and A.D. Baker, vol. 4, Academic Press (1984) p. 153 [14] N.V. Smith, Rep. Prog. Phys. 51, 1227 (1988).

[15] F.J. Himpsel, Surf. Sci. Rep. 12, 1 (1990).

[16] P.A. Dowben, Z. Phys. Chemie, 202, 227 (1997)

[17] P.A. Dowben, B. Xu, J. Choi, and E. Morikawa, "Band Structure and orientation of molecules adsorbates on surfaces by angle resolved electron spectroscopies." in: Handbook

of Thin Film Materials, vol. 2 Characterization and Spectroscopy of thin Films, 61-113 (2002).

[18] J. Xiao, Ph.D. thesis, 2009, University of Nebraska-Lincoln.

[19] P. A. Dowben, L. G. Rosa, C. C. Ilie and J. Xiao, J. Electron Spectrosc. Relat. Phenom., 174, 10, (2009).

[20] J. Xiao and P. A. Dowben, J. Mater. Chem., 2009, 19, 2172; J. Xiao, A. Sokolov and P. A. Dowben, Appl. Phys. Lett., 90, 242907, (2007).

[21] B. Xu, J. Choi, A. N. Caruso and P. A. Dowben, Appl. Phys. Lett., 80, 4342, (2002); J. Xiao and P. A. Dowben, J. Phys.: Condens. Matter, 21, 052001, (2009).

[22] J. Choi, C. N. Borca, P. A. Dowben, A. Bune, M. Poulsen, S. Pebley, S. Adenwalla, S. Ducharme, L. Robertson, V. M. Fridkin, S. P. Palto, N. Petukhova and S. G. Yudin, Phys. Rev. B: Condens. Matter Mater. Phys., 61, 5760, (2000);

[23] A. Sokolov, C.-S. Yang, L. Yuan, S.-H. Liou, R. Cheng, H.-K. Jeong, T. Komesu, B. Xu, C. N. Borca, P. A. Dowben and B. Doudin, Europhys. Lett., 58, 448, (2002).

[24] J. Zhang, D. N. McIlroy, P. A. Dowben, H. Zeng, G. Vidali, D. Heskett and M. Onellion, J. Phys.: Condens. Matter, 7, 7185, (1995); D. N. McIlroy, J. Zhang, P. A. Dowben and D. Heskett, Mater. Sci. Eng., A, 217–218, 64, (1996).

[25] D.-Q. Feng, D. Wisbey, Ya. B. Losovyj, Y. Tai, M. Zharnikov and P. A. Dowben, Phys. Rev. B: Condens. Matter Mater. Phys., 74, 165425, (2006).

[26] Y. Losovyj, I. Ketsman, E. Morikawa, Z. Wang, J. Tang and P. A. Dowben, Nucl. Instrum. Methods Phys. Res., Sect. A, 582, 264, (2007).

[27] P. A. Dowben, D. LaGraffe and M. Onellion, J. Phys.: Condens. Matter, 1, 6571, (1989).

[28] J. Hormes, J. D. Scott and V. P. Suller, Synchrotron Radiat. News, 19, 27, (2006).

[29] J. Hormes, J. D. Scott and V. P. Suller, Synchrotron Radiat. News, 19, 27, (2006).

[30] Y. Losovyj, K. Morris, L. Rosa, J. D. Scott and P. A. Dowben, Nucl. Instrum. Methods Phys. Res., Sect. A, 582, 258, (2007).

[31] C. M. Evans, J. D. Scott and E. Morikawa, Rev. Sci. Instrum., 73, 1557, (2002).

[32] J. Choi, M. Chipara, B. Xu, C. S. Yang, B. Doudin, P.A. Dowben, Chem. Phys. Lett., 343, 193 (2001).

[33] D. K. Chambers, S. Karanam, D. Qi, S. Selmic, Y. B. Losovyj, L.G. Rosa, P. A. Dowben, Appl. Phys. A, 80, 483 (2005).

[34] P. A. Dowben, D. LaGraffe, and M. Onellion, J. Phys. Cond. Matt. 1, 6571 (1989).

[35] M.P. Seah, M.E. Jones, and M.T. Anthony, Surface and Interface Analysis 6, 242 (1984); M.P. Seah, Surface and Interface Analysis 20, 243 (1993).

[36] C.N. Borca, T. Komesu, and P.A, Dowben, J. Electron Spectr. Relat. Phenom. 122, 259 (1976).

[37] D.C. Harris, M.D. Bertolucci, Symmetry and Spectroscopy, Oxford University Press, New York, 1978; M. Tinkham, Group Theory and Quantum Mechanics, McGraw-Hill, New York, 1964; S.J. Joshua, in: D.F. Brewer (Ed.), Symmetry Principles and Magnetic Symmetry in Solid State Physics, IOP publishing, New York, 1991.

[38] D.F. Heath, P.A. Sacher, Appl. Opt. 5 937 (1966).

[39] K. Watanabe, T. Nakayama, J. Mottl, J. Quant. Spectrosc. Radiat. Transf. 2 369 (1962).

[40] O. Kizilkaya, J. D. Scott, E. Morikawa, J. D. Garber and R. S. Perkins, Rev. Sci. Instrum., 76, 13703, (2005).

[41] O. Kizilkaya, A. Prange, U. Steiner, E. C. Oerke, J. D. Scott, E. Morikawa and J. Hormes, Nucl. Instrum. Methods Phys. Res., Sect. A, 582, 274, (2007).

[42] A. Gruverman, O. Auciello and H. Tokumoto, Ann. Rev. Mat. Sci., 28, 101 (1998).

[43] Ravel and M. Newville, J. Synchrotron Rad., 12, 537, (2005).

[44] L. G. Rosa, P. A. Jacobson, P. A. Dowben, J. Phys. Chem. B 110, 7944-7950, (2006).

[45] P. A. Dowben, L. G. Rosa, C. C. Ilie, Z. Phys. Chemie 222, 755-778, (2008).

[46] D. Deutsch, A. Natan, Y. Shapira, L. Kronik, J. Am. Chem. Soc. 129, 2989-2997, (2007); M. L. Sushko, A. L. Shluger, Adv. Func. Mat. 18, 2228-2236, (2008).

[47] A.V. Bune, V.M. Fridkin, S. Ducharme, L.M. Blinov, S.P. Palto, A.V. Sorokin, S.Yudin, and A. Zlatkin, Nature 391, 874, (1998).

[48] S. Ducharme, S.P. Palto, V.M. Fridkin, in: Handbook of Surfaces and Interfaces of Materials, Ferroelectric and Dielectric Films, Vol. 3, 546-592, (2002).

[49] L.M. Blinov, V.M. Fridkin, S.P. Palto, A.V. Bune, P.A. Dowben, S. Ducharme, Uspekhi Fizicheskikh Nauk [Russian edition vol.] 170, 247-262, (2000); Physics Uspekhi [English edition volume] 43, 243-257, (2000).

[50] P.A. Jacobson, L.G. Rosa, C.M. Othon, K. Kraemer, A.V. Sorokin, S. Ducharme, P.A. Dowben, Appl. Phys. Lett. 84, 88, (2004).

[51] L.G. Rosa, P.A. Jacobson, P.A. Dowben, J. Phys. Chem. B 109, 532, (2005).

[52] L.G. Rosa, I.N. Yakovkin, P.A. Dowben, J. Phys. Chem. B 109, 14189, (2005).

[53] L.G. Rosa, J. Xiao, Ya.B. Losovyj, Y. Gao, I.N. Yakovkin, X.C. Zeng, P.A. Dowben, J. Am. Chem. Soc. 127, 17261, (2005).

[54] J. Xiao, A. Sokolov, P.A. Dowben, Appl. Phys. Lett. 90, 242907, (2007).

[55] P.A. Dowben, J. Xiao, B. Xu, A. Sokolov, B. Doudin, Appl. Surf. Sci. 254, 4238-4244, (2008).

[56] H. Qu, Wei Yao, T. Garcia, J. Zhang, A.V. Sorokin, S. Ducharme, P.A. Dowben, V.M. Fridkin, Appl. Phys. Lett. 82, 4322, (2003).

[57] L. Cai, H. Qu, C. Lu, S. Ducharme, P.A. Dowben, J. Zhang, Phys. Rev. B 70, 155411, (2004).

[58] J. Choi, P.A. Dowben, S. Ducharme, V.M. Fridkin, S.P. Palto, N. Petukhova, S.G. Yudin, Phys. Lett. A 249, 505, (1998).

[59] J. Choi, C.N. Borca, P.A. Dowben, A. Bune, M. Poulsen, S. Pebley, S. Adenwalla, S. Ducharme, L. Robertson, V.M. Fridkin, S.P. Palto, N. Petukhova, A.V. Sorokin, Phys. Rev. B 61, 5760, (2000).

[60] C.N. Borca, S. Adenwalla, J. Choi, P.T. Sprunger, S. Ducharme, L. Robertson, S. P. Palto, J. Liu, M. Poulsen, V. M. Fridkin, H. You, P.A. Dowben, Phys. Rev. Lett. 83, 4562, (1999).

[61] J. Choi, P.A. Dowben, S. Pebley, A. Bune, S. Ducharme, V.M. Fridkin, S.P. Palto, N. Petukhova, Phys. Rev. Lett. 80, 1328, (1980).

[62] S. Palto, L. Blinov, E. Dubovik, V. Fridkin, N. Petukhova, A. Sorokin, K. Verkhovskaya, S. Yudin, A. Zlatkin, Europhys. Lett. 34, 465, (1996).

[63] J. Choi, S.-J. Tang, P.T. Sprunger, P.A. Dowben, V.M. Fridkin, A.V. Sorokin, S.P. Palto, N. Petukhova, S.G. Yudin, J. Phys. Cond. Matter 12, 4735, (2000).

[64] L.G. Rosa, Ya.B. Losovyj, J. Choi, P.A. Dowben, J. Phys. Chem. B 109, 7817, (2005).

[65] J. Xiao, L.G. Rosa, M. Poulsen, D.-Q. Feng, D. S. Reddy, J.M. Takacs, L. Cai, J. Zhang, S. Ducharme, P.A. Dowben, J. Phys. Cond. Matter 18, L155, (2006).

[66] L. Cai, X. Wang, Y. Darici, P. A. Dowben,J. Zhang, J. Chem. Phys. 126, 124908, (2007).

[67] J. Choi, E. Morikawa, S. Ducharme, P.A. Dowben, Matt. Lett. 59, 3599, (2005).

[68] M. Qin, K. Yao, Y. C. Liang, Appl. Phys. Lett. 93, 122904 (2008).

[69] Q.-Z. Yang, O. Siri, P. Braunstein, Chem. Commun., 2005, 2660-2662; Q. -Z. Yang, O. Siri, H. Brisset, P. Braunstein, Tetrahedron Lett., 47, 5727-5731, (2006).

[70] J. Xiao, Z.-Z. Zhang, D. Wu, L. Routaboul, P. Braunstein, B. Doudin, Ya. B. Losovyj, O. Kizilkaya, L. G. Rosa, C. N. Borca, A. Gruverman, P. A. Dowben, Phys. Chem. Chem. Phys. 12, 10329–10340, (2010).

[71] S. Dunn, D. Cullen, E. Abad-Garcia, C. Bertoni, R. Carter, D. Howorth, and R. W. Whatmore, Appl. Phys. Lett. 85, 3537, (2004).

Chapter 3 Altering the Static Dipole on Surfaces though Chemistry: *p*-benzoquinonemonoimine Zwitterionic Compounds

3.1 Introduction

In this chapter, we investigate thin films made of small molecules with a large intrinsic dipole and significant flexibility in their design. This allows us to take advantage of the tunability of the pendant groups for varying the density and nature of the chemical attachment to the surface, with the aim of gaining a better insight into the origin and control of the interface dipole [1-13]. We compare several different zwitterionic compounds of the *p*-benzoquinonemonoimine type (see in figure 3.1 i.e. $C_6H_2(\cdots NHR)_2(\cdots O)_2$, where R = H, *n*-$C_4H_9$, C_3H_6-S-CH_3, C_3H_6-O-CH_3, CH_2-C_6H_5, etc.) obtained by oxidation of *N*-alkyldiaminoresorcinols. The diversity of functions that can be incorporated in the pendant groups [14, 15, 16, 17] provides a unique opportunity for systematic studies of interface interactions for a family of closely related molecules, much like those studies undertaken for the metal (II) phthalocyanines [9, 18], or icosahedral *closo*-carboranes [13]. We systematically observe the molecular films, with homogenous films of thickness below 1 nm, fully covering the Au surface even for a variety of different attachments involving the R pendant group. This allows us to take advantage of the tunability of the pendant groups for varying the density and nature of the chemical attachment to the surface, with the aim of gaining a better insight into the origin and control of the interface dipole. We compare these different zwitterionic compounds and the diversity of functions that can be incorporated in the pendant groups provides a unique opportunity for systematic studies of interface

interactions for a family of closely related molecules, much like those studies undertaken for the metal (II) phthalocyanines , or icosahedral *closo*-carboranes.

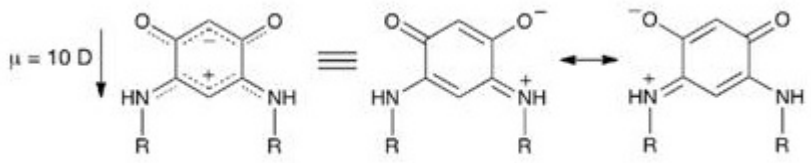

Figure 3.1 Representation of the family of the zwitterion studied. Zwitterionic compounds of the *p*-benzoquinonemonoimine type, $C_6H_2(\cdots NHR)_2(\cdots O)_2$, where R = H, *n*-$C_4H_9$, C_3H_6-S-CH_3, C_3H_6-O-CH_3, CH_2-C_6H_5, etc.).

Given the wide range of possible substituents on the quinonoid zwitterionic core (Figure 3.1) [14, 15, 16, 17], the study of their influence on the bonding and electronic structure is essential for further materials development using this class of compounds "by design". In the present work, we change the different functional R groups with the objective of modifying the molecular-substrate interactions, without significant alterations of the strong intrinsic electric dipole.

In this chapter, we show that ultra-thin films of *p*-benzoquinonemonoimine compounds of good coverage can be readily formed on Au, and exhibit properties tunable by the choice of the pendant R groups. These molecules exhibit very efficient interface dipole screening, thus the *p*-benzoquinonemonoimine type zwitterionic compounds may become organic materials of interest for their interfacial electronics properties. We show

that organized films, exhibiting crystallinity, can be closely packed on substrates, and may be n-type conductors.

3.2 The Characterization of *p*-benzoquinonemonoimine Zwitterionic Compounds

The schematics of *p*-benzoquinonemonoimine Zwitterionic Compounds are shown in figure 3.2. As described in Chapter 2, the zwitterions **1**, **2** and **5** ($C_6H_2(\cdots NHR)_2(\cdots O)_2$, where R = H, *n*-$C_4H_9$, CH_2-C_6H_5, respectively) were synthesized according to established procedures [17]. Zwitterions **3** and **4** can be synthesized using two methods: (A) the "one pot synthesis", in which addition of amine to a suspension of diaminoresorcinol dihydrochloride in ethanol yielded smoothly the zwitterions; or (B) reaction of an amine with the "parent zwitterion" **1.**

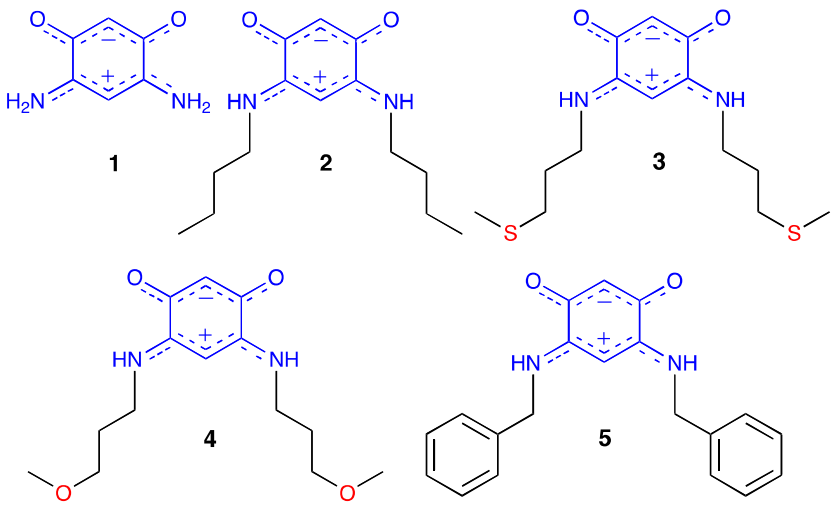

Figure 3.2 Zwitterionic compounds with different pendant groups studied in this chapter.

Single crystals of zwitterions **3** and **4** were obtained at room temperature by slow diffusion of pentane into a dichloromethane solution of **3** or **4**. Table 3.1 summaries bond lengths of the "C_6 core" which are experimentally determined by X-ray crystallography. They are similar to those observed in the structures of related zwitterions [15, 16, 17].

Interestingly, the bond lengths C(3)-C(4) and C(4)-C(5), C(3)-O(1) and C(5)-O(2) distances are almost equal. Likewise (C(1)-C(6) and C(1)-C(2)) as well as (C(2)-N(1) and C(6)-N(2)) are similar, respectively. All these distances are intermediate between those for single and double bonds. However, C(3)-C(2) and C(5)-C(6) distances are much longer and are consistent with single bonds. Based on these metrical data, these zwitterions are well described as two fully delocalized 6 electrons systems (trimethyne oxonol part: O···C···CH···C···O and the trimethyne cyanine part: N···C···CH···C···N) connected by two C-C single bonds.

Zwitterion **3**		Zwitterion **4**	
C(3)-C(4)	1.404	C(3)-C(4)	1.393
C(4)-C(5)	1.392	C(4)-C(5)	1.392
C(3)-C(2)	1.514	C(3)-C(2)	1.522
C(5)-C(6)	1.531	C(5)-C(6)	1.526
C(1)-C(2)	1.386	C(1)-C(2)	1.388
C(1)-C(6)	1.392	C(1)-C(6)	1.389
C(3)-O(1)	1.253	C(3)-O(1)	1.249
C(5)-O(2)	1.256	C(5)-O(2)	1.247
C(2)-N(1)	1.327	C(2)-N(1)	1.319
C(6)-N(2)	1.313	C(6)-N(2)	1.318

Table 3.1 Interatomic Distances (Å) observed in zwitterions **3** and **4**.

Since thiol or disulfide terminal functionalities are among the most obvious choices for strengthening the molecular anchoring, following the extensive literature on self-assembled monolayers [22, 23], we attempted but failed to isolate pure zwitterions **6** and **7** (Figure 3.3).

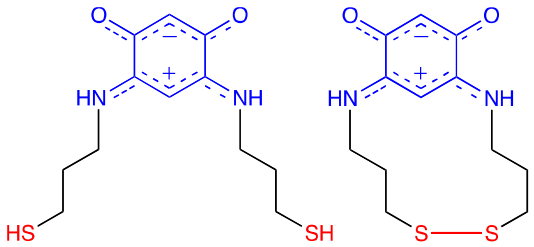

Figure 3.3 Zwitterions with thiol or disulfide terminal functions.

Alternatively, thioether terminal groups, are easier to synthesize and more stable towards oxidation than thiol or disulfide analogues. Their successful attachment to gold, especially when weaker interactions are needed, as in the case of molecular rotors, has been reported by several groups [24, 25, 26, 27].

XPS studies of thioether zwitterion **3** on gold revealed however significant decomposition caused by high fluences of low energy electrons and possibly other irradiation. The fact that we did not observe any trace of decomposition of the butyl zwitterion **2** on gold (although much care was given to keeping the total fluences low) suggests that S-C bonds may be the weakest part of the molecule after adsorption [20]. In order to confirm this assumption, we synthesized the zwitterion **4** differing only from **3** by replacing sulfur by oxygen atoms. The high solubility of the zwitterion **4** in organic

solvents and water also provides an opportunity to study the influence of the nature of the solvent on the functionalization of gold by zwitterionic compounds.

3.3 Adsorption of *p*-benzoquinonemonoimine Zwitterionic Compounds on Surfaces

The *p*-benzoquinonemonoimine zwitterions **2-4** were deposited on clean gold substrates from CH_2Cl_2 or EtOH solutions, and the zwitterions **1**, **5**, from CH_2Cl_2 solutions due to their poor solubility. Quartz crystal microbalance (QCM) experiments were performed to estimate the adsorbed mass of the layer and the kinetics for surface adsorption. We used a commercial system (QCM-E4, Q-Sense AB, Sweden) that allowed parallel processing of several devices, providing greater confidence in the reproducibility and facilitating comparisons between molecules **2** and **4**. Figure 3.4 shows the frequency changes as a function of time upon formation of the molecular films for zwitterions **2** and **4**. While several injections were necessary for zwitterion **4** to get a maximum number of molecules adsorbed onto the surface, only one injection was needed for zwitterion **2**. Successive EtOH washing can eliminate a significant fraction of the deposit, especially in the case of zwitterion **4**, where approximately half of the adsorbed molecules are removed from the surface by rinsing. However, after extensive washing, the residual QCM frequency shifts and the low dissipation values, in the same order of magnitude for both cases, indicate a remarkably stable thin molecular adsorption. Using Sauerbrey equation, the adsorbed mass can be estimated between 1 and 2 monolayers for both molecules. We deduce therefore that a thin film adsorbs rather rapidly, with typical isothermal adsorption kinetics showing layer saturations in the tens of mins range. Subsequent growth or reorganization has slower kinetics, and is reversible with time or through washing. For the

thickness dependence data shown in the subsequent sections, we used typical overnight dipping of the substrate in the solution, and successive washing cycles as simple means to obtain films of decreasing thickness value.

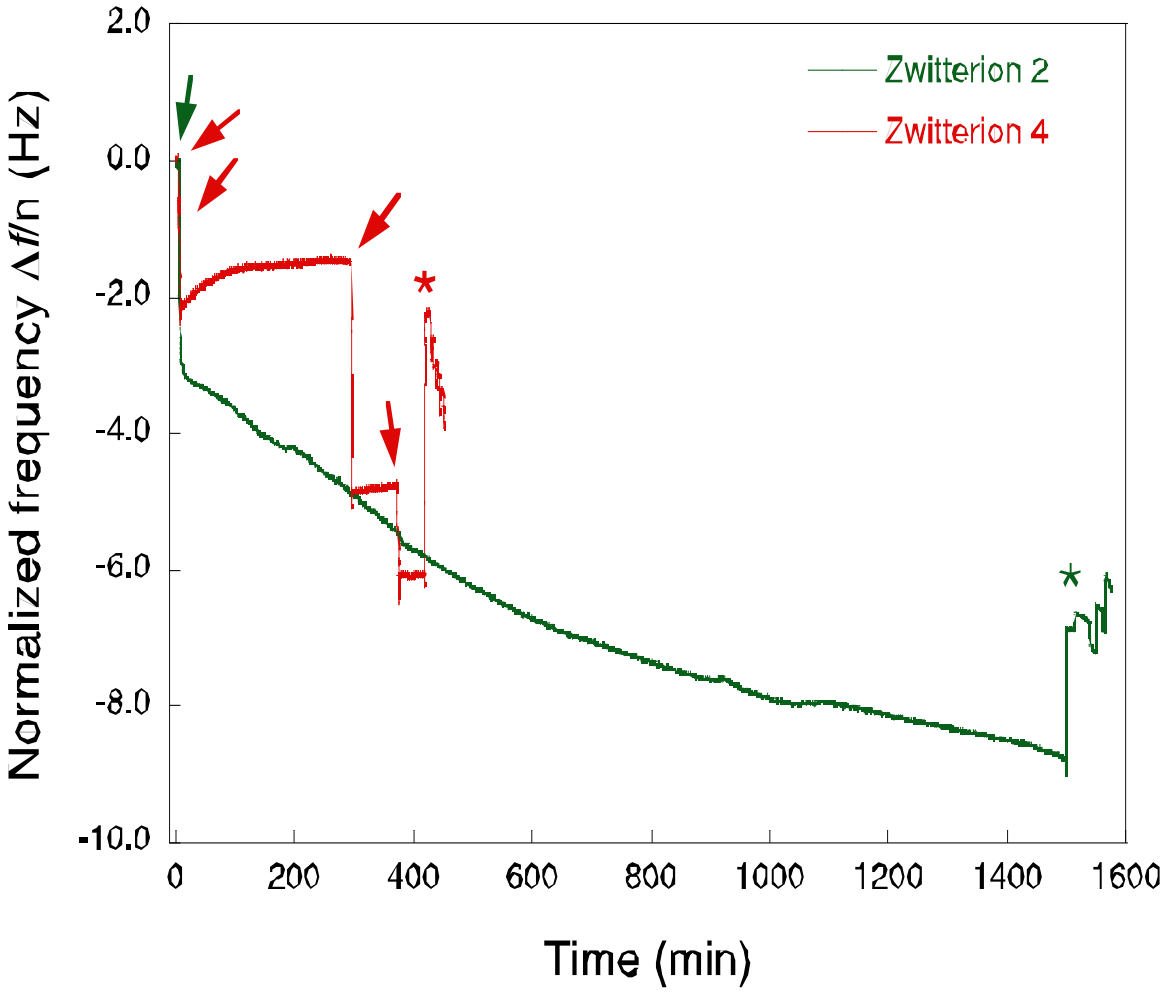

Figure 3.4 Evolution of the normalized frequency, measured at 35 MHz by QCM-D, as a function of time for the adsorption of zwitterions **2** (green) and **4** (red) on Au. Arrows indicate zwitterion injections and asterisks correspond to EtOH rinsing steps.

The quartz crystal microbalance (QCM) studies were also performed on substrates other than gold, confirming that the butyl zwitterion **2** can also be adsorbed on SiO_2 substrates, with less dense packing likely related to the lack of crystallinity. The differences in the adsorption of the butyl zwitterion **2** and the ether zwitterion **4** is also reflected in the indications of extensive and higher ordered crystal packing for **2**.

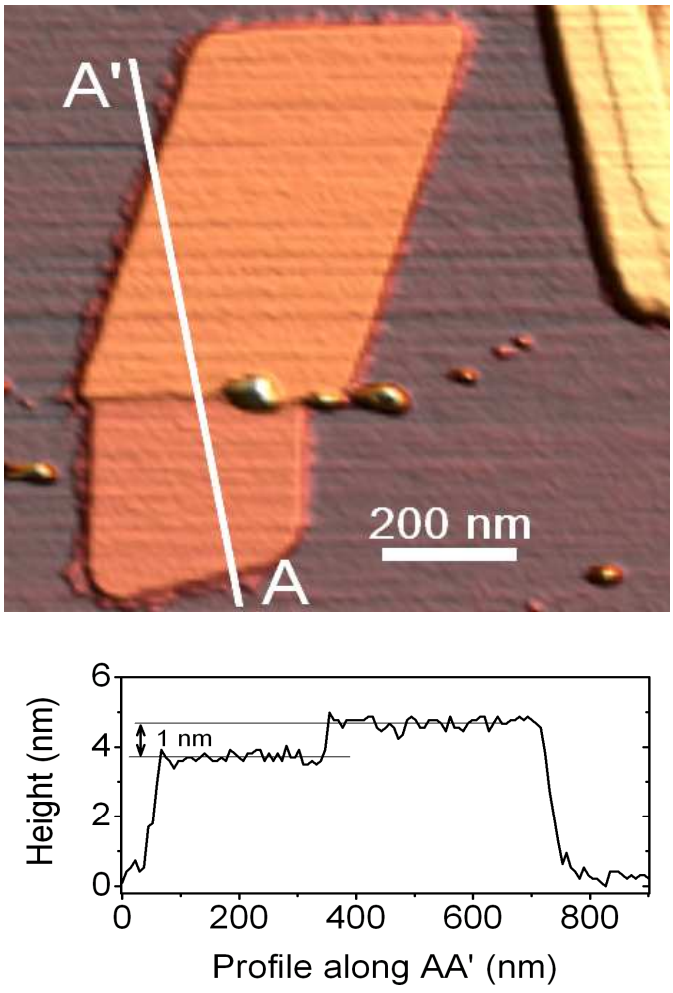

Figure 3.5 Atomic force microcopy mapping of butyl zwitterion **2** adsorbed on mica. The topography scan reveals thin crystals with typical 1-nm steps, corresponding to a bilayer of molecules (note that the top right crystal shows identical step height).

Atomic force microscopy (AFM) imaging was performed on atomically flat mica substrates and indicated the growth of thin flat crystals, made of a few molecular layers, with steps corresponding to a double molecular layer (Figure 3.5). The packing of the compound made of dipolar molecules always show antiparallel alignment of successive dipoles planes, minimizing the electrostatic dipole-dipole energy, and is expected to be a dominant factor in growing such ultra thin films. This type of packing is consistent with two molecules per unit cell, as inferred from the band structure, as discussed below.

3.4 Bonding to the Au Substrate

Partial insight into the molecule to substrate interactions was gained by core level X-ray photoemission spectra (XPS) taken with a SPECS X-ray source with a Mg anode ($h\nu$ = 1253.6 eV). We found that the molecules are stable on the time scale of the spectrsocopy measurements, except in the case of molecule **3**. The zwitterion is more fragile and shows evidence of decomposition with initial electron fluxes in inverse photoemission, and this decomposition may also occur in the X-ray photoemission, although we exercised caution throughout these studies by using limited total X-ray fluxes and incident photon intensities to limit the extent of photodecomposition, and the X-ray photoemission results are very reproducible. Unambiguous indications of bonding through the iminium/enamine groups have been provided in the case of butyl pendant groups (**2**) [20]. The previously reported [20] 0.5 ± 0.2eV nitrogen 1s core level shift, seen for **2**, was not observed for increasing molecular coverages of either 3 or 4 adsorbed on gold from solution, but the binding energies are in line with the expected N 1s core levels for a variety of similar organic compounds with amine and amide groups [28].

A clear sulfur $2p_{3/2}$ and 2s core level shift with increasing coverage is found for molecule 3 (Figure 3.6). This 1.1 $\pm$ 0.1 eV increase in binding energy (-162.3 $\pm$ 0.2 eV to -163.4 $\pm$ 0.2 eV for the S $2p_{3/2}$) is much larger, but similar in character to the N 1s core level shift observed with zwitterion 2. We interpret these core level shifts as indicative of binding of the molecule to gold largely through sulfur, in the thin film limit. We cannot exclude bonding through the iminium/enamine groups, but if such bonding occurs, it is very weak. The S $2p_{3/2}$ core level binding energies (-162.3 $\pm$ 0.2 eV) are in good agreement with the sulfur core level binding energies observed for alkane thiol self-assembled monolayers on gold [22], biphenyldimethyldithiol self-assembled monolayers on gold [25] and benzyl dithiobenzoate on gold [26], but somewhat larger than the core level binding energies (-162.1 eV) observed for biphenylthiols on gold [27]. We thus assume that in general the *p*-benzoquinonemonoimine zwitterions bind to the substrate through the thioether pendant groups situated on the electron-poor side of the dipole. We expect a dipole orientation along the direction normal to the surface, but unlike the detailed studies performed on molecule **2** (we will discussed it later in Chapter 4), the angle-resolved photoemission results are inconclusive as to the molecular orientation.

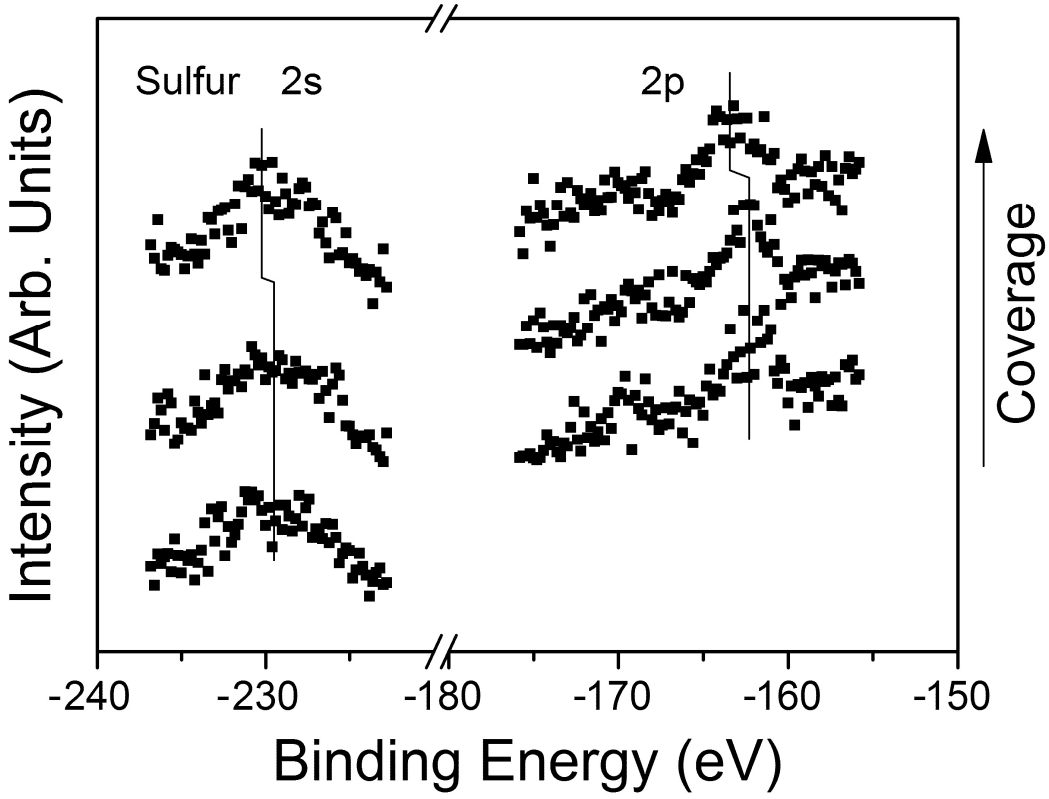

Figure 3.6 The S 2s and 2p core levels X-ray photoemission spectra for increasing coverages on gold of the thioether functionalized *p*-benzoquinonemonoimine zwitterion (molecule **3**). The main peak shifts are indicated by vertical bars.

3.5 Electronic Properties

The surface electronic properties were investigated using a combination of photoemission and inverse techniques. The ultraviolet photoemission (UPS) and inverse photoemission (IPES) spectra were taken in a single ultrahigh vacuum chamber to characterize the placement of both occupied and unoccupied molecular orbitals of the adsorbates as a function of adsorbate film coverage (thickness).

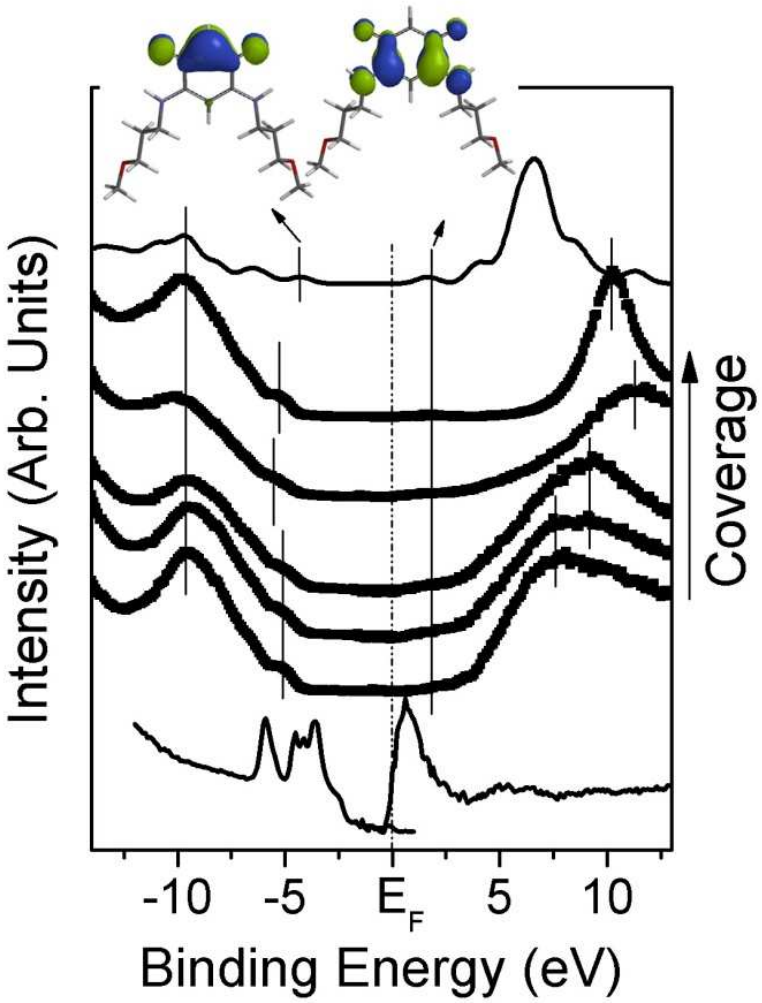

Figure 3.7 Coverage dependant photoemission and inverse photoemission (thick lines) of molecule **4** adsorbed on Au at room temperature. The bottom thin line corresponds to clean Au substrate, taken as reference spectra. The top thin line is the model calculation of the single molecule density of states, using a semi-empirical approach PM3 uncorrected for matrix elements and final state effects. The HOMO and LUMO are indicated by vertical bars and depicted by molecular orbital schematics as insets on the top of the figure. All the other shifted peaks are also indicated by vertical bars. The top experimental spectrum is taken from the sample in ethanol, instead of CH_2Cl_2, which is used for all the other spectra.

The decreasing thickness notation in Figure 3.7 relates to successive washing cycles, confirmed by the increase of the Au 4d core level. The expected extinction of valence band electron emission, as well as the Au substrate core level signals, of the buried gold substrate indicate that the thin film limit of our organic films is below 3 nm. Indeed, some molecular films are as thin as 1 nm, reaching the single to double monolayer coverage. This can be inferred from the occurrence of metal-induced gap states revealed by small features within the HOMO-LUMO bandgap (see the discussion in [20]). Such states are expected at the interface, and should become extinct for a thickness greater than 2 nm, because of the very short mean free paths of the low energy electrons detected in photoemission experiments. No indication of bare Au spectroscopic features was found for all thicknesses and all species of Figure 3.8, where comparison spectra are shown for molecules **1**-**5**. This provides strong evidence that the molecular films cover the substrate remarkably well. We estimate that the pinholes do not exceed 2% of the surface.

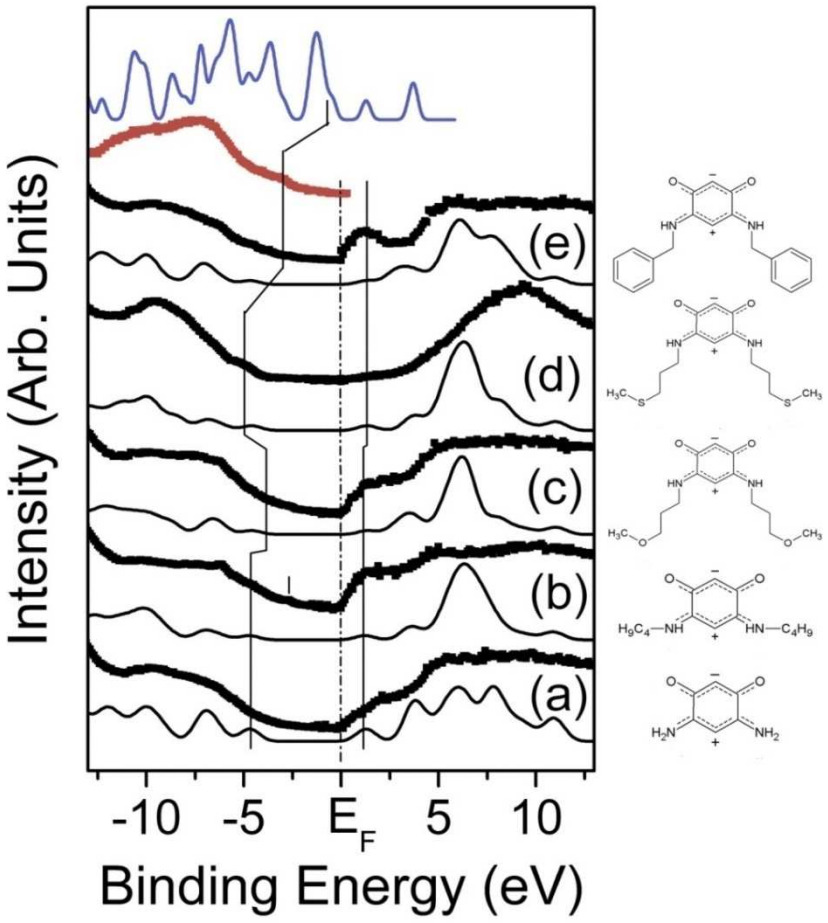

Figure 3.8 The combined photoemission and inverse photoemission spectra (thick lines) of p-benzoquinonemonoimine zwitterionic compounds ($C_6H_2(\cdots NHR)_2(\cdots O)_2$), where R is (a) H, (b) *n*-C_4H_9, (c) C_3H_6-S-CH_3, (d) C_3H_6-O-CH_3 or (e) CH_2-C_6H_5, on gold. The film thickness is in the range 0.5 - 1 nm. Model calculations of the single molecule density of states, using a semi-empirical approach PM3 uncorrected for matrix elements and final state effects are shown for comparison as a thin line for each species. The right side of the figure shows the schematic structure of each molecule. For the benzyl substituted zwitterion (zwitterion **5**), angle-resolved photoemission taken at 40 eV (as opposed to helium I radiation for the other molecules) is shown. Density functional calculations that include band structure effects are shown for this benzyl substituted zwitterion **5** (blue).

Experimental spectra were compared with the simplest single molecule calculated density of states (as in a gas phase experiment), based on simplistic single molecule semiempirical method NDO-PM3 (neglect of differential diatomic overlap, parametric model number 3) model calculations based on Hartree-Fock formalism. Geometry optimization of each of the *p*-benzoquinonemonoimine zwitterion systems was performed by obtaining the lowest restricted Hartree-Fock energy states. The calculated density of states (DOS) were obtained by applying equal Gaussian envelopes of 1 eV full width half maximum to each molecular orbital to account for the solid state broadening in photoemission and then summing. This model density of states calculations were rigidly shifted in energy, largely to account for the influence of work function on the orbital energies and no correction was made for molecular interactions and final state effects. We estimate that the HOMO-LUMO gap for the *p*-benzoquinonemonoimine compounds should retain a value of ca. 5.7 to 5.9 eV, being robust and stable with little variation for a wide variation of pendent groups, as both the HOMO and LUMO are dominated by molecular orbitals localized on the *p*-benzoquinonemonoimine zwitterion core. For the functionalized zwitterions **3** and **4** the observed HOMO-LUMO gaps from the combined photoemission and inverse photoemission slightly differs from the calculated ones. For the zwitterion **3**, we expect a HOMO-LUMO gap of 5.7 eV and observe gap of 5 eV or less, whereas the zwitterion **4** exhibits a larger gap of 6.3 eV, even larger than the calculated value of 5.9 eV.

For the benzyl substituted zwitterion **5**, the angle-resolved photoemission spectrum taken at 40 eV (using synchrotron radiation, as opposed to helium I radiation used for the other molecules) has been added (red curve in figure 3.8) to illustrate that for this zwitterion

compound, the single molecule calculation fails to provide a good approximation of the HOMO-LUMO gap (red).

The key experimental finding of photoemission and inverse photoemission data (Figures 3.7 and 3.8) is the observation that the position of the Fermi level energy of the Au substrate (used as zero reference energy states for the photoemission and inverse photoemission) is very close to the conduction band edge. This is to say that the placement of the lowest unoccupied molecular orbitals (LUMO) of the adsorbed molecules **1, 2, 3** and **5** is very close to the substrate Fermi level. In the case of zwitterion **4**, the molecular orbital alignment continues to retain the substrate Fermi level in the middle of the gap, as usually expected in organic dielectric thin films without electronic interactions with the substrate. We also systematically observe very limited charging effects in either photoemission or inverse photoemission, and the expected final state effects [29] that should occur with increasing molecule films thickness are surprisingly small. We infer therefore that these molecular films have good charge transfer properties, confirmed by the good band alignment between the LUMO of the molecules and the valence band edge of the metallic substrate (Figure 3.8). We interpret these results as an indication of the Au substrate becoming an electron donor. This is intuitively reasonable if we consider that in the molecular layers, the positively charged side of the molecular core is situated at a short distance to the interface. From a device point-of-view, we conclude that Au is a well-matched electron injector in these films. It also opens the possibility to create an n-type semiconductor material of significant mobility, that is a highly desirable property in the field of molecular electronics.

Remarkable properties are specifically found for molecule **5** (*p*-benzoquinonemonoimine zwitterion with benzyl pendant groups), which forms a molecular film that exhibits a density of states overlapping the Fermi level of the Au substrate. One can therefore speculate that the molecular films of this zwitterion species on gold are very close to a semi-metal. This was confirmed by the total absence of charging effects, even when cooling down the sample down to 100 K. Here the absence of final state effects in either photoemission or inverse photoemission (i.e. with either holes or electrons), combined with almost a complete absence of photovoltaic charging, indicates that these molecular films are not dielectrics. Occurrence of available states at the Fermi level of Au is likely related to the crystalline nature of these molecular films. This assumption is confirmed by modeling of the density of states beyond single molecule approximation to account for the observed density of states. This is the only zwitterion within the series investigated, where the experimental HOMO-LUMO gap from the combined photoemission and inverse photoemission is far smaller than suggested by the single molecule calculation. While the single molecule calculation for this benzyl substituted zwitterion **5** fails to provide a good approximation of the HOMO-LUMO gap, density functional calculations that include band structure effects have been performed for this zwitterion (blue line in Figure 3.8) and provide a HOMO-LUMO gap that is too small. This is typical for such DFT calculations [30]. The DFT first-principles calculations are performed in the framework of density functional theory as implemented in the DMol^3 code [31]. The PW91 generalized gradient approximation (GGA) was used for the exchange-correlation functional because of the better performance of GGA than the local density approximation (LDA) in many molecular systems. All the electrons were considered

equally, and the double numerical plus polarization (DNP) basis set, which is comparable to the 6-31G** basis set, was used. The convergence tolerance for the self-consistent field is 2.72×10^{-6} eV, and the molecular structures were optimized till the maximum force was below 0.054 eV/Å. We indeed observed that butyl and benzyl pendant groups allow self-organization in the packing of ultra-thin films, resulting in a crystalline structure. We will discuss the relating band mapping experiments of butyl and benzyl substituted zwitterions (zwitterions **2** and **5**) in details later in Chapter 5.

3.6 Conclusion

In this chapter, we have shown that small molecules of the *p*-benzoquinonemonoimine type, with significant intrinsic dipoles, can be adsorbed on conducting surfaces. We fabricated very thin films (less than 2 nm), with high surface coverages (few pin holes) and very good screening of the interface dipoles. Thickness dependent studies showed limited invariance of the electronic spectroscopic features, which can generally be modeled as independent molecular energies. Even if benzyl, butyl and methoxy substituents are not considered, a priori, as strong anchoring groups, their presence on the N-substituent of the zwitterion provide some important features. Firstly, these groups interact with the gold surface and help stabilize the molecule on the surface. In chapter 4, we will show our observation of some participation of the alkyl substituent to surprisingly strong anchoring of butyl substituted zwitterions on gold [30]. It is also known in the literature that aromatic substituents develop some interactions with gold [35]. Secondly, the substituent influence the organization of molecules on the surface. For example, the steric hindrance of the group may lead to increased distances between adjacent molecules, or

well-organized structures can be obtained byπ-stacking [36]. We found that crystalline ordering of the *p*-benzoquinonemonoimine molecules was possible, with the related □-stacking promoting conductivity in the thin films that was mostly evidenced by the occurrence of molecular density of states at the substrate Fermi level and significant intrinsic conductivity of this type of molecules. We will discuss conductance property of *p*-benzoquinonemonoimine molecules in detail in chapter 5. The interface molecular films can therefore play an important role for organic electronics devices, creating ideally a highly conductive interface with metallic electrodes, promoting efficient carrier injection in an organic film.

References

[1] S. Braun, W. R. Salaneck, M. Fahlman, Adv. Mater. 21, 1450–1472 (2009).

[2] S. Karthäuser, J. Phys. Cond. Matter 23, 013001, (2011).

[3] Y. Yuan, T. J. Reece, P. Sharma, S. Poddar, S. Ducharme, A. Gruverman, Y. Yang, J. Huang, Nature Materials, 13 FEBRUARY 2011 | DOI: 10.1038/NMAT2951.

[4] H. Ma, H.-L. Yip, F. Huang, A. K.-Y. Jen, Adv. Funct. Mater. 20, 1371–1388, (2010).

[5] I. G. Hill, A. Rajagopal, A. Kahn, Y. Hu, Appl. Phys. Lett. 73, 662-664, (1998).

[6] H. Ishii, K. Sugiyama, E. Ito, K. Seki, Adv. Mater. 11, 605-625, (1999).

[7] X. Y. Zhu, Surf. Sci. Rept. 56, 1-83, (2004).

[8] N. Koch, N. Elschner, J. Schwartz, A. Kahn, Appl. Phys. Lett. 82, 2281-2883, (2003).

[9] S. Kera, Y, Yabuuchi, H. Yamane, H. Setoyama, K. K. Okudaira, A. Kahn, N. Ueno, Phys. Rev. B, 70, 085304, (2004).

[10] P.A. Dowben, L.G. Rosa, C.C. Ilie, J. Xiao, J. Electron Spectroscopy and Related Phenomena, 174, 10–21, (2009).

[11] V.S. L'vov, R. Naaman, V. Tiberkevich, Z. Vager, Chem. Phys. Lett., 381, 650-653, (2003).

[12] D. Cahen, R. Naaman, Z. Vager, Adv. Funct. Mater., 15, 1571-1578, (2005).

[13] S. Balaz, A. N. Caruso, N. P. Platt, D. I. Dimov, N. M. Boag, J. I. Brand, Y. B. Losovyj, P. A. Dowben, J. Phys. Chem. B, 111, 7009-7016, (2007).

[14] P. Braunstein, O. Siri, J.-P. Taquet, M.-M. Rohmer, M. Bénard, R. Welter, J. Am. Chem. Soc. 125, 12246–12256, (2003); P. Braunstein, O. Siri, P. Steffanut, M. Winter, Q.-Z. Yang, C. R. Chimie, 9, 1493-1499, (2006); P. Braunstein, O. Siri, J.-p.Taquet, Q.-Z. Yang, Angew. Chem., Int. Ed., 45, 1393-1397, (2006); J.-p. Taquet, O. Siri, P. Braunstein,

R. Welter, Inorg. Chem., 43, 6944-6953, (2004); Q.-Z. Yang, A. Kermagoret, M. Agostinho, O. Siri, P. Braunstein, Organometallics, 25, 5518-5527, (2006).

[15] O. Siri, P. Braunstein, Chem. Commun., 208-209, (2002).

[16] Q.-Z. Yang, O. Siri, P. Braunstein, Chem. Eur. J., 11, 7237-7246, (2005).

[17] Q.-Z. Yang, O. Siri, P. Braunstein, Chem. Commun., 2660-2662, (2005); Q.-Z. Yang, O. Siri, H. Brisset, P. Braunstein, Tetrahedron Lett., 47, 5727-5731, (2006).

[18] X. Lu, K. W. Hipps, X. D. Wang, U. Mazur, J. Am. Chem. Soc., 118, 7197-7202, (1996); J. Xiao, P. A. Dowben, J. Materials Chem., 19, 2172-2178, (2009); P.A. Dowben, J. Xiao, B. Xu, A. Sokolov, B. Doudin, Appl. Surf. Sci., 254, 4238-424, (2008).

[19] A. Sawicka, P. Skurski, J. Simons, Chem. Phys. Lett,. 362, 527-533, (2002); Y. Haas, S. Zilberg, J. Am. Chem. Soc., 126, 8991-8998, (2004).

[20] J. Xiao, Z. Zhang, D. Wu, L. Routaboul, P. Braunstein, B. Doudin, Y. B. Losovyj, O. Kizilkaya, L. G. Rosa, C. N. Borca, A. Gruverman, P. A. Dowben, Phys. Chem. Chem. Phys., 12, 10329 – 10340, (2010).

[21] Kappa CCD Operation Manual; Nonius BV: Delft, The Netherlands, 1997; Sheldrick, G. M. SHELXL97, Program for the Refinement of Crystal Structures; University of Gottingen, Germany, 1997.

[22] C. Vericat, M. E. Vela, G. A. Benitez, J. A. M. Gago, X. Torrelles, R. C. Salvarezza, J. Phys.: Condens. Matter, 18, R867-R900, (2006).

[23] V. Kriegisch, C. Lambert, Topics in Current Chemistry, 258, 257-313, (2005); F. Tao,; L. Bernasek Steven, Chem. Rev., 107, 1408-1453, (2007); J. C. Love, L. A. Estroff, J. K. Kriebel, R. G. Nuzzo, G. M. Whitesides, Chem. Rev., 105, 1103-1170, (2005); R. G. Nuzzo, D. L. Allara, J. Am. Chem. Soc.,105, 4481-4483, (1983); R. G. Nuzzo, B. R.

Zegarski, L. H. Dubois, J. Am. Chem. Soc., 109, 733-40, (1987); C. Vericat, M. E. Vela, G. Benitez, P. Carro, R. C. Salvarezza, Chem. Soc. Rev., 39, 1805-1834, (2010).

[24] T. Weidner, A. Kraemer, C. Bruhn, M. Zharnikov, A. Shaporenko, U. Siemeling, F. Traeger, Dalton Trans., 2767-2777, (2006); M. Mannini, L. Sorace, L. Gorini, F. M. Piras, A. Caneschi, A. Magnani, S. Menichetti, D. Gatteschi, Langmuir, 23, 2389-2397, (2007); J. Noh, Y. Jeong, E. Ito, M. Hara, J. Phys. Chem. C, 111, 2691-2695, (2007); H. Jian, J. M. Tour, J. Org. Chem.,68, 5091-5103, (2003); O. Cavalleri, M. Vignolo, G. Strano, C. Natale, R. Rolandi, S. Thea, M. Prato, G. Gonella, M. Canepa, A. Gliozzi, Bioelectrochemistry, 63, 3-7, (2004); H. L. Tierney, A. E. Baber, E. C. H. Sykes, A. Akimov, A. B. Kolomeisky, J. Phys. Chem. C, 113, 10913-10920, (2009); A. E. Baber, H. L. Tierney, E. C. H. Sykes, ACS Nano 2, 2385-2391, (2008); E. Menozzi, R. Pinalli, E. A. Speets, B. J. Ravoo, E. Dalcanale, D. N. Reinhoudt, Chem. Eur. J.,10, 2199-2206, (2004); S. Zhang, L. Echegoyen, Tetrahedron, 62, 1947-1954, (2006); M. Mannini, D. Rovai, L. Sorace, A. Perl, B. J. Ravoo, D. N. Reinhoudt, A. Caneschi, Inorg. Chim. Acta 361, 3525-3528, (2008).

[25] A. D. Jewell, H. L. Tierney, A. E. Baber, E. V. Iski, M. M. Laha, E. C. H. Sykes, J. Phys.: Condens. Matter, 22, 264006/1-264006/11, (2010).

[26] D. O. Bellisario, A. D. Jewell, H. L. Tierney, A. E. Baber, E. C. H. Sykes, J. Phys. Chem. C, 114, 14583-14589, (2010).

[27] H. L. Tierney, A. D. Jewell, A. E. Baber, E. V. Iski, E. C. H. Sykes, Langmuir, 26, 15350-15355, (2010).

[28] M. E. Zoloff Michoff, P. Velez, E. P. M. Leiva, J. Phys. Chem. C 113, 3850-3854, (2009); F. Iori, S. Corni, R. Di Felice, J. Phys. Chem. C 112, 13540-13545, (2008); P. F. Cafe, A. G. Larsen, W. Yang, A. Bilic, I. M. Blake, M. J. Crossley, J. Zhang, H.

Wackerbarth, J. Ulstrup, J. R. Reimers, J. Phys. Chem. C 111, 17285-17296, (2007); J. Gong, T. Yan, C. B. Mullins, Chem. Commun. 761-763, (2009); A. Sivanesan, S. A. John, Langmuir 24, 2186-2190, (2008); M. Barber, J. A. Conner, M. F. Guest, I. H. Hillier, M. Schwarz, M. Stacy, J. Chem. Phys, Soc. Faraday Trans. II 69, 551, (1973); B. J. Lindberg, J. Hedman, Chem. Script. 7, 155, (1975); T. Yoshida, S. Sawada, Bull. Chem. Soc. Jpn. 47, 50, (1974); K. B. Yatsimirskii, V. V. Nemoshalenko, Y. P. Anazarenko, V. G. Aleshin, Y. I. Bratushko, E. P. Moiseenko, Chem. Phys. Lett. 52, 481, (1977).

[29] J. E. Ortega, F. J. Himpsel, D. Li, P. A. Dowben, Solid State Commun. 91, 807, (1994); P. A. Dowben, Surface Science Repts. 40, 151, (2000); N. Sato, K. Seki, H. J. Inokuchi, J. Chem. Soc. Faraday Trans. II 77, 1621, (1981); H. Fukagawa, H. Yamane, T. Kataoka, S. Kera, M. Nakamura, K. Kudo, N. Ueno, Phys. Rev. B 73, 245310, (2006); P. G. Schroeder, C. B. France, J. B. Park, B. A. Parkinson, J. Phys. Chem. B 107, 2253-2261, (2003).

[30] S. Kümmel, L. Kronik, Rev. Mod. Phys. 80, 3, (2009); F. Bechstedt, F. Fuchs, G. Kresse, Phys. Stat. Solidi B 246, 1877, (2009); T. Stein, L. Kronik, R. Baer, J. Am. Chem. Soc. 131, 2818, (2009); M.-S. Liao, Y. Lu, S. Scheiner, J. Comp. Chem. 24, 623, (2003); I. N. Yakovkin, P. A. Dowben, Surface Review and Lett., 14, 481, (2007).

[31] B. Delley, J. Chem. Phys. 92, 508, (1990); B. Delley, J. Chem. Phys.113, 7756, (2000).

[32] P.A. Dowben, B. Xu, J. Choi, E. Morikawa, in: Handbook of Thin Film Materials, 2, 61-113, (2002); E.W. Plummer, W. Eberhardt, Adv. Chem. Phys. 49, 533, (1982); H.-P. Steinrück, Vacuum 45, 715, (1994).

[33] N.T. Kemp, H. Majjad, P. Lunca Popa, G. Dalmas, B. Doudin, ECS Transactions, 16, 3-10, (2009).

[34] H.B. Akkerman, B. de Boer, J. Phys.: Condens. Matter 20, 013001, (2008).

[35] A. J. Britton, A. Rienzo, J. N. O'Shea, K. Schulte, J. Chem. Phys., 133, 094705/1-094705/7, (2010); W.-K. Chen, M.-J. Cao, S.-H. Liu, C.-H. Lu, Y. Xu, J.-Q. Li, Chem. Phys. Lett., 417, 414-418, (2006); P. Gao, M. J. Weaver, J. Phys. Chem., 89, 5040-5046, (1985); C. Schuster, U. Schwingenschloegl, Chem. Phys. Lett., 468, 75-78, (2009); D. Syomin, J. Kim, B. E. Koel, G. B. Ellison, J. Phys. Chem. B, 105, 8387-8394, (2001).

[36] J. Brede, M. Linares, S. Kuck, J. Schwoebel, A. Scarfato, S.-H. Chang, G. Hoffmann, R. Wiesendanger, R. Lensen, P. H. J. Kouwer, J. Hoogboom, A. E. Rowan, M. Broering, M. Funk, S. Stafstroem, F. Zerbetto, R. Lazzaroni, Nanotechnology, 20, 275602/1-275602/10, (2009); P. Guaino, D. Carty, G. Hughes, O. McDonald, A. A. Cafolla, Appl. Phys. Lett., 85, 2777-2779, (2004); B. Han, Z. Li, T. Wandlowski, A. Blaszczyk, M. Mayor, J. Phys. Chem. C, 111, 13855-13863, (2007); T. Huang, Z. Hu, A. Zhao, H. Wang, B. Wang, J. Yang, J. G. Hou, J. Am. Chem. Soc., 129, 3857-3862, (2007); P. Jiang, K. Deng, D. Fichou, S.-S. Xie, A. Nion, C. Wang, Langmuir, 25, 5012-5017, (2009); V. A. Langlais, Y. Gauthier, H. Belkhir, O. Maresca, Phys. Rev. B 72, 085444/1-085444/7, (2005); F. Lux, G. Lemercier, C. Andraud, G. Schull, F. Charra, Langmuir 22, 10874-10876, (2006); L. S. Pinheiro, M. L. A. Temperini, Surf. Sci., 464, 176-182, (2000); N. Sakai, A. L. Sisson, T. Buergi, S. Matile, J. Am. Chem. Soc., 129, 15758-15759, (2007); A. L. Sisson, N. Sakai, N. Banerji, A. Fuerstenberg, E. Vauthey, S. Matile, Angew. Chem., Int. Ed., 47, 3727-3729, (2008); G. S. Tulevski, M. L. Bushey, J. L. Kosky, S. J. T. Ruter, C. Nuckolls, Angew. Chem., Int. Ed., 43, 1836-1839, (2004).

Chapter 4 The Interface Bonding and Orientation of a Butyl Pendant Groups Zwitterion

4.1 Introduction

There is considerable interest in the study of molecular adsorbate systems with well-defined intrinsic electrostatic properties [1–12]. Two-dimensional arrangements of large adsorbates (compared to, say, CO) with large electric dipoles can exhibit strong intermolecular interactions [2, 4, 12–15]. One key issue is whether these cooperative effects within an adsorbate layer of larger dipolar molecules resemble those observed and well characterized for small adsorbate molecules like CO [8], or if there is a need to revise our views of intermolecular adsorbate interactions (based on our models of CO) when investigating larger organic adsorbates. Furthermore, since the interplay between the interface dipole interactions and the interface chemistry is not always readily distinguishable [1, 2, 6, 7], there is much value in the investigation of adsorbates with extremely large dipoles. In addition, a dominant electrostatic dipole, in a relatively high symmetry molecule, provides new routes to investigate interface interactions and can result in enhanced selectivity of specific spectroscopically dipole active transitions, therefore assisting in the interpretation of vibronic fine structure in photoemission and related spectroscopies.

Instrinsic molecular dipoles can lead to preferential adsorption on electrostatically biased substrates [1–7]. While planar aromatic species, alkane thiol-functionalized polyphenyls (at low coverages), or macrocyclic metal centered organometallics tend to lie flat, this orientation is not always adopted at an interface [6, 7]. When external electrostatic

fields are present, the interface chemical bonding, affinity energies, the molecule–molecule interactions, as well as the electrostatic dipolar molecule–substrate interactions all contribute to the total energy of the adsorbate-substrate system. Changing the balance between chemical bonding and the electrostatic dipolar interactions can lead to substantial changes in the molecular orientation [1–4, 6, 7] as well as molecular conformation [5]. In general, if electrostatics alone are considered, an adsorbed molecule with a large intrinsic dipole should adopt an orientation on a conducting substrate that places the dipole along the surface normal, as a result of the formation of an image dipole in the substrate [3]. Such arguments do not apply to nonconducting substrate [3]. Adsorbate dipole interactions with solid surfaces are, unfortunately, often complicated by the influence of the substrate (including band structure effects) [1, 16, 17] and strong perturbations due to the metal substrate surface charges that induce large interface dipoles [18]. Ferroelectric materials provide a unique opportunity to investigate dipole interactions with adsorbates [6]. This makes it possible to undertake experiments that may provide insights into the role of the static dipole on the vibrational modes of the adsorbate molecule. In prior studies where a comparison between molecular adsorption on a conducting substrate (like gold) and a ferroelectric substrate was possible, molecules like metal phthalocyanines [7] and dodecane [19] with small intrinsic electric dipoles appeared to adopt bonding orientations dominated by the interface chemistry, and were only slightly influenced by the dipoles of the ferroelectric substrate. The interactions of more polar molecules with a ferroelectric substrate were, however, seen to be more significant, and dipole orientation may matter [6, 7, 19].

In Chapter 3, we introduced a family of small quinonoid molecules. Here we expand our studies on just one zwitterions, as shown in figure 4.1, in this case (6Z)-4-(butylamino)-6-(butyliminio)-3-oxocyclohexa-1,4-dien-1-olate. This zwitterion is later shown to be ideal molecular systems for the study of adsorbate dipole interactions.

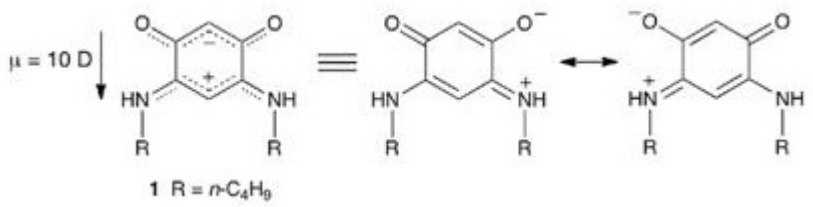

Figure 4.1 The molecule of study: (6Z)-4-(butylamino)-6-(butyliminio)-3-oxocyclohexa-1,4-dien-1-olate $C_6H_2(\underline{\cdots}NHR)_2(\underline{\cdots}O)_2$, where R = *n*-$C_4H_9$, indicating the resonance structures involving the cationic nitrogen iminium and enamine functional groups and the anionic oxygen enolate and ketonic groups, respectively.

The electric dipole of this zwitterion, when adsorbed on a metal surface (and most substrates) should not be switchable, which makes this molecule more like an electret if they adopt a preferential orientation upon adsorption. Each dipole associated with the zwitterionic ‘‘core’’ should affect the intermolecular interaction and could ultimately influence the molecular packing on metal surfaces, just like in the case of CO adsorption on metal surfaces [8, 16, 27], but this may be balanced by the strength and nature of the interface bonds. To assess the role of the dipole interactions at a surface, in this chapter, we mainly discuss the deposition of a zwitterion compound of figure 4.1 (where R=n-C_4H_9 for solubility reasons) on conducting (gold) substrate, and leave the discussion of selective

deposition of this zwitterion molecule onto specific ferroelectric domains of periodically poled lithium niobate substrate to Chapter 7.

. In this chapter, we will show that for gold substrate, the zwitterion adopts a preferential orientation with the plane of its ‘‘C6 core’’ along the surface normal. This simplified geometry of strong dipole alignment provides a symmetry simplification allowing better identification of the vibrational modes responsible for Frank-Condon scattering revealed in the fine spectroscopic signature in the photoemission spectrum.

4.2 Modeling Procedure

As a guide to the interpretation of the experimental data, we have performed simple model calculations of electronic structure of the p-benzoquinonemonoimine zwitterion. The calculated electronic structure of the zwitterion of figure 4.1 is based on simplistic single molecule semi-empirical method NDO-PM3 (neglect of differential diatomic overlap, parametric model number 3) model calculations. Geometry optimization of this zwitterion system was performed by obtaining the lowest restricted Hartree–Fock energy states. Our model PM3 calculations are a simplistic semi-empirical single molecule ground state calculation based on the quinoid molecule alone and do not include any substrate corrections, nor include any additional atoms.

The model molecular orbital intensities obtained from these calculations have not been corrected for matrix element effects, yet the comparisons with experiment are still often successful [6, 7, 11, 29, 31], as shown here. For both figure 4.2 and 4.3, the calculated density of states (DOS) is only an approximation based on the molecular orbital placement of the free molecule and was obtained by applying equal Gaussian envelopes of 1 eV full

width half maximum to each molecular orbital (or both 1 and 2 eV full width half maximum to each molecular orbital, in the case of figure 4.3) to account for the solid state broadening in photoemission and then summing. The calculated density of states have been rigidly shifted in energy, largely to account for the influence of work function on the orbital energies without corrections for molecular interactions and final state effects.

Better model calculational methods are certainly possible and should be explored, but outside the scope of this chapter. Our preference for the simplistic semiempirical calculations used here in calculating the electronic structure, as opposed to using density functional theory, as is used to model the vibrational modes, stems from problems associated with density functional theory (DFT) when it comes to electronic structure. DFT is notorious for underestimating the band gap in some cases by a factor 2 or more [43] (particularly for some of the larger molecular systems, or systems with considerable charge transfer). DFT orbital energies generally require some rescaling for comparison with experiment [44], particularly for final state spectroscopies like photoemission and inverse photoemission.

4.3 The Bonding and Orientation of a Zwitterion, with Pendant Alkyl chains, Adsorbed on Gold

An upright configuration of the p-benzoquinonemonoimine zwitterion with the dipole along the surface normal would allow for a dense packing along one direction (p-benzoquinonemonoimine zwitterion plane to plane packing). Support for a dense packing between adjacent molecules may be inferred [8, 32, 46] from the intermolecular dispersion of about 400 meV, obtained by emission angle dependent photoemission indicating an

intermolecular spacing of about 3.2 $\pm$0.2 Å , with two molecules per period in the direction perpendicular to the zwitterion core plane but parallel to the plane of the Au surface [47]. This is consistent with the molecule core (Figure 4.1) being aligned upright and with the plane of the molecular core lying close to the surface normal as discussed below. The p-benzoquinonemonoimine band dispersion, along one in-plane direction, is close to the value of 350 meV observed for thin crystalline films of sexiphenyl grown on Cu(110), with an interplanar spacing of 3.8 Å [46].

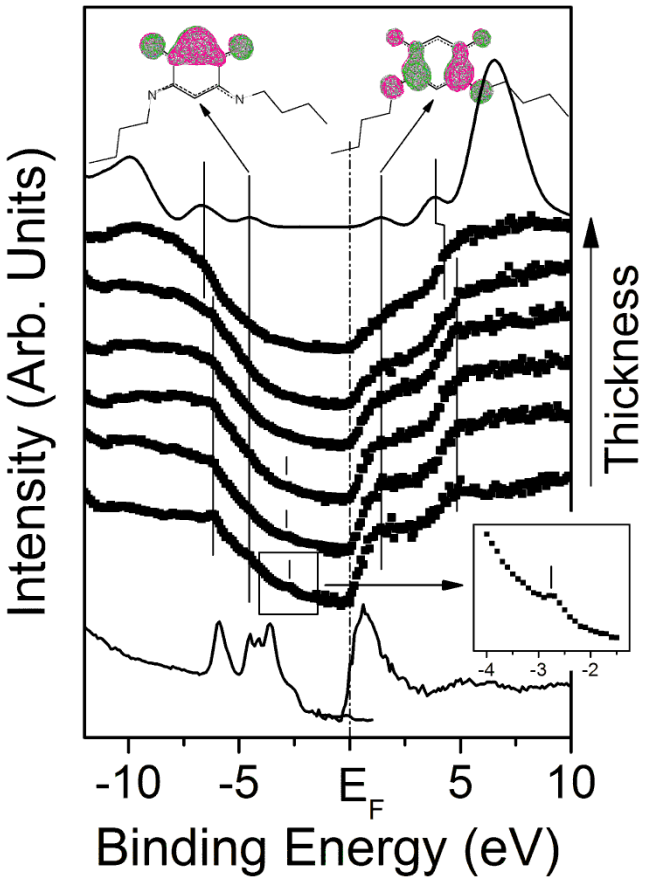

Figure 4.2 The coverage dependent photoemission (left) and inverse photoemission spectra (right) (thick lines) of the p-benzoquinonemonoimine zwitterion, of figure 4.1, adsorbed on Au at room temperature.The bottom thin line is clean Au substrate spectrum used as a reference. The top thin line is the model calculation of the single molecule density of states, using a semi-empirical approach PM3 uncorrected for matrix elements and final state effects. The HOMO and LUMO are indicated by vertical thin lines and the pertinent molecular orbitals are schematically depicted as insets on the top of the figure. The molecular orbital shifts, as a function of changing molecular coverage, are also indicated by vertical lines. The inset on the right is an expanded section of the photoemission spectra highlighting the metal induced gap state.

The coverage dependent photoemission and inverse photoemission spectra of the zwitterion of figure 4.1, shown in figure 4.2, indicates that even the thinnest films obscure the Au substrate signal, and are therefore without pinholes. This is consistent with our atomic force microscope images that show that the zwitterion films on gold tend to be uniform, even for films that are multiple molecular monolayers thick [47]. The photoemission and inverse photoemission spectra of the adsorbed zwitterion on gold indicate a highest occupied molecular orbital (HOMO) to lowest unoccupied molecular orbital (LUMO) gap of 5.8 to 6.0 eV which has been estimated from the vertical (peak) energies, with corrections for the measured instrumental line widths. These experimental values are consistent with our expectations of 5.8 eV (indicated at the top of figure 4.2) based on simplistic single molecule semiempirical methods (NDO-PM3). In spite of experimental and theoretical approximations in estimating the gap, the agreement is satisfactory.

The combined photoemission and inverse photoemission spectra, shown in figure 4.2, also provide indications of interactions between the p-benzoquinonemonoimine zwitterions and the gold substrate. Interface interactions with the gold substrate, are evident from the changes in the spectra with increasing molecular film thickness. While the experimental HOMO–LUMO gap matches theory, there is evidence of a weak metal-induced gap state (MIGS) within the HOMO–LUMO gap, in the photoemission spectra of the thinner molecular films. This is indicated by a short vertical bar in figure 4.2, and highlighted in the expanded inset to figure 4.2. This state is consistent with gold acting as electron donor and indicates a strong molecular interaction with the substrate and may be attributed to an interfacial molecular orbital formed upon bonding with the gold substrate. Similarly, the

shift in some molecular orbitals upon formation of the molecular multilayer films, as well as the disappearance of the occupied state (MIGS) within the HOMO–LUMO gap for the thicker films is also indicative of strong bonding of this zwitterion to the gold substrate.

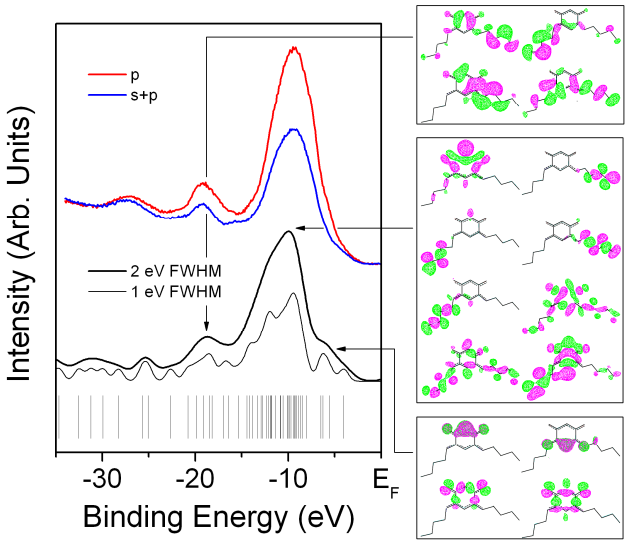

Figure 4.3 Light polarization dependent photoemission spectra of the zwitterion, of figure 4.1, adsorbed on Au at room temperature. The spectra compared are with the **E** of the plane polarized light more along the surface normal (red line) obtained with a light incidence angle of 70^0 and with a component of **E** of the plane polarized light more in the plane of the surface (blue line) obtained with a light incidence angle of 45^0 both taken with a photon energy of 50 eV. For comparison, two model calculations of density of states were performed by applying equal Gaussian envelopes of 1 eV (black thin line) and 2 eV (black thick line) full width half maximum to each molecular orbital. The calculated molecular orbitals are shown on the bottom as vertical bars at the bottom of the Figure. The schematics of the pertinent theoretical molecular orbitals (from the same calculation) of the three major peaks, at binding energies in the vicinity of the HOMO, the -10 eV peak and the -18 eV peak, are indicated and shown on the right side as three inset panels.

These MIGS photoemission features are also strong indications that the smallest coverage corresponds to films thinner than 1 nm. Together with the fact that contributions to the spectra from the gold substrate are absent from the thinnest films data, figure 4.2 provides compelling evidence that this zwitterion molecule can adsorb and form homogeneous films not exceeding a few monolayers.

The light polarization dependent photoemission of figure 4.3 provides further evidence that in a multilayer, the molecules of figure 4.1 adopt a preferential orientation when adsorbed on gold. The molecular orbitals associated with the zwitterion core as well as those of the alkyl chain, which have strong C–H bond weight, exhibit enhanced contributions to the photoemission spectra taken with a light incidence angle that places the **E** vector more along the surface normal. The angle resolved photoemission results of figure 4.3 therefore indicate that the preferential orientation adopted upon adsorption on gold places the zwitterion core plane parallel with the surface normal, while the two butyl pendant groups lie parallel with the surface, likely in opposite directions, as indicated in figure 4.4. Some of the zwitterion core contributions to the photoemission feature at about -8 eV binding energy are expected to be enhanced with the **E** vector (of the incident light) parallel with the surface. Although there are six molecular orbitals of b_1 or b_2 symmetry, there are 8 molecular orbitals of a_1 symmetry, assuming the C_{2v} point group symmetry. Analysis of the light polarization dependent photoemission spectra of figure 4.3, in the context of photoemission selection rules [8, 16, 27], strongly favors placement of the zwitterion core molecular alignment parallel to the surface normal, or an ‘‘upright’’ bonding configuration. Because of the photoemission selection rules, the light polarization dependent photoemission above does not directly distinguish whether this zwitterion largely

bonds to the surface through the oxygen or through the nitrogen groups. Other evidence, however, provided below, establishes that the bonding does occur through the latter functional groups.

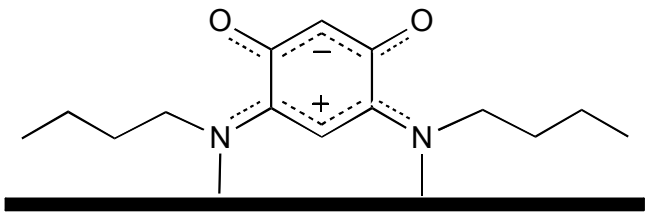

Figure 4.4 A sketch of a possible interaction mode between the zwitterions (6Z)-4-(butylamino)-6-(butyliminio)-3-oxocyclohexa-1, 4-dien-1-olate $C_6H_2(\underline{\cdots}NHR)_2(\underline{\cdots}O)_2$, where R = *n*-$C_4H_9$ and the gold surface, consistent with the data presented here for molecules at the gold interface. See text for details on the possible deprotonation of the N bounded atoms.

The ‘‘upright’’ orientation for this zwitterion, with the molecular plane parallel to the surface normal, is similar to that of pyridine adsorbed on Ir (111) [48] through the nitrogen. However pyridine generally bonds neither ‘‘upright’’ nor ‘‘flat’’ but rather orients the planar molecular axis tilted with respect to the surface normal as in the case of adsorption on Pd(111) [49] and Cu (110) [50].

The X-ray photoemission data (Figure 4.5) implicate bonding of this zwitterion to the gold substrate through the nitrogen functions. Because this generates steric hindrance, there

is some decrease of the core to N asymmetric modes (schematically illustrated in figure 4.6) intensity.

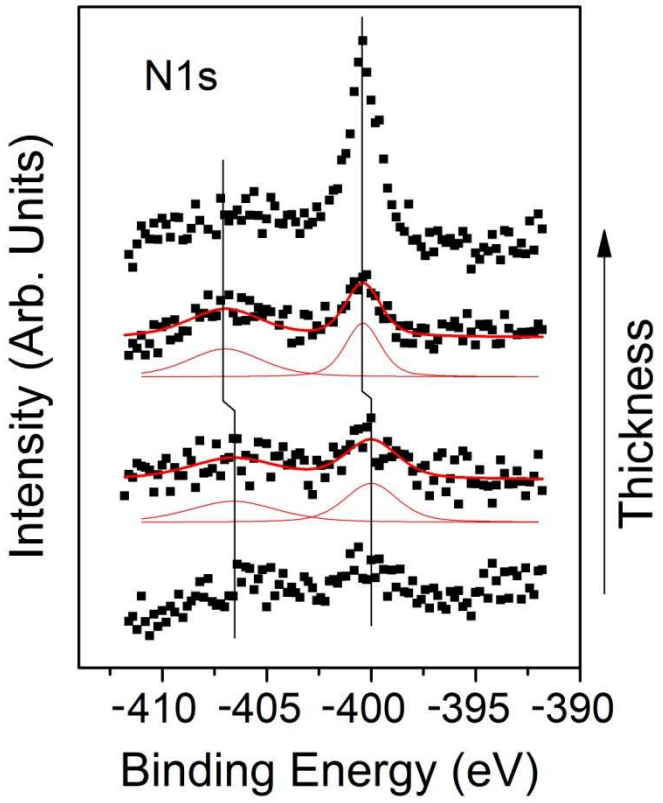

Figure 4.5 X-Ray photoemission spectra for N 1s core level of adsorbed p-benzoquinonemonoimine zwitterion of figure 4.1 and 4.4, for increasing molecular film thickness on Au at room temperature. The main peaks and the shake-off side peaks are indicated by vertical bars (see text).The XPS spectra were taken under low total flux conditions to preserve adsorbate molecular integrity.

The N 1s core level binding energy shifts with changes in zwitterion film thickness on gold also confirm our hypothesis of the p-benzoquinonemonoimine zwitterion bonding to gold through the nitrogen groups. The X-ray photoemission spectra provide some evidence for a shift in the N 1s core level photoemission binding energies with increasing zwitterions molecular coverage, as seen in figure 4.5. The N 1s core level binding energy shift of about 0.5 + 0.2 eV to smaller binding energies, with decreasing molecular coverage, is likely the result of charge donation to the electrophilic nitrogen at gold substrate interface. This is consistent with expectations as is a competition between the molecule–substrate and molecule–molecule interactions [2, 4, 12–15] that would generally favor a dipole reduction due to intermolecular dipole–dipole interactions.

Such zwitterion bonding to gold through the nitrogen atoms is consistent with the observation of an occupied state (MIGS) within the HOMO–LUMO gap of this zwitterion for the thinner molecular films as seen in figure 4.2. If we suppose that the N 1s core level binding energy shift results from increased substrate screening, as seen with molecular systems [51–54], such shifts should continue to occur to increasingly higher binding energies with increasing film thickness and should not be sensitive to the R substituent in the zwitterions. This is not observed with the coverage dependent adsorption of p-benzoquinonemonoimine zwitterions with thioether and alkyl methyl ether pendant (R) groups on gold [47]. A bonding of this p-benzoquinonemonoimine zwitterion to gold, through the nitrogen groups, also supports our contention that the molecular zwitterion core plane is placed largely along the surface normal. The exact nature of the bonding between the nitrogen groups and gold cannot, as yet, be specified more precisely. Interaction

involving the carbon of an imidazolium type bond on gold [55] cannot, a priori, be excluded.

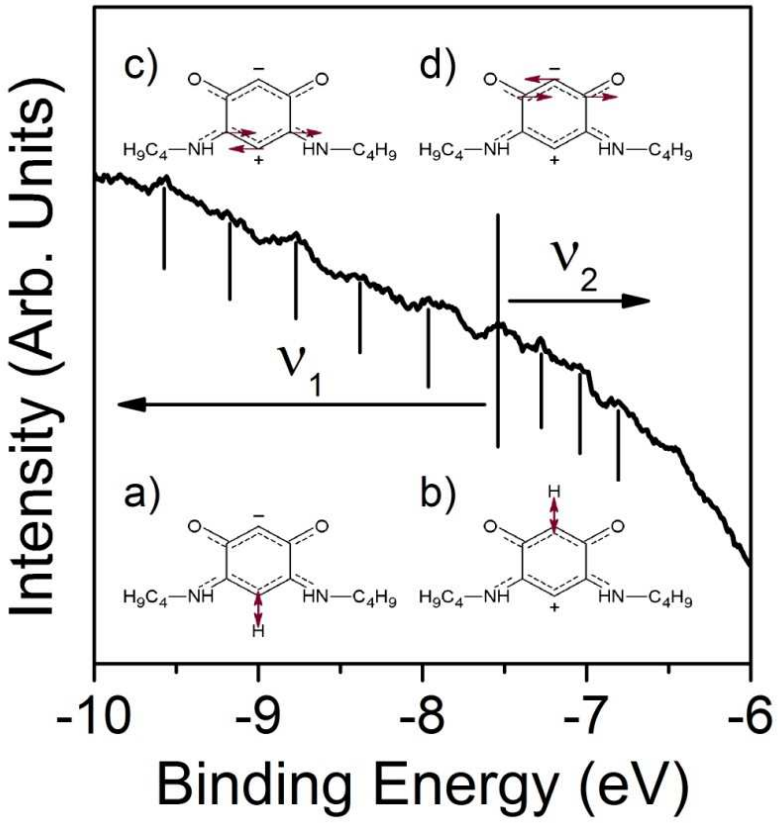

Figure 4.6 High resolution photoemission of the zwitterions (6Z)-4-(butylamino)-6-(butyliminio)-3-oxocyclohexa-1,4-dien-1-olate $C_6H_2(\underline{\cdots}NHR)_2(\underline{\cdots}O)_2$, where R = *n*-$C_4H_9$ absorbed on Au at room temperature. The vibronic fine structure to the high resolution photoemission is seen to have two distinct vibrational contributions. Possible origins of these vibronic contributions to the photoemission spectra are indicated (see text), with energies of (a) 3126 cm^{-1}, (b) 3227 cm^{-1}, (c) 1609 cm^{-1}, and (d) 1678 cm^{-1} assuming the higher point group symmetry of C_{2v} (see text).

The presence of a shake-off side peak, accompanying the N 1s main peak, as seen in figure 4.5, at 6 to 7 eV larger binding energies is consistent with the strong dipole excitations possible for the zwitterion of figure 4.1 and 4.4, leaving a two hole bound final state, for which the expected energy of a shake-off would be at 6 to 7 eV, or about the value of the HOMO–LUMO gap. The other possibility for the higher binding energy satellite N 1s feature is an unscreened final state at higher binding energy, as has been seen at 5 to 6 eV larger binding energy for molecular nitrogen (N_2) adsorbed on a variety of metal substrates [56]. The energy difference between the screened and unscreened final states, in the case of adsorbed molecular nitrogen (N_2), is apparent in the model of Schönhammer and Gunnarsson [57]. The latter explanation is less likely as the N 1s satellite actually decreases in intensity with increasing coverage, thus is unlikely to be the unscreened final state and more likely to be the screened two hole bound final state.

The binding energy of the main (fully screened) N 1s core level at -400.0 $\pm$0.2 eV, increasing to -400.5 $\pm$0.2 eV (with increasing film thickness), is somewhat larger than NH amide binding energies (-399.7 eV) of polyamide-6,6 films on Cu and Pt [58], and much larger than the binding energies typically observed for pyridine (-399.3 eV) [59] or aniline ($PhNH_2$) (-399.4 eV) [60], although slightly less than the N 1s binding energies observed for $EtCHNH_2COOH$ (-400.6 eV) [61], and CH_3CHNH_2COOH (-401.0 eV) [62].

Our results for the interactions of the p-benzoquinonemonoimine zwitterion, $C_6H_2(\underline{\cdots}NHR)_2(\underline{\cdots}O)_2$, where R = *n*-$C_4H_9$, to gold through the nitrogen are consistent with the literature data reporting anchoring of molecules by a gold–nitrogen interaction [8, 48, 51, 63–66]. The nature of the Au–N interaction is, however, not yet fully elucidated. While Bilic et al. proposed that the anchoring of ammonia [67] or pyridine [68] on gold is mainly

a naturally dispersive bond, a significant contribution to bonding may arise from image charge polarization. In a more conventional manner, Ford and coworkers [69] considered the Au–N interaction to have a more covalent contribution (a donation/back-donation mechanism) with some charge-transfer character. Similar to the situation observed here for this p-benzoquinonemonoimine zwitterion, Ford and coworkers [69] observed that all the alkylamines studied adopted orientations perpendicular or near-perpendicular to the surface with the nitrogen–substituent bonds arranged symmetrically with respect to the surface, as was seen for pyridine adsorbed on Ir(111) [48]. In the case of arylamines [69], the aromatic ring was found to lie flat on the surface, as does, surprisingly, pyridine adsorbed on Pd(110) [70].

We can therefore consider the multiple experimental indications as consistent with the picture that the molecules interact strongly with the gold substrate through the two nitrogen functional groups, keeping the zwitterionic properties of the adsorbate. Owing to the significant interaction energy, the first layer of molecules on gold may be constituted by deprotonated zwitterion compounds, as schematically indicated in figure 4.4. Subsequent molecular layers do not appear to deprotonate, and it may be that only a fraction of the molecules at the gold interface in fact deprotonate. Deprotonation of amines on gold surfaces has been reported by several authors [71–73, 66]. Braunstein's group also found that some transition metal precursors are able to deprotonate the N–H group of these zwitterions at room temperature [74–76].

4.4 Franck–Condon Scattering from a P-benzoquinonemonoimine Zwitterion on Gold

Another approach to exploring the molecular configuration and orientation, in the presence of a local electric dipole field is to study the vibronic fine structure in photoemission. The existence of contributions of the vibrational modes to the photoemission spectra of the molecular orbitals of gas phase [77–87] and adsorbed [85–91] molecules has long been recognized. For molecules in the gas phase larger than CO and small alkanes, the vibronic fine structure in the photoemission or photoionization spectra can be quite complex [79–91]. Based on the time scale of the vibrations, the photoemission electronic transition time scale is negligible, so the nuclei do not change their positions or momenta during the electronic (photoemission) transition, but only after it has occurred. Furthermore, the vibrational modes that couple to the photoemission process must share the same symmetry as the electronic transition. Thus with a preferential orientation that favors a high point group symmetry, only select modes will likely be observed in the photoemission fine structure. If the molecule has a large dipole, the strong dipole vibrational modes of specific symmetry will couple better in the photoemission final state, although the precise matrix elements are not readily ascertained from first principles.

These considerations can be expressed more precisely by considering the photoemission process as an electronic dipole transition from the initial vibrational state ν of the ground state E_0, to some vibrational state $\nu'$of an excited electronic state E_1. Given that the overall wave-functions are the product of the individual electronic, vibrational and spin wave-functions, the separation of the electronic and vibrational wave-functions is a fundamental assumption of the Born–Oppenheimer approximation and core to the Franck–

Condon principle. The probability amplitude in terms of separate electronic, vibrational and spin contributions is

$$P = \langle \psi_e' \psi_v' \psi_s' | \mu | \psi_e' \psi_v' \psi_s' \rangle \qquad 4.1$$

$$= \langle \psi_e' \psi_v' \psi_s' | (\mu_e + \mu_N) | \psi_e \psi_v \psi_s \rangle$$

$$= \langle \psi_e' \psi_v' \psi_s' | \mu_e | \psi_e \psi_v \psi_s \rangle + \langle \psi_e' \psi_v' \psi_s' | \mu_N | \psi_e \psi_v \psi_s \rangle$$

$$= \underbrace{\langle \psi_v' | \psi_v \rangle}_{\text{Franck-Condon Factor}} \quad \underbrace{\langle \psi_e' | \mu_e | \psi_e \rangle}_{\text{Orbital selection rules}} \quad \underbrace{\langle \psi_s' | \psi_s \rangle}_{\text{Spin selection rule}}$$

$$+ \langle \psi_e' | \psi_e \rangle \langle \psi_v' | \mu_N | \psi_v \rangle \langle \psi_s' | \psi_s \rangle$$

The first integral is the vibrational overlap integral, also called the Franck–Condon factor. The remaining two integrals contributing to the probability amplitude determine the molecular orbital photoemission selection rules and the spin selection rules. These selection rules do appear to apply and have recently been demonstrated not only in gas phase photoemission of molecules larger than CO and small alkanes [80–87], but also for molecular thin films [90–91]. Generally though, the Franck–Condon principle is not strictly obeyed in these molecular systems, as noted elsewhere [87], and photo-hole perturbations of the vibronic fine structure in high resolution photoemission are common and very difficult to model accurately.

Nonetheless, the resulting Frank-Condon vibronic fine structure can be observed in high resolution photoemission [77–88, 90, 91], and has been observed for the p-benzoquinonemonoimine zwitterion adsorbed on gold, as seen in figure 4.6. Two vibrational modes are evident in the high resolution photoemission spectra, as indicated in figure 4.6, with characteristic vibrational energies (denoted by the vertical bars in figure 4.6)

in the energy regions of ν_1= 0.41 $\pm$0.01 eV (3291$\pm$90 cm^{-1}) and ν_2= 0.25$\pm$0.01 eV (2016$\pm$110 cm^{-1}).

As just noted, the vibrational modes must share the same symmetry and couple to the ionized final state of the molecule, in order to provide the observed photoemission vibronic fine structure, seen in figure 4.6. Because the vibronic fine structure occurs in the region of-7 to-10 eV binding energies, where the molecular orbitals are strongly enhanced with incident light that places **E** more along the surface normal (Figure 4.3), the associated vibrational modes are most likely to be of a1 irreducible representation symmetry, particularly at binding energies closer to -9 to -10 eV, assuming a C_{2v} point group symmetry for this adsorbed p-benzoquinonemonoimine zwitterion. Given that this zwitterion dipole is placed largely along the surface normal (as discussed in the prior section), this means that the a_{1u} core stretching modes (schematic a and b in figure 4.6), at 3126 cm^{-1} and 3227 cm^{-1} are the likely origin of the vibronic fine structure at ν_1= 0.41$\pm$0.01 eV (or 3291$\pm$90 cm^{-1}), observed in the photoemission spectra. These vibrational modes are observed to be at lower energies in the electronic ground state.

At smaller binding energies of -7 eV or less, vibronic coupling to b_1 and b_2 electronic states is more likely (Figure 4.4). These vibronic contributions to the photoemission fine structure of ν_2= 0.25 $\pm$0.01 eV (i.e. 2016$\pm$110 cm^{-1}) occur at much higher vibrational energies than the b_1 dipole active modes of the electronic ground state. The largely b_1 symmetry vibrational core to NH asymmetric modes (schematic c of figure 4.6), at 1609 cm^{-1} and the asymmetric oxygen to core mode (schematic d of figure 4.6) at 1678 cm^{-1} may well be the dominant contributions to the vibronic fine structure in the high resolution photoemission at binding energies of -7 eV or less (Figure 4.6).

Because the vibronic structure occurs in the photoemission final state, there could be a ‘‘stiffening’’ of the associated ground states vibrational modes by as much as 300 to 400 cm^{-1}, as has been observed in prior measurements of the vibronic photoemission fine structure [87,90,91].

The vibrational modes that dominate the photoemission fine structure are symmetry restricted by molecular orientation. The observation of different vibronic fine structures at different photoemission binding energies is consistent with our placement of the p-benzoquinonemonoimine zwitterion core dipole (of figure 4.1 and 4.4) along the surface normal. Can the selective excitation of specific vibrational modes in the photoemission final state be recreated in the electronic ground state? Recent density functional theory calculations [92] suggest that the influence of the substrate on the hole-vibration coupling for molecular systems like pentacene should be larger than the perturbations caused by intermolecular interactions. The test is the adsorption of the p-benzoquinonemonoimine zwitterion in a similar orientation in a strong static electric field and using a similar infrared absorption selection rule geometry to see if the dipole active vibrational spectra are dominated by these two features in the region of 2000 to 3300 cm^{-1}.

4.5 Conclusion

Adsorption studies have shown that strong interactions develop between the zwitterionic p-benzoquinonemonoimine compound ($C_6H_2(\cdots NHR)_2(\cdots O)_2$, where R = *n*-$C_4H_9$) (Figure 4.1) and a conducting substrate (gold). The core of the zwitterion tends to align preferentially along the surface normal, likely because of the image charge and/or the substrate dipole. In the case of adsorption on gold, the zwitterion bonds to the gold through the nitrogen groups, with the alkyl chains parallel to the surface. We observe a significant bonding strength to gold. This suggests, but does not prove, that the N–Au interaction has a significant covalent character, implying loss of the N–H hydrogen atom of the precursor molecule. We also found remarkable molecular coverage properties, with experimental evidence that very thin films (below 1 nm) fully cover the Au substrates.

The static dipole field, in the mean field in the photoemission final state (as seen in the vibrational fine structure contributions to the valence band photoemission), perturbs the adsorbate vibrational states. Strong local dipole fields created owing to the photo-hole in the photoemission final state [93], can lead to vibrational mode stiffening of the dipole active modes associated with the nitrogen groups of the zwitterion. This is reflected in the change of energy of the asymmetric vibrational mode linking the core of the zwitterion molecule to the nitrogen, increasing from 1500 $\pm$50 cm^{-1} (Au substrate) to 2016$\pm$110 cm^{-1} (photoemisson final state). This expected perturbation of the adsorbate vibrational states can finally be observed because these adsorbed zwitterions molecules adopt a preferential orientation leading to very restrictive selection rules, simplifying the otherwise complex vibrational mode spectra.

The selective deposition of molecules $C_6H_2(\underline{\cdots}NHR)_2(\underline{\cdots}O)_2$, where R = *n*-$C_4H_9$ onto specific ferroelectric domains has also been demonstrated for a spatially periodically poled ferroelectric surface (Periodically Poled Lithium Niobate substrate), which we will discuss in detail in Chapter 7.

References

[1] V. S. Lvov, R. Naaman, V. Tiberkevich and Z. Vage, Chem. Phys.Lett., 381, 650, (2003).

[2] D. Cahen, R. Naaman and Z. Vager, Adv. Funct. Mater., 15, 1571, (2005).

[3] C. G. Duan, W. N. Mei, W. G. Yin, J. J. Liu, J. R. Hardy, S. Ducharme and P. A. Dowben, Phys. Rev. B: Condens. Matter Mater. Phys.,69, 235106, (2004); M. Kuehn and H. Kliem, Phys.Status Solidi B, 245, 213, (2008).

[4] W. Guo, S. X. Du, Y. Y. Zhang, W. A. Hofer, C. Seidel, L. F. Chi, H. Fuchs and H.-J. Gao, Surf. Sci., 603, 2815, (2009).

[5] M. Feng, L. Gao, Z. Deng, W. Ji, X. Guo, S. Du, D. Shi, D. Zhang, D. Zhu and H. Gao, J. Am. Chem. Soc., 129, 2204, (2007); P. A. Lewis, C. E. Inman, F. Maya, J. M. Tour, J. E. Hutchison and P. S. Weiss, J. Am. Chem. Soc., 127, 17421, (2005); H. J. Gao, K. Sohlberg, Z. Q. Xue, H. Y. Chen, S. M. Hou, L. P. Ma, X. W. Fang, S. J. Pang and S. J. Pennycook, Phys. Rev. Lett., 84, 1780, (2000).

[6] P. A. Dowben, L. G. Rosa, C. C. Ilie and J. Xiao, J. Electron Spectrosc. Relat. Phenom., 174, 10, (2009).

[7] J. Xiao and P. A. Dowben, J. Mater. Chem., 19, 2172, (2009); J. Xiao, A. Sokolov and P. A. Dowben, Appl. Phys. Lett., 90, 242907, (2007).

[8] P. A. Dowben, J. Choi, E. Morikawa and B. Xu, ‘‘The Band Structure and Orientation of Molecular Adsorbates on Surfaces by Angle-Resolved Electron Spectroscopies’’, in Handbook of Thin Films, ed. H. S. Nalwa, Characterization and Spectroscopy of Thin Films, Academic Press, ch. 2, vol. 2, pp. 61–114, (2002).

[9] H. Ishii, K. Sugiyama, E. Ito and K. Seki, Adv. Mater., 11, 605, (1999).

[10] X. Y. Zhu, Surf. Sci. Rep., 56, 1, (2004).

[11] S. Balaz, A. N. Caruso, N. P. Platt, D. I. Dimov, N. M. Boag, J. I. Brand, Ya. B. Losovyj and P. A. Dowben, J. Phys. Chem. B, 111, 7009, (2007).

[12] A. Natan, L. Kronik, H. Haick and R. T. Tung, Adv. Mater., 19, 4103, (2007).

[13] D. Taguchi, N. Kajimoto, T. Manaka and M. Iwamoto, J. Chem. Phys., 127, 044703, (2007).

[14] A. Natan, Y. Zidon, Y. Shapira and L. Kronik, Phys. Rev. B: Condens. Matter Mater. Phys., 73, 193310, (2006).

[15] D. Deutsch, A. Natan, Y. Shapira and L. Kronik, J. Am. Chem.Soc., 2007, 129, 2989; M. L. Sushko and A. L. Shluger, Adv.Funct. Mater., 18, 2228, (2008).

[16] E. W. Plummer and W. Eberhardt, Adv. Chem. Phys., 49,533, (1982); N. V. Richardson and A. M. Bradshaw, in Electron Spectroscopy: Theory, Techniques and Aplications, ed. C. R. Brundle and A. D. Baker, Academic Press, San Diego, vol. 4, p. 153, (1984).

[17] P. A. Dowben, A. Miller, H.-J. Ruppender and M. Grunze, Surf. Sci., 193, 336, (1988).

[18] J.K.Nørskov, S.Holloway andN.D. Lang, Surf. Sci., 137, 65, (1984).

[19] Y. Yun and E. I. Altman, J. Am. Chem. Soc., 129, 15684, (2007).

[20] L. Onsager, J. Am. Chem. Soc., 58, 1486, (1936).

[21] O. Siri and P. Braunstein, Chem. Commun., 208, (2002).

[22] P. Braunstein, O. Siri, J.-P. Taquet, M.-M. Rohmer, M. Be´nard and R. Welter, J. Am. Chem. Soc., 125, 12246, (2003).

[23] A. Sawicka, P. Skurski and J. Simons, Chem. Phys. Lett., 362, 527, (2002).

[24] D. Delaere, P. C. Nam and M. T. Nguyen, Chem. Phys. Lett., 382, 349, (2003).

[25] H. T. Le, P. C. Nam, Y. L. Dao, T. Veszpremi and M. T. Nguyen, Mol. Phys., 101, 2347, (2003).

[26] Y. Haas and S. Zilberg, J. Am. Chem. Soc., 126, 8991, (2004).

[27] P. A. Dowben, Z. Phys. Chem., 202, 227, (1997).

[28] Q.-Z. Yang, O. Siri and P. Braunstein, Chem. Commun., 2005, 2660; Q.-Z. Yang, O. Siri, H. Brisset and P. Braunstein, Tetrahedron Lett., 47, 5727, (2006).

[29] B. Xu, J. Choi, A. N. Caruso and P. A. Dowben, Appl. Phys. Lett., 2002, 80, 4342; J. Xiao and P. A. Dowben, J. Phys.: Condens. Matter, 21, 052001, (2009).

[30] J. Choi, C. N. Borca, P. A. Dowben, A. Bune, M. Poulsen, S. Pebley, S. Adenwalla, S. Ducharme, L. Robertson, V. M. Fridkin, S. P. Palto, N. Petukhova and S. G. Yudin, Phys.Rev. B: Condens. Matter Mater. Phys., 61, 5760, (2000); A. Sokolov, C.-S. Yang, L. Yuan, S.-H. Liou, R. Cheng, H.-K. Jeong, T. Komesu, B. Xu, C. N. Borca, P. A. Dowben and B. Doudin, Europhys. Lett., 58, 448, (2002).

[31] J. Zhang, D. N. McIlroy, P. A. Dowben, H. Zeng, G. Vidali, D. Heskett and M. Onellion, J. Phys.: Condens. Matter, 7, 7185, (1995); D. N. McIlroy, J. Zhang, P. A. Dowben and D. Heskett, Mater. Sci. Eng., A, 217–218, 64, (1996).

[32] D.-Q. Feng, D. Wisbey, Ya. B. Losovyj, Y. Tai, M. Zharnikov and P. A. Dowben, Phys. Rev. B: Condens. Matter Mater. Phys., 74, 165425, (2006).

[33] J. Xiao, L. G. Rosa, M. Poulsen, D.-Q. Feng, S. Reddy, J. M. Takacs, L. Cai, J. Zhang, S. Ducharme and P. A. Dowben, J. Phys.: Condens. Matter, 18, L155, (2006).

[34] J. Choi, P. A. Dowben, S. Ducharme, V. M. Fridkin, S. P. Palto, N. Petukhova and S. G. Yudin, Phys. Lett. A, 249, 505, (1998).

[35] Y. Losovyj, I. Ketsman, E. Morikawa, Z. Wang, J. Tang and P. A. Dowben, Nucl. Instrum. Methods Phys. Res., Sect. A, 582, 264, (2007).

[36] P. A. Dowben, D. LaGraffe and M. Onellion, J. Phys.: Condens. Matter, 1, 6571, (1989).

[37] J. Hormes, J. D. Scott and V. P. Suller, Synchrotron Radiat. News, 19, 27, (2006).

[38] Y. Losovyj, K. Morris, L. Rosa, J. D. Scott and P. A. Dowben, Nucl. Instrum. Methods Phys. Res., Sect. A, 582, 258, (2007).

[39] C. M. Evans, J. D. Scott and E. Morikawa, Rev. Sci. Instrum., 73, 1557, (2002).

[40] O. Kizilkaya, J. D. Scott, E. Morikawa, J. D. Garber and R. S. Perkins, Rev. Sci. Instrum., 76, 13703, (2005).

[41] O. Kizilkaya, A. Prange, U. Steiner, E. C. Oerke, J. D. Scott, E. Morikawa and J. Hormes, Nucl. Instrum. Methods Phys. Res., Sect. A, 582, 274, (2007).

[42] A. Gruverman, O. Auciello and H. Tokumoto, Annu. Rev. Mater. Sci., 28, 101, (1998).

[43] S. Kümmel and L. Kronik, Rev. Mod. Phys., 2008, 80, 3; F. Bechstedt, F. Fuchs and G. Kresse, Phys. Status Solidi B, 246, 1877, (2009); T. Stein, L. Kronik and R. Baer, J. Am. Chem. Soc., 131, 2818, (2009); M.-S. Liao, Y. Lu and S. Scheiner, J. Comput. Chem., 24, 623, (2003); N. Yakovkin and P. A. Dowben, Surf. Rev. Lett., 14, 481, (2007).

[44] A. M. Scheer, G. A. Gallup and P. D. Burrow, Chem. Phys. Lett., 2008, 466, 131; A. M. Scheer and P. D. Burrow, J. Phys. Chem. B, 110, 17751, (2006).

[45] C. Waldfried, D. Welipitiya, C. W. Hutchings, H. S. V. de Silva, G. A. Gallup, P. A. Dowben, W. W. Pai, J. Zhang, J. F. Wendelken and N. M. Boag, J. Phys. Chem. B, 101, 9782, (1997).

[46] G. Koller, S. Berkebile, M. Oehzelt, P. Pusching, C. Ambrosch-Draxi, F. P. Netzer and M. G. Ramsey, Science, 317, 351, (2007).

[47] L. Routaboul, P. Braunstein, J. Xiao, Z. Zhang, B. Doudin, Ya. B. Losovyj, O. Kizilkaya and P. A. Dowben, G. Delmas and V. Da Costa, in preparation.

[48] J. U. Mack, E. Bertel and F. P. Netzer, Surf. Sci., 159, 265, (1985).

[49] F. P. Netzer and J. U. Mack, J. Chem. Phys., 79, 1017, (1983); F. P. Netzer and J. U. Mack, Chem. Phys. Lett., 95, 492, (1983).

[50] Z. T. Giessel, O. Schaff, R. Lindsay, P. Baumgartel, M. Polcik, A. M. Bradshaw, A. Koebbel, T. McCabe, M. Bridge, D. R. Lloyd and D. P. Woodruff, J. Chem. Phys., 110, 9666, (1999).

[51] A. Sivanesan and S. A. John, Langmuir, 24, 2186, (2008).

[52] N. Sato, K. Seki and H. J. Inokuchi, J. Chem. Soc., Faraday Trans. 2, 77, 1621, (1981).

[53] H. Fukagawa, H. Yamane, T. Kataoka, S. Kera, M. Nakamura, K. Kudo and N. Ueno, Phys. Rev. B: Condens. Matter Mater. Phys., 73, 245310, (2006).

[54] P. G. Schroeder, C. B. France, J. B. Park and B. A. Parkinson, J. Phys. Chem. B, 107, 2253, (2003).

[55] R. Atkin, S. Z. El Abedin, R. Hayes, L. H. S. Gasparotto, N. Borisenko and F. Endres, J. Phys. Chem. C, 113, 13266, (2009).

[56] J. C. Fuggle, E. Umbach, D. Menzel, K. Wandelt and C. R. Brundle, Solid State Commun., 27, 65, (1978); J. Stohr and R. Jaeger, Phys. Rev. B: Condens. Matter, 26, 4111, (1982); M. Grunze, J. Fuhler, M. Neumann, C. R. Brundle, D. J. Auerbach and J. Behm, Surf. Sci., 139, 109, (1984); C. R. Brundle, P. S. Bagus, D. Menzel and K. Hermann, Phys.

Rev. B: Condens. Matter, 24, 7041, (1981); E. Umbach, Solid State Commun., 51, 365, (1984).

[57] K. Schönhammer and O. Gunnarsson, Solid State Commun., 23, 691, (1977); K. Schönhammer and O. Gunnarsson, Solid State Commun., 26, 399, (1978); O. Gunnarsson and K. Schönhammer, Phys. Rev. Lett., 41, 1608, (1978).

[58] C. Bureau, F. Valin, G. Lecayon, J. Charlier and V. Detalle, J. Vac. Sci. Technol., A, 15, 353, (1997).

[59] M. Barber, J. A. Conner, M. F. Guest, I. H. Hillier, M. Schwarz and M. Stacy, J. Chem. Soc., Faraday Trans. 2, 69, 551, (1973).

[60] B. J. Lindberg and J. Hedman, Chem. Script., 7, 155, (1975).

[61] T. Yoshida and S. Sawada, Bull. Chem. Soc. Jpn., 47, 50, (1974).

[62] K. B. Yatsimirskii, V. V. Nemoshalenko, Y. P. ANazarenko, V. G. Aleshin, Y. I. Bratushko and E. P. Moiseenko, Chem. Phys.Lett., 52, 481, (1977).

[63] M. E. Zoloff Michoff, P. Velez and E. P. M. Leiva, J. Phys. Chem.C, 113, 3850, (2009).

[64] F. Iori, S. Corni and R. Di Felice, J. Phys. Chem. C, 112, 13540, (2008).

[65] P. F. Cafe, A. G. Larsen, W. Yang, A. Bilic, I. M. Blake, M. J. Crossley, J. Zhang, H. Wackerbarth, J. Ulstrup and J. R. Reimers, J. Phys. Chem. C, 111, 17285, (2007).

[66] J. Gong, T. Yan and C. B. Mullins, Chem. Commun., 761, (2009).

[67] A. Bilic, J. R. Reimers, N. S. Hush and J. Hafner, J. Chem. Phys., 116, 8981,(2002).

[68] A. Bilic, J. R. Reimers and N. S. Hush, J. Phys. Chem. B, 106, 6740, (2002).

[69] R. C. Hoft, M. J. Ford, A. M. McDonagh and M. B. Cortie, J. Phys. Chem. C, 111, 13886, (2007).

[70] F. P. Netzer, G. Rangelov, G. Rosina and H. B. Saalfeld, J. Chem. Phys., 89, 3331, (1988).

[71] I. Gallardo, J. Pinson and N. Vila, J. Phys. Chem. B, 110, 19521, (2006).

[72] R. A. Ojifinni, J. Gong, D. W. Flaherty, T. S. Kim and C. B. Mullins, J. Phys. Chem. C, 113, 9820, (2009).

[73] J. Gong and C. B. Mullins, Acc. Chem. Res., 42, 1063, (2009).

[74] Q.-Z. Yang, O. Siri and P. Braunstein, Chem.–Eur. J., 11, 7237, (2005).

[75] P. Braunstein, O. Siri, P. Steffanut,M.Winter and Q.-Z. Yang, C. R. Chimie, 9, 1493, (2006).

[76] Q.-Z. Yang, A. Kermagoret, M. Agostinho, O. Siri and P. Braunstein, Organometallics, 25, 5518, (2006).

[77] E.Heilbronner, K. A. Muszkat and G. Schazublin, Helv. Chim. Acta, 54, 58, (1971); J.M.Hollas and T.A. Sutherley, Mol. Phys., 21,183, (1971); J. M. Hollas and T. A. Sutherley, Mol. Phys., 22, 213, (1971).

[78] W. C. Price, ‘‘Ultraviolet Photoelectron Spectroscopy: Basic Concepts and Spectra of Small Molecules’’, in Electron Spectroscopy: Theory Techniques and Applications, ed. C. R. Brundle and A. D. Baker, Academic Press, New York, vol. 1, p. 151, (1977).

[79] E. Heilbronner and J. P. Maier, ‘‘Some Aspects of Organic Photoelectron Spectra’’, in Electron Spectroscopy: Theory Techniques and Applications, ed. C. R. Brundle and A. D. Baker, Academic Press, New York, vol. 1, p. 151, (1977).

[80] N. E. Gruhn, D. A. da Silva, T. G. Bill, M. Malagoli, V. Coropceanu, A. Kahn and J.-L. Brédas, J. Am. Chem. Soc., 124, 7918, (2002).

[81] V. Coropceanu, M. Malagoli, D. A. da Silva Filho, N. E. Gruhn, T. G. Bill and J.-L. Brédas, Phys. Rev. Lett., 89, 275503, (2002).

[82] J.-L. Brédas, D. Beljonne, V. Coropceanu and J. Cornil, Chem. Rev., 104, 4971, (2004).

[83] M. Malagoli, V. Coropceanu, D. A. da Silva Filho and J.-L. Brédas, J. Chem. Phys., 120, 7490, (2004).

[84] R. S. Sánchez-Carrrera, V. Coropceanu, M. Malagoli, D. A. da Silva Filho, R. Freidlein, W. Osikowicz, R. Murdey, C. Suess, W. R. Salaneck and J.-L. Brédas, J. Phys. Chem. B, 110, 18904, (2006).

[85] F. Evangelista, V. Carravetta, G. Stefani, B. Jansik, M. Alagia, L. Nazionale, S. Stranges and A. Ruocco, J. Chem. Phys., 126, 124709, (2007).

[86] H. Yamane, S. Nagamatsu, H. Fukagawa, S. Kera, R. Friedlein, K. K. Okudaira and N. Ueno, Phys. Rev. B: Condens. Matter Mater. Phys., 72, 153412, (2005).

[87] S. Kera, H. Yamane and N. Ueno, Prog. Surf. Sci., 84, 135, (2009).

[88] S. Kera, H. Yamane, I. Sakurgai, K. K. Okudaira and N. Ueno, Chem. Phys. Lett., 364, 93, (2002).

[89] J. W. Gadzuk, Phys. Rev. B: Solid State, 1976, 14, 5458; J. W. Gadzuk, Phys. Rev. B: Condens. Matter, 20, 515, (1979).

[90] L. G. Rosa, Ya. B. Losovyj, J. Choi and P. A. Dowben, J. Phys. Chem. B, 109, 7817, (2005).

[91] L. G. Rosa, J. Jiang, F. W. Li, J. Xiao, E. Utreras, O. V. Lima, J. Alvira, Ya. B. Losovyj and L. Tan, J. Phys. Chem. C, 114, 1015, (2010).

[92] P. B. Paramonov, V. Coropceanu and J.-L. Brédas, Phys. Rev. B: Condens. Matter Mater. Phys., 78, 041403, (2008).

[93] J. E. Ortega, F. J. Himpsel, D. Li and P. A. Dowben, Solid State Commun., 1994, 91, 807. 10340.

Chapter 5 Band Mapping and Electron Pockets at the Fermi Level for *p*-benzoquinonemonoimine Zwitterion

5.1 Introduction

Organic materials are commonly regarded as electrical insulator with a large range of application in electronics, biomedical and pharmaceutical purposes. This is largely true even today when we observed man made organic materials in our surroundings. However, electrical conduction on organic materials began to draw attention of scientists. Even today questions such as underlying mechanism of electron mobility, synthesis of materials with determine conductivity properties, which electronic state promotes conduction, are current subject of research for scientist in materials and nanotechnology research. The field of organic semiconductors has developed from a fundamental laboratory discovery into a manufacturing technological material for a large range of thin- film electronics applications [1-3] , which benefits from the compatibility of organic materials with large area, low-cost, room temperature solution processing and direct-write printing. Since their discovery organic semiconductor applications today include emissive light emitting diodes, flat panel displays, and low cost thin film transistor circuits on flexible substrates [4].

One of the general issues in molecular electronics is the transport through organic molecules. The hybridization of molecular orbitals to form band structure has been studied for nearly three decades [5-9], and is a fairly well established phenomenon. With larger molecular species, intramolecular band structure is far more likely and commonly observed [10-12]. Such intramolecular band dispersion has been found in self-assembled monolayers [11, 12], including polyphenyl species [12]. In contrast, because of the very small effective

Brillouin zone (requiring exceptionally good wave vector resolution) and the generally very small intermolecular interactions, band structure resulting from intermolecular interactions is generally not observed for ordered assemblies of large molecules, with only a few exceptions [5-13].

The study of the details of transport mechanisms in organic systems has demonstrated that, not only do interface dipoles and valence band electronic structure symmetry play a role, but that there is a strong dependence on molecular vibrations [14-20] that couple to the transport properties through electronic structure. Organic semiconducting systems, such as anthracene [21], on the other hand, are characterized by their high degree of electron localization and molecular polarization that dominates the physics of excited states and transport phenomena. These organics have small intermolecular overlap, low dielectric constant, localized charges on individual molecules, and large polarizabilities involving charges and induced and permanent electric dipoles [22-25]. This can be enhanced by suitable functionalization, as we have demonstrated here for the horizontal and vertical anthracene isomers of the silane complexes.

The quinonoid zwitterions, although electrically neutral as a whole, carry positive and negative charges on different parts of the molecule. The positive charge is delocalized between the amino groups over 4 bonds involving 6π electrons, while the negative charge is spread likewise between the oxygen atoms [26-28]. The result is a large electric dipole that is formed across the across the "benzene" like plane of the benzoquinonemonoimine "core"; this makes these zwitterionic compounds fascinating candidates for the study the electronic structure. These molecules have not only had a very strong local dipole, but the delocalized benzene π molecule of the zwitterion "core" loses aromatic character due to the

large charge separation. Large dipolar molecules tend to be good dielectrics, but obviously the molecular packing and orientation can enhance or suppress the dielectric properties. In this chapter, we will discuss the band structure and electron pockets on the (6Z)-4-(benzylamino)-6-(benzylliminio)-3-oxocyclohexa-1,4-dien-1-olate zwitterion isomer of the benzoquinonemonoimine family *(p*-benzoquinonemonoimine zwitterion with benzyl pendant groups, zwitterions **5**).

5.2 Electron Pockets at the Fermi Level and Band Structure

5.2.1 Theoretical Approaches

The zwitterion calculations, it was applied a plane-wave-based density functional theory (DFT) method within the Perdew-Burke-Ernzerhof (PBE) generalized gradient approximation [39], which was implemented in the CASTEP computer code (Accelyrs Inc. San Diego, CA) [40]. The wave functions were expanded in terms of a plane-wave basis set with a kinetic energy cutoff of 300 eV, which with adopted ultra soft pseudopotentials provided good convergence of calculated total energies and atomic forces [41]. The supercell was taken with the dimension a_x = 8.446 Å, b_y = 14.996 Å, c_z = 12.728 Å. The semiempirical (with a PM3 parameter set) theoretical calculations of the zwitterion on PVDF-TrFE were done with the HyperChem package [42], as previously described in the prior chapter.

5.2.2 Band Structure of the (6Z)-4-(benzylamino)-6-(benzylliminio)-3-oxocyclohexa-1,4-dien-1-olate Zwitterion

Combined photoemission and inverse photoemission spectra [30-34], were taken of the *p*-benzoquinonemonoimine zwitterion (Figure 5.1) on gold, for molecular coverages that range from nominally 0.5 nm to the thicker multilayer films [32]. As mentioned in chapter 2, the IPES were obtained by using variable kinetic energy incident energy electrons while detecting the emitted photons at a fixed energy (9.7 eV) using a Geiger-Müller detector [30-35]. The inverse photoemission spectroscopy was limited by an instrumental line width of approximately ~ 400 meV, as described elsewhere [33, 34]. In both photoemission and inverse photoemission measurements, the binding energies are referenced with respect to the Fermi edge ($E_F = 0$ eV) of gold in intimate contact with the sample surface and the photoemitted (UPS, XPS), in terms of $E-E_F$ (thus making occupied state energies negative).

Energy-dependent photoemission spectra were taken for the zwitterion thin film grown on the gold surface (Figure 5.1(b)), with the photoelectrons collected normal to the surface. In this particular experimental setup, the photon energy dependence of the photoemission spectra (relative to the Fermi level) can be exploited to determine the dispersion (change in binding energy) as a function of wave vector $k_{\perp}$ (along the surface normal). Such dispersion is observed here (Figure 5.1(a & b)) and is a consequence of the hybridization of molecular orbitals of adjacent zwitterion molecules fulfilling the criteria of Bloch's theorem [5, 43]. As shown in figure 5.1(b), the photoemission peak binding energies exhibit oscillatory behavior as a function of electron wave vector (proportional to the square root of electron kinetic energy). This is summarized in figure 5.1(b), where the

peak position for the -2.4 eV band is plotted against the $k_{\perp}$ vector. From this dispersion amplitude of 200 meV, not only is the crystallinity of the zwitterion film evident but also a bulk lattice parameter for along the surface normal can be derived.

From these values, we find that zwitterion crystal grown on the gold substrate here has a crystal layer spacing of 5.9 Å ($\pm$ 0.2 Å along the surface normal. This lattice parameter derived from the band dispersion can be assigned to the calculated value of 6.4 Å, along the Z to G direction (Figure 5.2(a-g)) of the O-O distances in the cubic zwitterion structures as shown in figures 5.2(a-f) [26, 27]. As seen in figure 5.1(b) and figure 5.2(g), the experimental dispersion is and average to band dispersions calculated along the Z to G figure 5.2(g), due to the limited resolution of the electron analyzer. The expectation that the inner potential U_{in} is negligible in an insulator is not completely borne out by the data. We find some evidence for a small inner potential corresponding to a wave vector of about 0.1 (0.3 Å-1, which increases with increasing energy (as is often observed with metals [44]). This corresponds to a very small inner potential energy correction but does tend to suggest that effects from the potential change across the surface boundary cannot be completely neglected. The electron mean free path at roughly 50 eV kinetic energy is generally accepted to be quite short [45-48], but as we see from the data here. Accordingly, we would expect that the electron mean free path for the photoelectrons in the zwitterion is much longer than is observed in metals, consistent with the longer mean free paths observed in organic systems [45]. The mean free path is clearly sufficient to observe that Bloch's theorem [5, 43] is fulfilled for the occupied molecular orbitals of zwitterion, although we do not observe photoelectrons from the gold substrate.

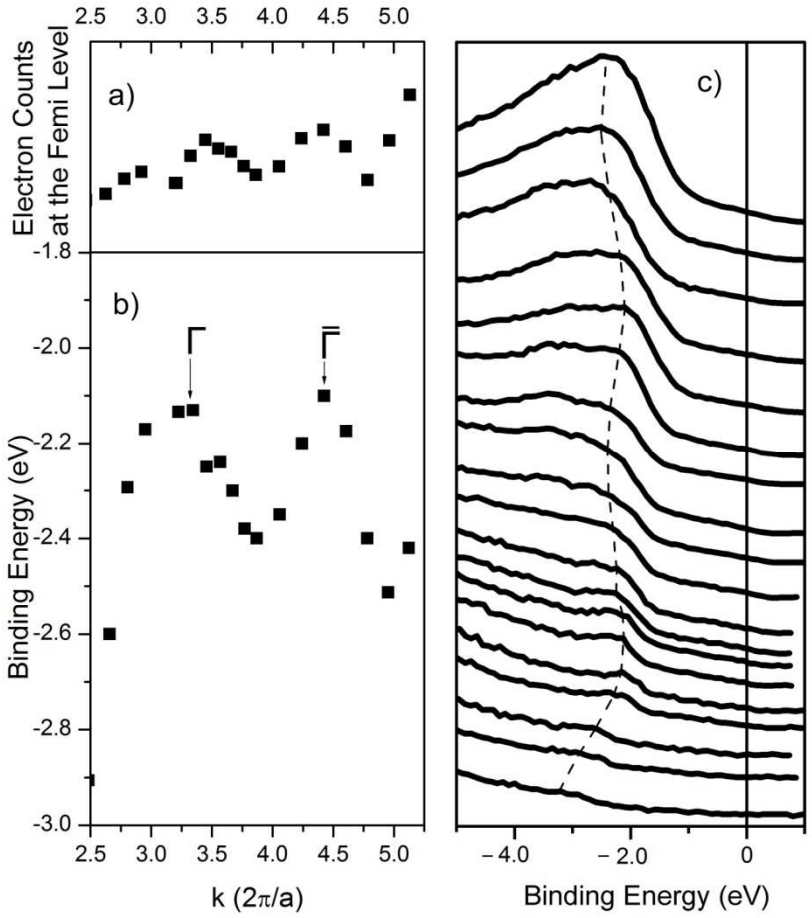

Figure 5.1 (a) Evidence of electron pockets, electron were collected normal to the surface at the Fermi Level, (b) band structure dispersion as a function of wave vector $k_{\perp}$, providing an experimental lattice of 5.9 Å along the surface normal and (c) energy-dependent photoemission spectra of zwitterion (6Z)-4-(benzylamino)-6-(benzylliminio)-3-oxocyclohexa-1,4-dien-1-olate on gold, showing evidence of band dispersion. The photoelectrons were collected along the surface normal.

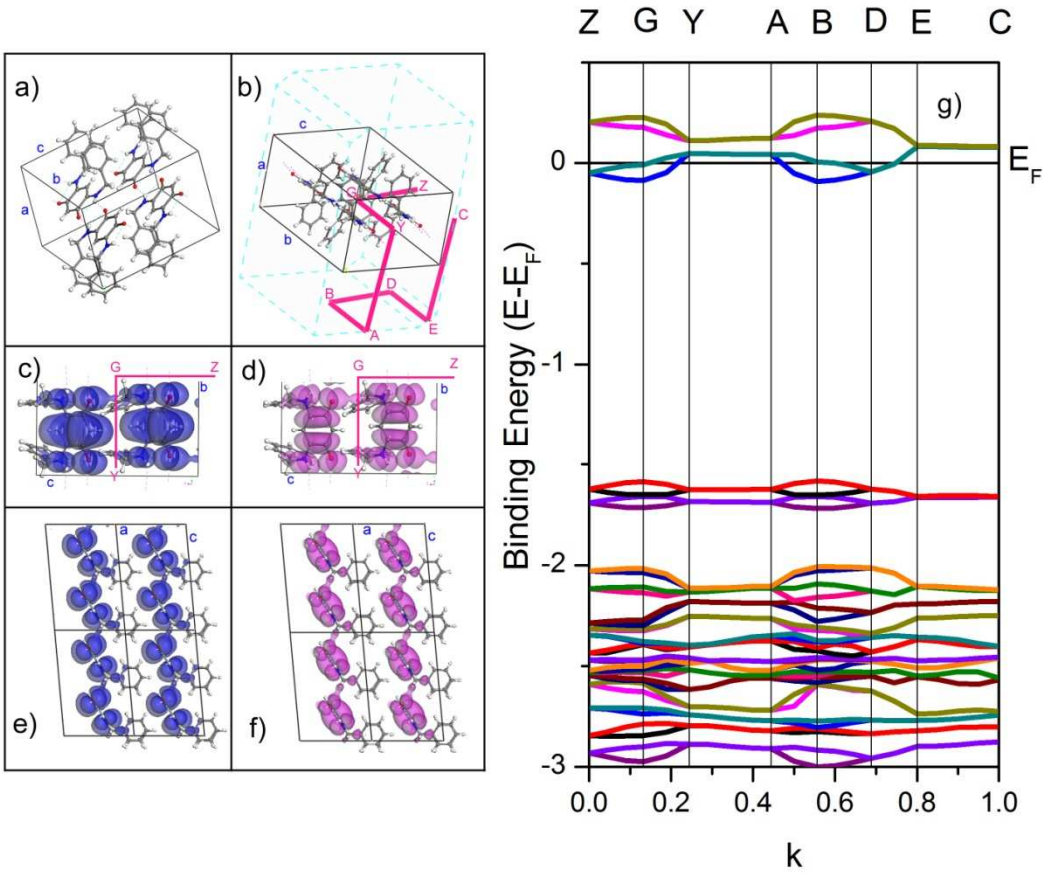

Figure 5.2 Band structure calculation of zwitterion (6Z)-4-(benzylamino)-6-(benzylliminio)-3-oxocyclohexa-1,4-dien-1-olate crystal. (a) crystal structure, (b) , (c) and (e) views of the highest valence band wave function density and (d) & (f) views of the lowest conduction band wave function density.

5.2.3 Electron Pockets at the Fermi Level of the (6Z)-4-(benzylamino)-6-(benzylliminio)-3-oxocyclohexa-1, 4-dien-1-olate Zwitterion

The electronic structure of the zwitterion is shown on figure 5.3 (a) measured by photoemission and inverse photoemission. The calculated density of states for the zwitterion (6Z)-4-(benzylamino)-6-(benzylliminio)-3-oxocyclohexa-1,4-dien-1-olate of chemical formula $C_6H_2(\cdots NHR)_2(\cdots O)_2$ where R =*n*-C_6H_5 is shown on figure 5.3 (b). In comparison a hydrogenated zwitterion $C_6H_2(\cdots NHR)_2(\cdots O)(\cdots OH)$ figure 5.3(c), a dehydrogenated zwitterion $C_6H_2(\cdots NHR)(\cdots NR)(\cdots O)_2$ Figure 3(d) were calculated by DFT and a dehydrogenated zwitterion $C_6H_2(\cdots NHR)(\cdots NR)(\cdots O)_2$ was calculated by semiempirical method figure 5.3 (e). The calculated spectra were aligned with respect to the -2.4 eV peak of the experimental photoemission spectra. In order to align the theoretical spectra to the experimental results the zwitterion density of states Figure 5.3(b) was shifted -1.58eV, the hydrogenated zwitterion Figure 5.3(c) did not require any shifts to be aligned with the experimental measurement, Figure 5.3(a). The dehydrogenated zwitterion Figure 5.3(d) was shifted -1.88 eV. The dehydrogenated zwitterion Figure 5.3(e) calculated with semiempirical methods was also shifted +2.95 eV with respect to the Fermi level. Band gap for the zwitterion experimental measurement was 1.66 eV Figure 5.3(a), for the calculated zwitterion 1.63 eV Figure 5.3(b), hydrogenated zwitterion 1.70 eV Figure 5.3(c), dehydrogenated zwitterion Figure 5.3(d) 1.83 eV and for the dehydrogenated zwitterion by semiempirical methods Figure 5.3(e) 1.93 eV.

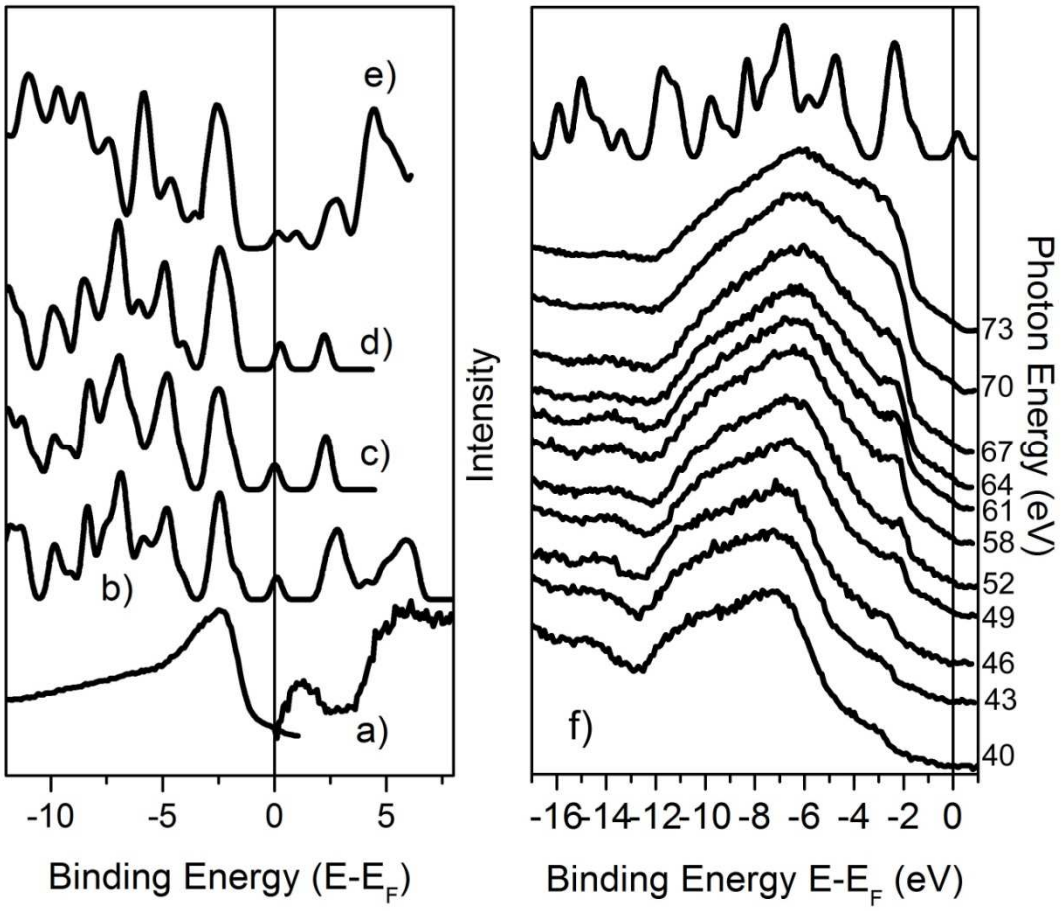

Figure 5.3 (a) Combined photoemission and inverse photoemission of the zwitterion zwitterions (6Z)-4-(benzylamino)-6-(benzylliminio)-3-oxocyclohexa-1,4-dien-1-olate, Density state calculation of: (b) the $C_6H_2(\underline{\cdots}NHR)_2(\underline{\cdots}O)_2$ where R =*n*-C_6H_5 zwitterion by DFT, (c) hydrogenated zwitterion $C_6H_2(\underline{\cdots}NHR)_2(\underline{\cdots}O)(\underline{\cdots}OH)$ by DFT, (d) dehydrogenated zwitterion $C_6H_2(\underline{\cdots}NHR)(\underline{\cdots}NR)(\underline{\cdots}O)_2$ by DFT and (e) zwitterion $C_6H_2(\underline{\cdots}NHR)(\underline{\cdots}NR)(\underline{\cdots}O)_2$ by semiempirical methods, (f) energy-dependent photoemission spectra of the $C_6H_2(\underline{\cdots}NHR)_2(\underline{\cdots}O)_2$ where R =*n*-C_6H_5.

Evidence of an electron pocket within 90 meV below the Fermi Level is a dominant feature in the spectra. Due to a conduction band crossing the Fermi Level, electron pockets

are formed, as shown on figure 5.1(a) and figure 5.2(g), were the photoelectron intensity current was measured at the Fermi level showing a periodic oscillation corresponding to approximately 6.3 Å or 1 $Å^{-1}$ wave number. As shown in figure 5.2(g) DFT band structure calculation a conduction band does crosses the Fermi level and shows periodicity along the Z-G direction as shown in figure 5.2 (b, d, f). The conduction band wave function density was plotted as a 3D view, Figure 5.2(d, f), of the total density along the Z-G direction showing an overlap of electron density between zwitterion molecules through the oxygen and the amine group of the next zwitterion molecule along the Z-G direction.

Besides, we observe the similar band mapping in butyl substituted zwitterions (zwitterions **2**). Figure 5.4 shows results from band mapping experiments, indicating that long range ordering exists in a direction normal to the zwitterion cores. The emission angle dependence of photoemission has been exploited to determine the dispersion (change in binding energy) as function of wave vector $k_{\|}$, the wave vector parallel to the surface of the film, using:

$$k_{\|} = \sqrt{\frac{2m}{\hbar^2} E_{kin}} \sin(\theta) = 0.512\sqrt{E_{kin}/eV} \sin(\theta)\ Å^{-1} \qquad 5.1$$

where the value of $k_{\|}$ can be estimated from the photoelectron kinetic energy (E_{kin}) and the photoemission emission angle (θ) [5, 49].

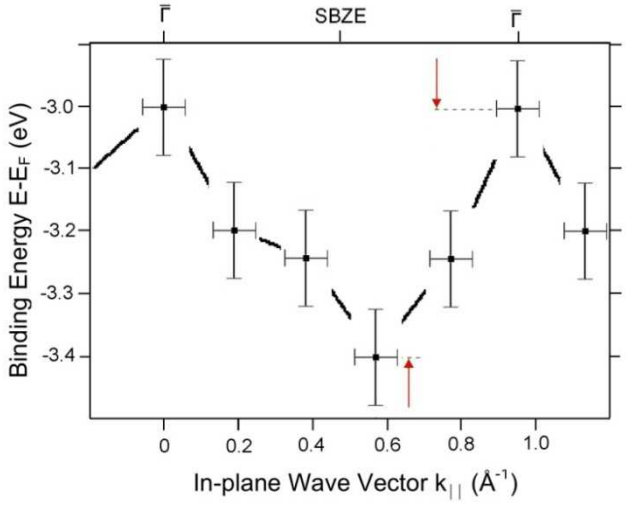

Figure 5.4 Dispersion of the intermolecular band from the HOMO molecular orbitals of zwitterion **2** molecules assembled on Au (111) in the reduced zone scheme. The red arrows indicate the extent of the disperions or effective band width of the highest occupied molecular orbtal along the zwitterion **2** molecular core π-π stacking direction.

Support for a dense packing between adjacent molecules of zwitterion **2** can be inferred from the intermolecular dispersion or band width of about 400 meV, obtained by emission angle dependent photoemission, as indicated in figure 5.4 (red arrows). This is a rather large band width (dispersion) for a molecular film and indicates a lattice with a period of 6.4± 0.2 Å ($2\pi/(k=0.98$ Å^{-1})), with two molecules per period in the direction perpendicular to the zwitterion ion core plane but parallel to the plane of the Au surface. This lattice spacing along one of the in-plane directions of the film indicates an intermolecular spacing of about 3.2 ± 0.2 Å, and is consistent with *p*-benzoquinonemonoimine zwitterionic core of molecule **2** aligned along the surface normal,

as discussed previously [32]. This short distance also opens the possibility of π-π stacking allowing good mobility charge transport.

5.3 Conclusion

The results demonstrate that Bloch's theorem applies to the wave vector dependence of the electronic band structure (where the molecular orbitals also combine to form bands) for a thin film of zwitterion (6Z)-4-(benzylamino)-6-(benzylliminio)-3-oxocyclohexa-1,4-dien-1-olate on gold substrate. Inter-molecular band dispersion has been previously observed for small adsorbates (like the molecular CO and N_2 and for large adsorbate molecular layers like pentancene, thione 2-mercatobenzoxazole and a very few other examples [50-55]. This comparison, by analogy at the very least, is possible because both these small and large adsorbate molecules tend to bond with the molecular axis ‘‘mostly’’ along the surface normal. Band dispersion and large electron pockets are observed in the photoemission spectra, this large electron pockets can be associated with an electronic state in which its electronic density is shared inter-molecularly through the oxygen to amino groups of the zwitterion crystal. Here we provide basic characterization of this large electron pocket, revealing its one dimensional origins. We propose a one dimensional electronic state as shown on the calculation figure 5.2(g), electronic band crossing the Fermi level and consequently a large number of free electron along Z-G direction on the zwitterion crystalline structure, in comparison other crystal directions do not contribute to electron states on the Fermi level, making it a quasi-one dimensional conductor.

References

[1] R. Friend, "Polymers show they're metal", Nature, 44, 37, (2006).

[2] V.I. Roldughin and V.V. Vysotskii, "Percolation properties of metal-filled polymer films, structure and mechanisms of conductivity", Progress in Organic Coatings, 39, 81, (2000).

[3] T. Ohta, A. Bostwick, T. Seyller, K. Horn and E. Rotenberg, "Controlling the electronic structure of bilayer graphene", Nature, 313, 951, (2006).

[4] G. Gustafsson, Y. Cao, G.M. Treacy, F. Klavetter, N. Colaneri and A.J. Heeger, "Flexible light-emitting diodes made from soluble conducting polymers", Nature, 357, 477, (1992).

[5] P. A. Dowben, B. Xu, J. Choi, & E. Morikawa, Band Structure and orientation of molecules adsorbates on surfaces by angle resolved electron spectroscopies. In: Handbook of Thin Film Materials, vol. 2, Characterization and Spectroscopy of thin Films, Hari Singh Nalwa (Ed.), Academic Press: A division of Harcourt, Inc. 61–113, (2002).

[6] E. W. Plummer, & W. Eberhardt, Adv. Chem. Phys., 49, 533, (1982).

[7] H.-P. Steinrück, Vacuum, 45, 715, (1994).

[8] F. Zwick, D. Jérome, G. Margaritondo, M. Onellion, J. Voit, and M. Grioni, Physical Review Letters, 81, 2974, (1998).

[9] C. Rojas, J. Caro, M. Grioni and J. Fraxedas, Surface Science, 482-485, 546, (2001).

[10] J. Choi, C. N. Borca, P. A. Dowben, A. Bune, M. Poulsen, S. Pebley, S. Adenwalla, S. Ducharme, L. Robertson, V.M. Fridkin, S. P. Palto, N. Petukhova, & S.G. Yudin, Phys. Rev. B, 61, 5760, (2000).

[11] D. Yoshimura, H. Ishii, Y. Ouchi, E. Ito, T. Miyamae, S. Hasegawa, K.K. Okudaira, N. Ueno, & K. Seki, Phys. Rev. B, 60, 9046, (1999).

[12] S. Narioka, H. Ishii, K. Edamatsu, K. Kamiya, S. Hasegawa, T. Ohta, N. Ueno, & K. Seki, Phys. Rev. B, 52, 2362, (1995).

[13] A. N. Caruso, R. Rajesekaran, G. Gallup, J. Redepenning, & P. A. Dowben, J. Phys. Cond. Matt., 16, 845 (2004).

[14] M. Galperin, A. Nitzan, M. Ratner, Inelastic effects in molecular junctions in the Coulomb and Kondo regimes: Nonequilibrium equationof- motion approach. Phys. ReV. 76 (035301), 1–10, (2007).

[15] H. Yamane, S. Nagamatsu, H. Fukagawa, S. Kera, R. Friedlein, K. K. Okudaira, N. Ueno, Hole-vibration coupling of the highest occupied state in pentacene thin films. Phys. ReV. B 72 (15), 153412, (2005).

[16] J. S. Seldenthuis, H. S. J. van der Zant, M. A. Ratner, J. M. Thijssen, Vibrational excitations in weakly coupled single-molecule junctions: A computational analysis. ACS Nano 2 (7), 1445–1451, (2008).

[17] A. Troisi, M. A. Ratner, Molecular signatures in the transport properties of molecular wire junctions: What makes a junction “molecular”? Small 2, 172-181, (2006).

[18] V. Mujica, M. Kemp, M. A. Ratner, Electron conduction in molecular wires. II. Application to scanning tunneling microscopy. J. Chem Phys. 101, 6856–6864, (1994).

[19] M. Galperin, A. Nitzan, M. Ratner, Inelastic effects in molecular junctions in the Coulomb and Kondo regimes: Nonequilibrium equationof- motion approach. Phys. ReV. B 76, 035301, (2007).

[20] V. Mujica, M. Kemp, M. Ratner, Electron conduction in molecular wires I. A scattering formalism. J. Chem. Phys. 101, 6849–6855, (1994).

[21] Luis G. Rosa, Jinyue Jiang, Freddy Wong Li, Jie Xiao, Emmanuel Utreras, Ocelio V. Lima, Jose Alvira, Ya. B. Losovyj and Li Tan, "Franck-Condon Coupling in Anthracene Isomers Self-assembled Layers and Symmetry Effects on the High Resolution Ultraviolet Photoemission Spectra (HRUPS)", Journal of Physical Chemistry C, 114, 1015 (2010).

[22] I. G. Hill, A. Kahn, Z. G. Soos, R. A. Pascal, Jr. Chargeseparation energy in films of p-conjugated organic molecules. Chem. Phys Lett. 327, 181–188, (2000).

[23] N. Koch, A. Kahn, J. Ghijsen, J.-J. Pireaux, J. Schwartz, R. L. Johnson, A. Elschner, Conjugated organic molecules on metal versus polymer electrodes: Demonstration of a key energy level alignment mechanics. Appl. Phys. Lett. 82 (8), 70–72, (2003).

[24] C. Wu, Y. Hirose, H. Sirringhaus, A. Kahn, Electron-hole interaction energy in the organic molecular semiconductor PTCDA. Chem. Phys. Lett. 272, 43–47, (1997).

[25] N. Karl, Charge carrier transport in organic semiconductors. Synth.Met. 133-134, 649–657, (2003).

[26] O. Siri, P. Braunstein, Chem. Commun. 208-209, (2002).

[27] P. Braunstein, O. Siri, J. Taquet, M. Rohmer, M. Bénard, R. Welter, J. Am. Chem. Soc. 125, 12246-12256, (2003).

[28] Q.Z. Yang, O. Siri, P. Braunstein, Chem. Commun. 2660–2662, (2005).

[29] Q. Z. Yang, O. Siri, H. Brisset, P. Braunstein, Tetrahedron Lett. 47, 5727–5731, (2006).

[30] P. A. Dowben, L. G. Rosa, C. C. Ilie, J. Xiao, J. Electron Spectrosc. Rel. Phenom. 174, 10-21, (2009).

[31] J. Xiao, P. A. Dowben, J. Materials Chem. 19, 2172-2178, (2009); J. Xiao, A. Sokolov, P. A. Dowben, Appl. Phys. Lett. 90, 242907, (2007).

[32] J. Xiao, Z. Zhang, D. Wu, L. Routaboul, P. Braunstein, B. Doudin, Ya. B. Losovyj, O. Kizilkaya, L. G. Rosa, C. N. Borca, A. Gruverman, and P. A. Dowben, "The interface bonding and orientation of a quinonoid zwitterion", Physical Chemistry Chemical Physics 12 10329 - 10340, (2010).

[33] B. Xu, J. Choi, A. N. Caruso, P. A. Dowben, Appl. Phys. Lett. 80, 4342-4344, (2002); J. Xiao, P. A. Dowben, J. Phys. Cond. Matter 21, 052001, (2009).

[34] D. -Q. Feng, D. Wisbey, Ya. B. Losovyj, Y. Tai, M. Zharnikov, P.A. Dowben, Phys. Rev. B 74, 165425, (2006).

[35] A. Ahmadi, G. Attard, J. Feliu, A. Rodes, Langmuir 15, 2420-2424, (1999); A.J. Gellman, ACS Nano 4, 5-10, (2010); G. A. Attard, J. Phys. Chem. B 105, 3158-3167, (2001); D. S. Sholl, A. J. Gellman, AICHE Journal 55, 2484-2490, (2009); G. Held, M. J. Gladys, Topics In Catalysis 48, 128-136, (2008); J.N. James, D.S. Sholl, Current Opinion In Colloid & Interface Science 13, 60-64, (2008); T. Greber, Z. Sljivancanin, R. Schillinger, J. Wider, B. Hammer, Phys. Rev. Lett. 96, 056103, (2006); A. Kuhnle, T. R. Linderoth, F. Besenbacher, J. Am. Chem. Soc. 128, 1076-1077, (2006).

[36] Y. Losovyj, I. Ketsman, E. Morikawa, Z. Wang, J. Tang, P.A. Dowben, Nucl. Instrumen. Methods Phys. Res. A 582, 264, (2007).

[37] P.A. Dowben, D. LaGraffe, M. Onellion, J. Phys. Cond. Matt. 1, 6571, (1989).

[38] J. Hormes, J.D. Scott, V.P. Suller, Synchrotron Radiation News 19, 27, (2006).

[39] J. P. Perdew, K. Burke, M. Ernzerhof, Phys. ReV. Lett. 77, 3865-3868, (1996).

[40] M. D. Segall, P. J. D. Lindan, M. J. Probert, C. J. Pickard, P. J. Hasnip, S. J. Clark, M. C. Payne, J. Phys.: Condensed Matter 14, 2717-2744, (2002).

[41] D. Vanderbilt, Phys. ReV. B 41, 7892-7895, (1990).

[42] L. G. Rosa, I. N. Yakovkin, P. A. Dowben, J. Phys. Chem. B 109, 14189, (2005).

[43] Luis G. Rosa, J. Xiao, Ya. B. Losovyj, Y. Gao, I.N. Yakovkin, X.C. Zeng and P.A. Dowben, "Crystalline Ice Grown on the Surface of the Ferroelectric Polymer Poly(vinylidene fluoride) (70%) and trifluoroethylene (30%)", Journal of the American Chemical Society, 127, 17261-17265, (2005).

[44] I. N. Yakovkin, J. Zhang, P. A. Dowben, Phys. ReV. B 63, 115408, (2001).

[45] C. J. Powell, Surf. Sci. 44, 29, (1974).

[46] D. R. Penn, J. Electron Spectrosc. Relat. Phenom. 9, 29, (1976).

[47] S. Tamura, C. J. Powell, D. R. Penn, Surf. Interface Anal. 17, 911, (1991).

[48] S. Tamura, C. J. Powell, D. R. Penn, Surf. Interface Anal. 21, 165, (1994).

[49] E.W. Plummer, W. Eberhardt, Adv. Chem. Phys. 49, 533, (1982); H.-P. Steinrück, Vacuum 45, 715, (1994).

[50] N. Koch, A. Vollmer, I. Salzmann, B. Nickel, H. Weiss, & J. P. Rabe, Phys. Rev. Lett., 96, 156803, (2006).

[51] C. Mariani, F. Allegretti, V. Corradini, G. Contini, V. Di Castro, C. Baldacchini, & M. G. Betti, Phys. Rev. B, 66, 115407, (2002).

[52] H.-P. Steinrück, J. Phys. Condensed Matt., 8, 6465, (1996).

[53] S. Hasegawa, T. Mori, K. Imaeda, S. Tanaka, Y. Yashita, H. Inokuchi, H. Fijimoto, K. Seki, & N. Ueno, J. Chem. Phys., 100, 6969, (1994).

[54] G. N. Gavrila, H. Mendez, T.U. Kampen, D. R. T. Zahn, D. V. Vyalikh,& W. Braun, Appl. Phys. Lett., 85, 4657, (2004).

[55] H. Yamane, & S. Kera, Phys. Rev. B, 68, 033102, (2003).

Chapter 6 Di-idobenzene Isomers Adsorptions on Molecule films of Quinonoid Zwitterion and PVDF

6.1 Di-idobenzene Isomers Adsorbed on Quinonoid Zwitterion: Lock and Key Adsorption Chemistry

Molecules possessing a strong intrinsic dipole can be used for testing if electrostatic dipolar interactions can lead to preferential adsorption on electrostatically biased substrates [1-27]. Both the magnitude of the molecular electrostatic dipole and the frontier orbital symmetry play a dominant role in the adsorption process. Even when intermolecular interactions do not involve any irreversible chemical reaction between the molecular species, there is a balance between the chemical interactions and the electrostatic dipolar interactions [1, 2, 9-26].

Insight into these problems was gained by comparing adsorption of isomeric molecules [28-49]. In this chapter, we investigate di-iodobenzene adsorption/absorption on the zwitterionic molecule (6Z)-4-(butylamino)-6-(butyliminio)-3-oxocyclohexa-1, 4-dien-1-olate [50-52], described in detail in Chapter 4.

Reversible adsorption of weakly adsorbed molecules has been shown to depend on the ferroelectric domain orientation of both organic [14, 15, 53, 54] and inorganic ferroelectrics [18, 19, 20, 25, 55, 56]. Such studies have largely investigated polar adsorbate molecules [14, 15, 18, 19, 20, 25, 53, 54, 55, 56], with the tacit assumption that non polar molecules should be insensitive the ferroelectric polarization domain orientation [18, 19, 20]. The chemistry of the surface can play a role and it would be rare, if not unusual, for the surface chemistry of positive and negative ferroelectric domains to be identical [24, 26]. In

this sense, non polar molecules would not be immune from the surface dipole direction of a ferroelectric surface. Not only would the non polar molecule respond to the surface dipole direction, as all molecules have a finite polarizability, but surface termination, stoichiometry and defect densities can differ with different dipole (polarization) directions.

This interplay between the surface chemical interactions and the electrostatic dipolar interactions can be explored by comparing adsorption of isomeric molecules that are both polar and non polar. The investigation of molecular isomeric effects with the adsorption of the different isomers of di-iodobenzene on molecular zwitterion films demonstrated that the frontier orbital symmetry can both play a dominant role in the adsorption process [57]. For a stronger substrate - adsorbate interaction, particularly reaction chemistry [55, 56], it remains unclear whether it is the differences in the static surface dipole or the differences in the surface chemistry that dominates. For ferroelectrics, the reaction chemistry suggests that it is the surface dipoles that matter, but there is no clear delineation of surface chemistry and surface dipoles where the surface chemistry is photoactivated [58-71].

At 150 K, the initial adsorption of all three isomers of diiodobenzene is found to be similar on a conducting but chemically fairly inert substrate like graphite [49], although a number of isomer-specific effects have been identified for the halogenated and substituted benzene adsorbates on surfaces [48,49]. Such small simple molecules provide a clear test of preferential isomer adsorption, particularly because their intrinsic dipole depends on the isomer: the dipole moment 1,2-di-iodobenzene is the largest with an experimentally determined value of 1.87 D [72] (1.856 D from density functional theory, with the PW91 exchange and correlation potential), while 1,3-di-iodobenzene is intermediate with a static dipole value of 1.19 D [72] (1.297 D from density functional theory), and of course 1,4-di-

iodobenzene has a zero net dipole moment. These different charge distributions are schematically illustrated in figure 6.1. It is, however, 1, 3-disubstituted benzene that shares the same symmetry as the C_6 core of the zwitterion substrate molecules. While molecular dipoles certainly have a profound influence on adsorption [1-27, 73-80], here we show that dipolar interactions alone cannot explain the preferential adsorption of one isomer of di-iodobenzene. The oxygen and nitrogen functional groups of this class of p-benzoquinonemonoimine zwitterions should also play a role, as potentially influencing the chemoselective adsorption chemistry of a "guest" molecule from the vapor [51, 52, 76].

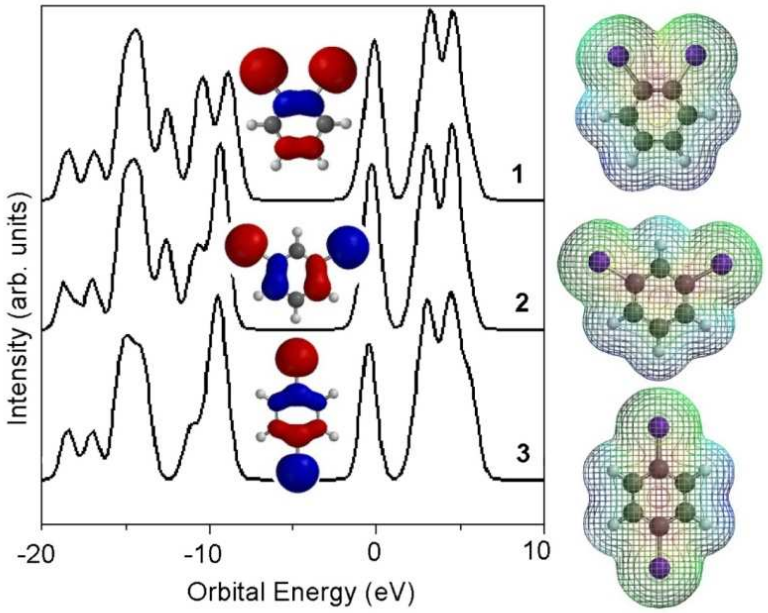

Figure 6.1 Model calculations of the (1) 1,2-di-iodobenzene, (2) 1,3-diiodobenzene, and (3) 1,4-di-iodobenzene density of states obtained by applying equal Gaussian envelopes of 1 eV (black thin line) full width half-maximum to each molecular orbital to account for the solid state broadening in photoemission and then summing but uncorrected for matrix elements and final state effects. The calculated molecular orbitals are shown as a function of orbital energy and are not referenced to any Fermi level. Also shown are the schematics of the highest occupied molecular orbital (HOMO) of each di-iodobenzene, placed between the occupied (left) and unoccupied (right) molecular orbitals. Also shown are schematic representations of the charge densities based on Mulliken charge populations.

6.1.1 Adsorption of Di-iodobenzene on p-benzoquinonemonoimine Zwitterion Molecular Films

The ultraviolet photoemission (UPS) and inverse photoemission (IPES) spectra were taken in a single ultrahigh vacuum chamber to study the placement of both occupied and unoccupied molecular orbitals of the combined zwitterion-di-iodobenzene molecular systems as a function of di-iodobenzene exposure to the samples at 150 K.

The studies were carried out at 150 K, well below the expected desorption temperature of the di-iodobenzenes [49]. Although we do note that while all three isomers of di-iodobenzene will adsorb on the ferroelectric copolymer polyvinylidene (70%) with trifluoroethylene (30%) (PVDF-TrFE) at 150 K, at 160 K, 1, 2-di-iodobenzene and 1, 3-di-iodobenzene do not readily adsorb on PVDF-TrFE, while 1, 4-di-iodobenzene will absorb. Each isomer of di-iodobenzene (Sigma-Aldrich >99% purity for 1, 2-di-iodobenzene and 1, 4-di-iodobenzene; >98% purity for 1,3-di-iodobenzene) was admitted to the vacuum chamber through a standard leak valve and thus absorbed or adsorbed on the zwitterion molecular films from the vapor. Exposures are denoted in Langmuirs (L), where 1 L = 1×10^{-6} Torr s. We believe that there is some photodecomposition because after many (10-20) cycles of absorption/adsorption at 150 K followed by extensive photoemission studies, and desorption at or below 300 K, a trace signal of the iodine 3d core level can be observed at room temperature. Samples were therefore routinely replaced after a maximum of a few cycles, to avoid any contribution from di-iodobenzene fragment contamination as a result of this photodissociation common to many halogenated benzenes.

All three isomers of diiodobenzene adsorb molecularly on 0.5-1 nm thick films of p-benzoquinonemonoimine zwitterions, with the substrates held at 150 K. The characteristic

molecular orbitals of 1, 2-di-iodobenzene, 1, 3-di-iodobenzene, and 1, 4-di-iodobenzene are clearly evident in the combined photoemission and inverse photoemission spectra, shown in figure 6.2 for zwitterion molecular films of identical thickness and preparation. There is, however, no indication of interactions of any of the di-iodobenzenes with the underlying Au substrate, confirming previous observations on clean graphite [49] and copper surfaces [47].

The combined photoemission and inverse photoemission spectra of the p-benzoquinonemonoimine zwitterion molecular films on Au indicate a highest occupiedmolecular orbital (HOMO) to lowest unoccupied molecular orbital (LUMO) gap of 5.8-6.0 eV for the thinner of the films. These experimental values are consistent with the calculated value of 5.8 eV based on the simplistic single molecule semiempirical method NDO-PM3 (neglect of differential diatomic overlap, parametric model number 3), as discussed in detail elsewhere [50].

With increasing exposure of all three isomers of di-iodobenzene, the apparent HOMO-LUMO gap increases, and features appear in the spectra (Figure 6.2) consistent with the molecular orbitals of the pertinent di-iodobenzenes, as seen in figure 6.1. There is agreement of the single molecule calculations with the combined photoemission and inverse photoemission, as seen in figure 6.2. Good agreement is found between the observed (Figure 6.2) and calculated (Figure 6.1 and top of Figure 6.2) levels of the molecular orbitals of the di-iodobenzenes. In fact, the various isomers of di-iodobenzene actually have a very similar electronic structure, as illustrated in figure 6.1, where the calculated density of states (DOS) was obtained by applying equal Gaussian envelopes of 1 eV full width half-maximum to each molecular orbital, to account for the solid state broadening in photoemission, and then summing. There should be differences from

expectations based on a single molecule and a thin film due to intermolecular interactions within the film (solid state effects) and band structure, and the model PM3 is a simplistic semiempirical single molecule ground state calculation not corrected for matrix element effects. Such comparisons with experiments are nevertheless often successful [9-14, 50, 75, 83, 84, 87, 88], as seen here, although the calculated orbital energies must be rigidly shifted in energy by about 5 eV, largely to account for the influence of work function.

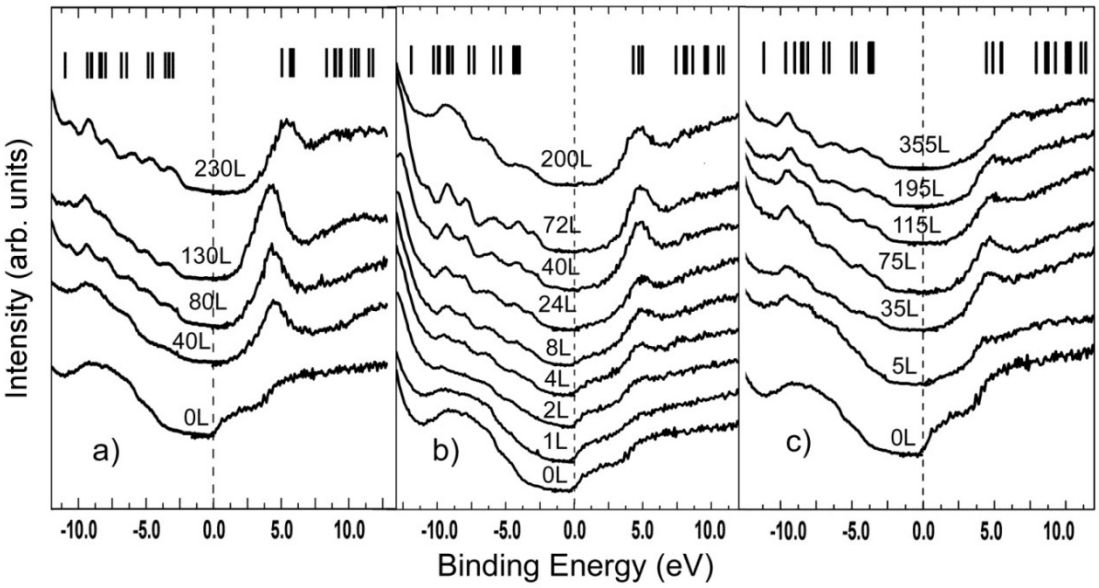

Figure 6.3 Combined photoemission and inverse photoemission of 1 nm thick p-benzoquinonemonoimine zwitterion molecular films as a function of (a) 1, 2-di-iodobenzene, (b) 1, 3-di-iodobenzene, and (c) 1, 4-di-iodobenzene exposure. The exposures were done with the p-benzoquinonemonoimine zwitterion molecular films maintained at 150 K, and exposure is denoted in Langmuirs (L), where 1 L = 1×10^{-6} Torr s. The bars at the top of each panel are the placement of the molecular orbitals rigidly shifted about 5 eV, approximately consistent with the work function. Binding energies are in terms of $E - E_F$.

The adsorption of all of the di-iodobenzenes on the p-benzoquinonemonoimine zwitterion molecular films is seen to be reversible with no characteristic molecular orbitals nor any iodine 3d core level signal evident upon annealing to room temperature. There are clear experimental indications that the isomers, while all adsorbing on the zwitterion molecular films, exhibit isomeric dependence. The exposure-dependent spectra of figure 6.2 reveal that the spectral features corresponding to the signature of diiodobenzene molecular orbitals appear at exposure values depending on the isomer. The 1,2-di-iodobenzene requires 60-80 L exposure to approximately 1 nm thick p-benzoquinonemonoimine zwitterion molecular films at 150 K; the 1,4-di-iodobenzene requires some 10-15 L exposure; and the 1,3-diiodobenzene requires only about 4 L exposure for the molecular orbitals to become evident in the combined photoemission and inverse photoemission spectra. Extending these observations to acoverage dependence on the isomer requires introducing the sticking coefficients S, assuming a linear relation between the exposure x and coverage y

$$y = \frac{S}{q}\left(\frac{x}{x_0}\right) \qquad 6.1$$

where x_0 is the exposure needed to form one monolayer of coverage (roughly 8×10^{18} molecules/m^2) and q is the ratio of adsorbate ionization cross section to that of N_2, neither established here. We may assume that the ionization gauge cross sections of all of the di-iodobenzenes are likely much higher than for nitrogen; for example, the toluene ionization gauge crosssection is 6.4 times greater than nitrogen [92], while it is a factor of 3.5 [92] to 5.7 [93] greater for benzene than nitrogen. Furthermore, one can reasonably assume that the ionization gauge cross section of each of the di-iodobenzenes is in fact similar, as has been

assumed elsewhere [49]. We therefore infer that the sticking coefficient of 1, 3-di-iodobenzene on p-benzoquinonemonoimine zwitterion molecular films is roughly 3-5 times larger than that observed for 1, 4-di-iodobenzene and 15 times larger than for 1, 2-di-iodobenzene adsorption at 150 K. This qualitative trend is even more apparent on thicker (2-3 nm thick) p-benzoquinonemonoimine zwitterion molecular films at 150 K, as detailed in the next section.

6.1.2 Isomeric Dependence of the Di-iodobenzene Adsorption on p-Benzoquinonemonoimine Zwitterion Molecular Films

Another approach to investigating the preferential adsorption and absorption of one particular isomer of di-iodobenzene is to look at the increase in the core level iodine signals with exposure time. This type of experiment was performed on thicker p-benzoquinonemonoimine zwitterion films, approximately 2-3 nm thick. As seen in figure 6.4, significant exposures of 1, 2-di-iodobenzene and 1, 4-di-iodobenzene to thick p-benzoquinonemonoimine zwitterion molecular films at 150 K are necessary for appreciable iodine $3d_{5/2}$ core level signals. This is in strongcontrast with iodine signals of 1, 3-di-iodobenzene adsorption/absorption, which is remarkably more efficient, as seen in figure 6.4. The iodine $3d_{5/2}$ X-ray photoemission core level signal for 1, 3-di-iodobenzene is roughly 70 times larger than observed for 1, 2-di-iodobenzene and 210-250 times larger than observed for 1, 4-di-iodobenzene, using in all cases thick p-benzoquinonemonoimine zwitterion molecular films at 150 K, as summarized in figure 6.4. Again, we see a strong preference for the adsorption/absorption of 1, 3-di-iodobenzene.

The 1, 3-di-iodobenzene exposure-dependent XPS spectra show very large shifts in the I 3d core level binding energies, as evident in figure 6.4. These increases in core level binding energies of ~ 2.5 eV ormore are far greater than observed for 1, 2- and 1, 4-di-iodobenzene (Figure 6.3). Since dissociative chemisorption can be excluded in all data of the adsorption systems we describe here, such large core level shifts should result fromstrong intermolecular interactions or from decreased screening from the substrate with increasing di-iodobenzene film thickness [49], resulting in larger photoemission final state binding energies [10, 94-96]. Both effects would lead to energy shifts, but such final state effects should lead to a decrease [96-98], not an increase, in core level binding energies with increasing di-iodobenzene coverages [49]. Changes in the final state screening [94-96], with increasing di-idodobenzene coverages, also tend to be excluded because there is no change in the HOMO-LUMO gap of the adsorbed 1,3-di-iodobenzenes, as seen in figures 6.2 and 6.6.

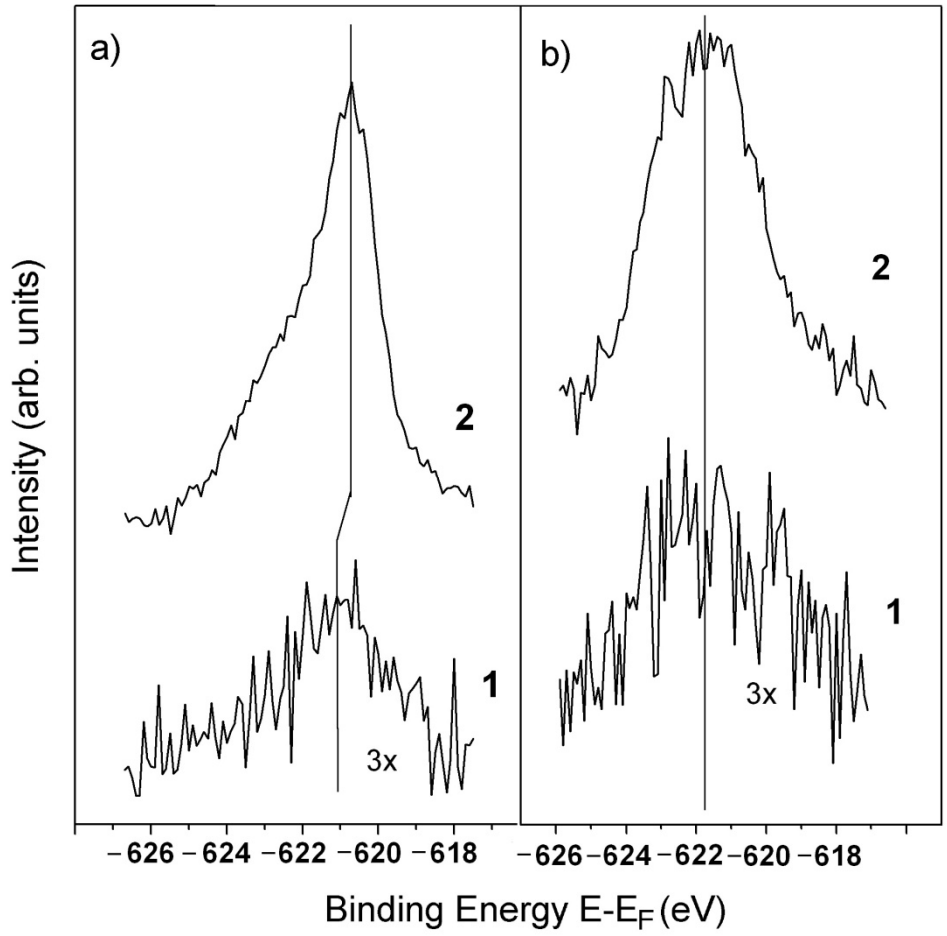

Figure 6.3 $3d_{5/2}$ iodine core level spectra following (a) 1, 2-di-iodobenzene adsorption (1, 5 L exposure; 2, 600 L exposure) and (b) 1, 4-diidobenzene adsorption (1, 250 L exposure; 2, 1200 L exposure) to zwitterion molecular films of identical 3 nm thickness and preparation. Binding energies are in terms of $E - E_F$.

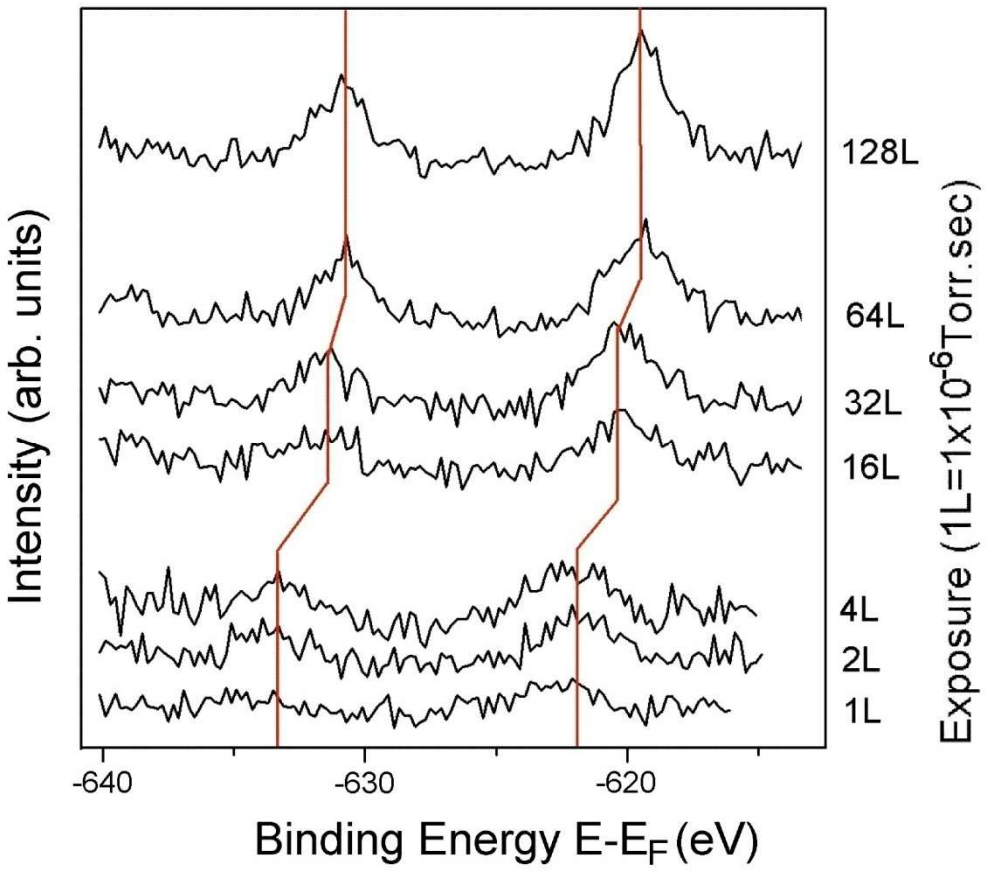

Figure 6.4 X-ray photoemission spectra for I 3d core levels of 1, 3-diiodobenzene adsorbed on 3 nm *p*-benzoquinonemonoimine zwitterions molecular films at 150 K. The core level binding energy shifts of both the I $3d_{5/2}$ and I $3d_{3/2}$ peaks are indicated by vertical bars (see text).

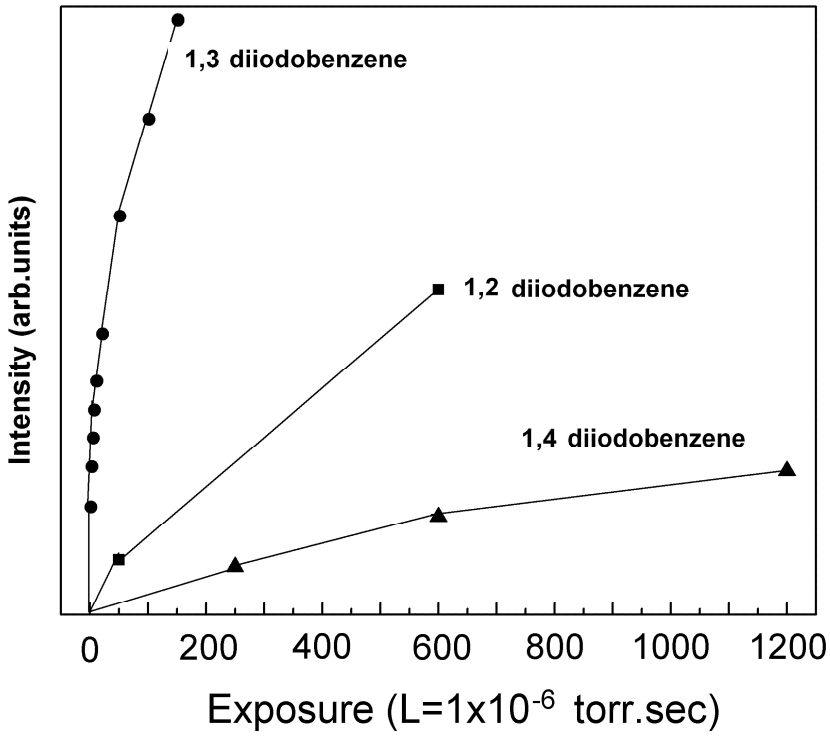

Figure 6.5 Iodine $3d_{5/2}$ core level intensities with increasing exposure of (■) 1,2-di-iodobenzene, (●) 1,3-di-iodobenzene, and (▲) 1,4-di-iodobenzene exposures to 3 nmthick p-benzoquinonemonoimine zwitterion molecular films maintained at 150 K. Exposures are denoted in Langmuirs (L), were 1 L = 1×10^{-6} Torr s.

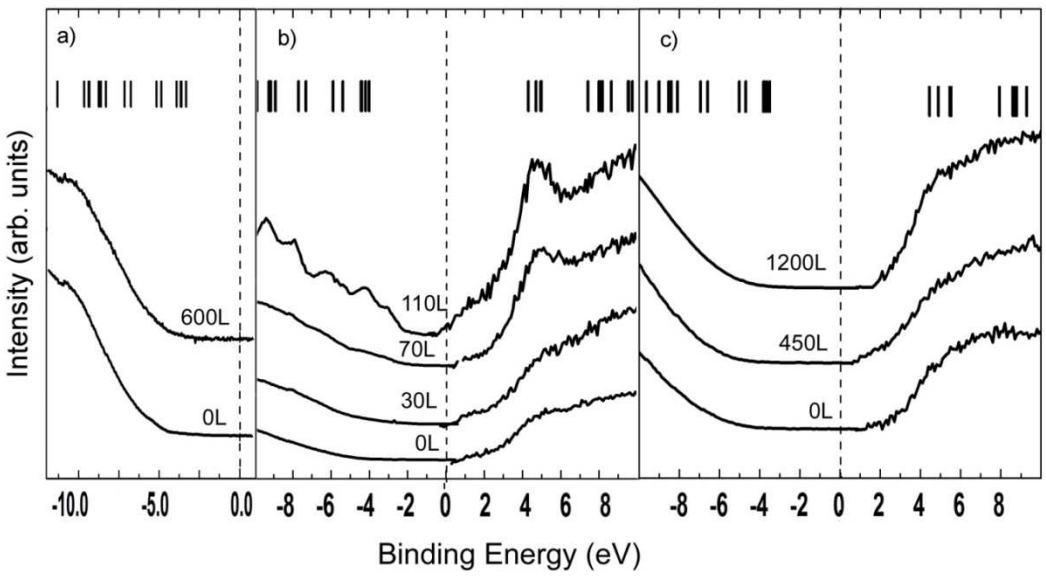

Figure 6.6 Combined photoemission and inverse photoemission of *p*-benzoquinonemonoimine zwitterion molecular films as a function of (a) 1, 2-diiodobenzene, (b)1,3-di-iodobenzene, and (c) 1,4-di-iodobenzene exposure. The p-benzoquinonemonoimine zwitterion molecular films, of identical 3 nm thickness and preparation, were maintained at 150 K, and exposure is denoted in Langmuirs (L), were 1 L = 1×10^{-6} Torr s. The bars at the top of each panel are the placement of the di-iodobenzene molecular orbitals rigidly shifted about 5 eV, approximately consistent with the work function. Binding energies are in terms of $E - E_F$.

Excluding final state effects, and molecular dissociation, the shifts observed in the I 3d core level shift with increasing 1, 3-diiodobenzene coverage can also originate from two different species: an absorbed phase of di-iodobenzene within the p-benzoquinonemonoimine zwitterion molecular films and an adsorbed phase, near or at the surface of the p-benzoquinonemonoimine zwitterion molecular films. With increasing

exposure to di-iodobenzene, the X-ray photoemission iodine signals appear well before the molecular orbital peaks appear in the combined photoemission and inverse photoemission spectra of figure 6.6. The larger probing depth for the iodine $3d_{5/2}$ core level photoemission feature is a result of the different electron mean free paths through the molecular film with the different electron spectroscopies. The different probing depths are related to significantly greater electron kinetic energies (633 eV) in XPS than the valence band photoemission (16 eV), with inverse photoemission being notoriously even more surface sensitive [99, 100]. The I 3d core level feature may be therefore representative of an absorbed phase of 1, 3-di-iodobenzene. It is only with the largest di-iodobenzene exposure values where sites in the vicinity or at the surface become populated and become evident in inverse photoemission and the low(er) photon energy valence band photoemission.

Accordingly, we can partially attribute these different I $3d_{5/2}$ core level binding energies to the differences between absorbed (621.9 $\pm$ 0.2 eV) and adsorbed (619.4 $\pm$ 0.4 eV) 1, 3-diiodobenzene. The initial iodine 3d5/2 core level binding energies for 1,3-di-iodobenzene (621.9 $\pm$ 0.2 eV), 1,2-di-iodobenzene (621.1 $\pm$ 0.4 eV), and 1,4-di-idobenzene (621.7 $\pm$ 0.4 eV) are significantly greater than the binding energy of 620.7 $\pm$ 0.1 eV observed for the initial molecular adsorption of all three isomers on graphite [49] and 1,4-di-idobenzene adsorption on the ferroelectric copolymer polyvinylidene (70%) with trifluoroethylene (30%) with a binding energy value of 620.8 $\pm$ 0.2 eV. While adsorption on a semimetal like graphite is difficult to compare to adsorption on a poorly conducting zwitterion film, the values obtained with dielectric ferroelectric copolymer polyvinylidene (70%) with trifluoroethylene (30%) should be similar if the intermolecular interactions are minimal. In any case, the change in the initial I $3d_{5/2}$ core level binding energy is toward

smaller binding energies with increasing di-iodobenzene coverages on pbenzoquinonemonoimine zwitterion molecular films at 150 K, in contrast to di-iodobenzene adsorption on graphite [49]. The core level binding energies support the contention that there are strong intermolecular interactions between the di-idobenzenes and p-benzoquinonemonoimine zwitterion molecules, especially for 1, 3-di-iodobenzene.

The far greater sticking coefficient and far larger core level binding energy shifts (I 3d5/2 decreasing from 621.9 $\pm$ 0.2 to 619.4 $\pm$ 0.1 eV) with increasing 1, 3-di-iodobenzene coverages suggest that this isomer favors strong π-π interactions with the adjacent p-benzoquinonemonoimine zwitterion molecules. The large iodine 3d core level shifts seen with 1,3-di-iodobenzene are also consistent with an absorbed phase of 1,3-di-iodobenzene followed by adsorption of a surface-related phase on the p-benzoquinonemonoimine zwitterion molecular film, with increasing exposure. Exposure of 1, 2-di-iodobenzene and 1, 4-diiodobenzene to the 3 nm thick p-benzoquinonemonoimine zwitterion molecular films at 150 K does not provide signature of di-iodobenzene molecular orbitals in the combined photoemission and inverse photoemission, even with significant exposure of several hundreds of Langmuirs. As seen in figure 6.6, the characteristic di-idobenzene molecular orbitals are only observed in the combined photoemission and inverse photoemission in the case of 1, 3-di-iodobenzene exposure to thicker (3 nm thick) zwitterion molecular films. Given that there are clear indications of di-iodobenzene adsorption from the core level photoemission, we must conclude that 1, 2-di-iodobenzene and 1, 4-di-iodobenzene exposures (in the range studied here) have only led to absorption within the bulk of the thicker 3 nm p-benzoquinonemonoimine zwitterion molecular films at 150 K, with no surface or near surface adsorption sites occupied. This goes a long way toward explaining

the smaller or negligible iodine X-ray photoemission core level shifts observed (Figure 6.3) for 1,2-di-iodobenzene and 1,4-di-iodobenzene.

These molecules are dielectrics, and even small core level shifts are not a good indication of future trends with continued diiodobenzene adsorption. The XPS core level binding energies will not and should not saturate at a specific value. With extensive adsorption, as when a di-iodobenzene ice is formed at the surface, there are changes to the overall dielectric properties of the combined molecular film, and final state effects will then dominate the photoemission spectra.

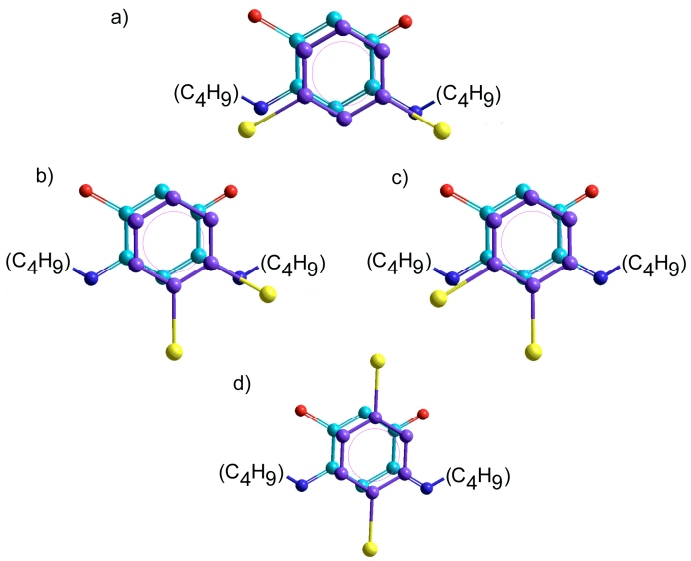

Figure 6.7 Lock and key configuration for the absorption interactions between the di-iodobenzene isomers and the p-benzoquinonemonoimine zwitterion: (a) 1, 3-di-iodobenzene, (b), (c) 1, 2-di-iodobenzene, (d) 1, 4-di-iodobenzene. Color code: nitrogen (dark blue), carbon (light blue and violet), iodine (yellow), oxygen (red).

6.1.3 Summary

Di-iodobenzene adsorption studies on molecular films of the zwitterionic p-benzoquinonemonoimine compound C_6H_2-(⋯NHR)$_2$(⋯O)$_2$ where R = n-C_4H_9 reveal that 1,3-diiodobenzene adsorption is strongly favored. This isomer of diiodobenzene shares the same symmetry as the C_6 core of the p-benzoquinonemonoimine zwitterion compound, suggesting that the frontier molecular orbital symmetry plays a dominant role in preferential isomeric adsorption. Indeed, the highest occupied molecular orbital (HOMO) of 1, 3-di-iodobenzene bears considerable resemblance to the lowest unoccupied molecular orbital (LUMO) of the core of the p-benzoquinonemonoimine zwitterions compound. This molecular recognition phenomenon should therefore be understood within models going beyond simple dipolar interactions, as there are indications that the HOMO of 1, 3-di-iodobenzene can strongly hybridize with the LUMO of this p-benzoquinonemonoimine zwitterion compound, if the relative orientation of figure 6.7 is adopted.

It is clear that there is one orientation of 1, 3-di-iodobenzene that favors strong π-π interactions (see Figure 6.7), with a concomitant electric dipole coalignment with the adjacent p-benzoquinonemonoimine molecules. The two orientations of 1, 2-di-iodobenzene that favor π-π interactions are shown in figure 6.7, with electric dipole coalignment, with the adjacent p-benzoquinonemonoimine molecules, but the alignment is imperfect and the symmetry not preserved. For 1,4-di-iodobenzene, there is one symmetry-preserving orientation that favors π-π interactions with the adjacent p-benzoquinonemonoimine molecules, but apart from some induced dipole in the 1,4-diiodobenzene, there is no expected real dipole alignment (see Figure 6.7). If the multiplicity of available favorable orientations based on dipole and π-π interactions is the

key factor determining preferential isomeric attachment, then absorption of 1, 2-diiodobenzene should be preferred, in contradiction with our experimental findings. Our experiments demonstrate that reversible isomer-selective adsorption chemistry of small molecules is indeed possible, with a preferential adsorption mechanism illustrating that symmetry does matter.

6.2 Di-idobenzene Isomers Adsorbed on PVDF: Dipole Orientation Mediated Chemistry at Polymer Surfaces

Now we turn to our investigation of di-iodobenzene adsorption/absorption on crystalline copolymers of polyvinylidene with trifluoroethylene (PVDF-TrFE), a molecular ferroelectric. As with some prior studies of adsorption on ferroelectric substrates [18], we compare a polar and nonpolar species, but by investigating two different isomers of di-iodobenzene, we compare molecules with far more similar surface chemistry than in prior investigations involving adsorption on ferroelectrics. Key to any fundamental understanding is performing the experiments at constant temperature, to eliminate pyroelectric contributions to the surface charge, a complication common to ferroelectric materials.

While molecular dipoles certainly have a profound influence in adsorption [1-7, 15, 53, 72-79], here we show that dipolar interactions alone cannot explain the preferential adsorption of one isomer of di-iodobenzene.

6.2.1 The Adsorption of Di-iodobenzene on Ferroelectric Films of the Copolymer 70% Vinylidene Fluoride with 30% Trifluoroethylene, P(VDF-TrFE 70:30)

In Section 2.5 and 2.7.3, Chapter 2, we have shown the fabrication and "non-contact" ferroelectric poling process of ultrathin ferroelectric films of the copolymer 70% vinylidene fluoride with 30% trifluoroethylene, P(VDF-TrFE 70:30) and discussed the ferroelectric domain orientations and hysteresis which were determined and imaged in ambient environment by means of piezoresponse force microscopy [118].

In our experiment, combined ultraviolet photoemission (UPS) and inverse photoemission (IPES) spectra [11, 14, 18, 75, 83, 85, 90, 76, 103, 111] were taken in a single ultrahigh vacuum chamber to study the placement of both occupied and unoccupied molecular orbitals of the combined di-iodobenzene – P(VDF-TrFE, 70:30) molecular film system, as a function of di-iodobenzene exposure to the samples at 150 K. The studies were carried out at 150 K, well below the expected desorption temperature of the di-iodobenzenes [49, 57]. Here, each isomer of di-iodobenzene (Sigma-Aldrich >99% purity for 1,2-di-iodobenzene and 1,4-di-iodobenzene; >98% purity for 1,3-di-iodobenzene) were admitted to the vacuum chamber through a standard leak valve, and thus absorbed or adsorbed on the zwitterion molecular films from the vapor. Exposures are denoted in Langmuirs (L), where 1 L=1x10^{-6}torr.sec.

Di-iodobenzene will adsorb molecularly on thin ferroelectric films of the copolymer 70% vinylidene fluoride with 30% trifluoroethylene, P(VDF-TrFE 70:30), with the substrates held at 150 K as seen in Figure 6.9. As with 1,2-di-iodobenzene, 1,3-di-iodobenzene and 1,4-di-iodobenzene adsorption on zwitterionic *p*-benzoquinonemonoimine compound $C_6H_2(\underline{\cdots}NHR)_2(\underline{\cdots}O)_2$ where R = *n*-C_4H_9 molecular films [57], the characteristic

molecular orbitals of 1,4-di-iodobenzene are clearly evident in the combined photoemission and inverse photoemission, shown in Figure 6.8. Indeed the combined photoemission and inverse photoemission spectra for 1, 4-di-iodobenzene adsorption on *p*-benzoquinonemonoimine zwitterion molecular films [57] and P(VDF-TrFE 70:30), shown here, are very similar.

We believe that there is some decomposition, at least with annealing of adsorbed di-iodobenzene on P(VDF-TrFE 70:30), because strong signal of the iodine 3d core level can be observed at room temperature and above with post exposure annealing of the sample, as indicated in Figure 6.9 for 1,4-di-idobenzene. Samples were therefore routinely replaced to avoid any contribution from di-iodobenzene fragment contamination, as a result of this dissociation common to all of the di-iodobenzenes adsorbed on the P(VDF-TrFE 70:30) substrates at 150 K. This strong chemisorption and possible decomposition is unlike with di-iodobenzene absorption/adsorption on the *p*-benzoquinonemonoimine zwitterion molecular films at 150 K, where many adsorption and desorption cycles (>20) were required for traces of the di-iodobenzene to remain at room temperature after annealing.

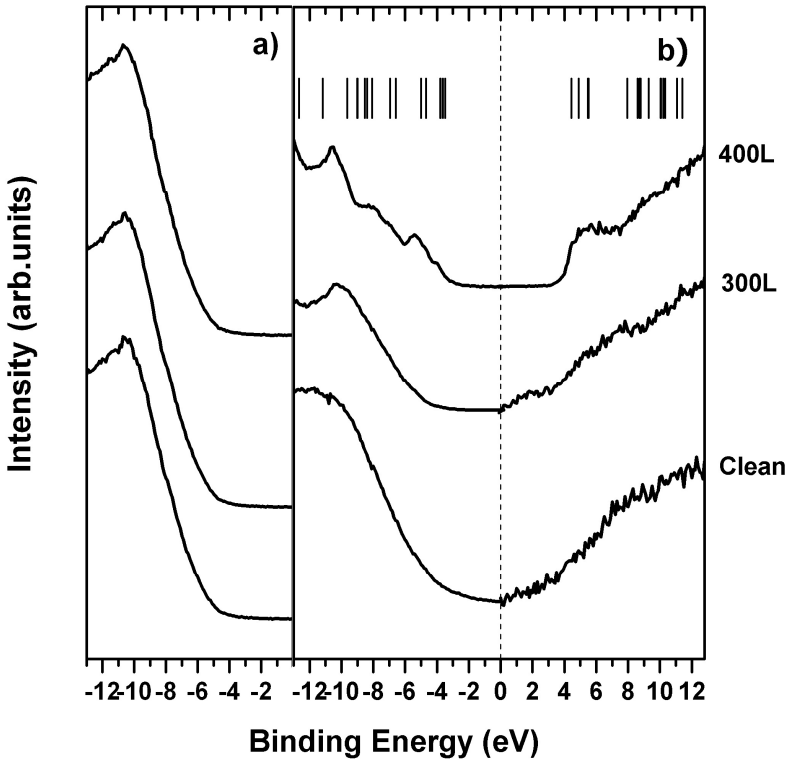

Figure 6.8 The combined photoemission and inverse photoemission of about 3 nm thick copolymer 70% vinylidene fluoride with 30% trifluoroethylene, P(VDF-TrFE 70:30) molecular films as a function of (a) 1,2-di-iodobenzene, (b) 1,4-di-iodobenzene exposure. The exposures were done with the P(VDF-TrFE 70:30) molecular films maintained at 150 K, and exposure is denoted in Langmuirs (L), where 1 L=1x10^{-6}torr.sec. The bars at the top of the panels on the right are the placement of the molecular orbitals rigidly shifted by about 5 eV, approximately consistent with the work function. Binding energies are referenced with respect to the Fermi edge in terms of E-E_F, thus making occupied state energies negative.

In spite of the possible fragmentation upon adsorption, the combined photoemission and inverse photoemission spectra of 1, 4-di-iodobenzene and the apparent HOMO-LUMO gap are consistent with the molecular orbitals of the 1, 4-di-iodobenzene, as seen in figure 6.8. There is agreement of the single molecule calculations with the combined photoemission and inverse photoemission, as seen in figure 6.8. Good agreement is found between the observed (Figure 6.8), and calculated (top of Figure 6.8) energy levels of the molecular orbitals of 1-4-di-iodobenzenes using a single molecule semiempirical molecular orbital calculation (PM3). There should be differences from expectations based on a single molecule and a thin film due to intermolecular interactions within the film (solid state effects) and band structure, and the semiempirical model PM3 is a simplistic semi-empirical single molecule ground state calculation not corrected for matrix element effects. This type of comparison with experiments has been, however, very successful in modeling all of the isomers of di-iodobenzene adsorbed/absorbed on *p*-benzoquinonemonoimine zwitterion molecular films [57], although, as seen here, the calculated orbital energies must be rigidly shifted in energy by about 5 eV, largely to account for the influence of work function.

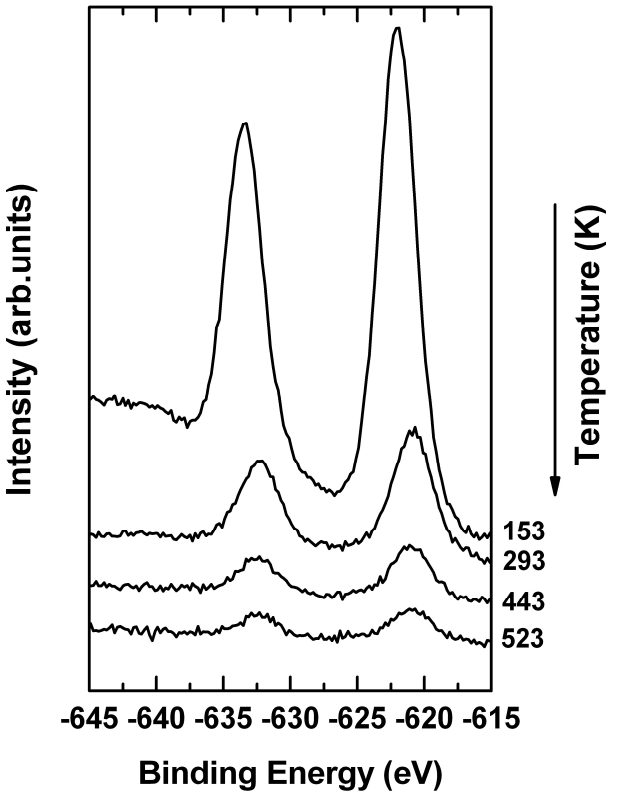

Figure 6.9 X-ray photoemission spectra for both the I $3d_{5/2}$ and I $3d_{3/2}$ core level features of 1,4-di-iodobenzene adsorbed on 3 nm thick copolymer 70% vinylidene fluoride with 30% trifluoroethylene, P(VDF-TrFE 70:30) molecular films following exposures of 400 Langmuirs at 150 K. The P(VDF-TrFE 70:30) molecular film has been poled up. Binding energies are referenced with respect to the Fermi edge in terms of $E-E_F$, thus making occupied state energies negative.

The initial iodine $3d_{5/2}$ core level binding energies for 1,2-di-iodobenzene and 1,4-di-idobenzene adsorption on the ferroelectric copolymer polyvinylidene (70%) with trifluroethylene (30%) are similar, with a binding energy value of 620.8 ± 0.2 eV. These

values are close to the core level binding energies observed with initial 1,2-di-iodobenzene (621.1±0.4 eV) and 1,4-di-idobenzene (621.7±0.4 eV) adsorption/absorption on on *p*-benzoquinonemonoimine zwitterion molecular films [57], and extremely similar to the binding energy of 620.7±0.1 eV observed for the initial molecular adsorption of all three isomers on graphite [49]. While this also suggests that the initial adsorption of di-iodobenzenes on P(VDF-TrFE 70:30) at 150 K is indeed molecular, this does not exclude partial dissociation nor does this exclude strong chemisorption.

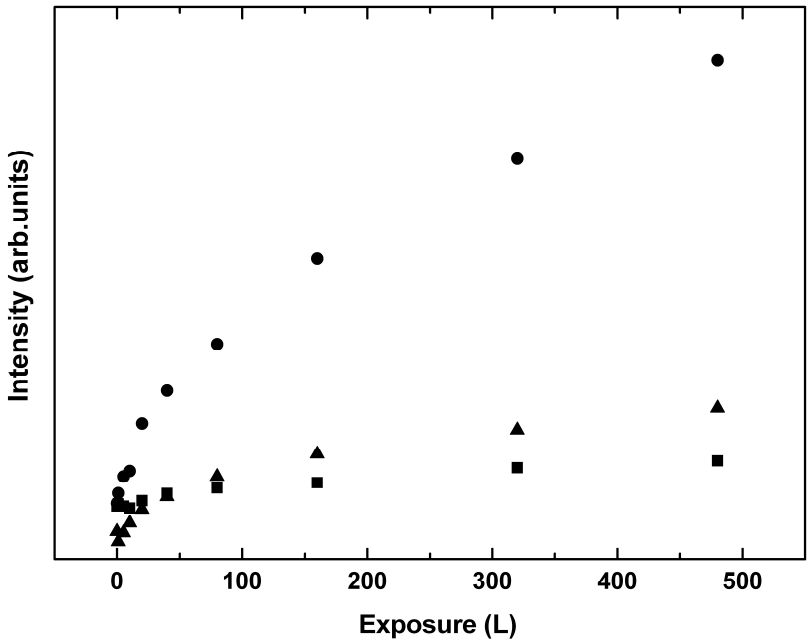

Figure 6.10 The iodine $3d_{5/2}$ core level intensities with increasing exposure of (■) 1,2-di-iodobenzene, (▲)1,3-di-iodobenzene and (●) 1,4-di-iodobenzene exposures to 3 nm thick copolymer 70% vinylidene fluoride with 30% trifluoroethylene, P(VDF-TrFE 70:30) molecular films maintained at 150 K. Exposures are denoted in Langmuirs (L), were 1 L=1x10^{-6}torr.sec. The P(VDF-TrFE 70:30) molecular films have all been poled up.

What is clear is that the appearance of the di-iodobenzene molecular orbitals requires very large exposures of 1, 2-di-iodobenzene, compared to 1, 4-di-iodobenzene, for adsorption on the P(VDF-TrFE 70:30) substrates held at 150 K. In other words, the initial sticking coefficient of 1, 2-di-iodobenzene on the P(VDF-TrFE 70:30) substrates held at 150 K is low compared to that for 1,4-di-iodobenzene. Either 1, 2-di-iodobenzene does not readily adsorb on the P(VDF-TrFE 70:30) substrate, or the fact that the films are naturally poled up after growth inhibits 1,2-di-iodobenzene adsorption on the P(VDF-TrFE 70:30) substrates. As demonstrated below, we show that in fact the latter is true. This suggestion that 1,4-di-iodobenzene adsorption on P(VDF-TrFE 70:30) substrates held at 150 K is more facile than 1,2-di-iodobenzene adsorption, as indicated by the combined photoemission and inverse photoemission spectra that is reflected in the iodine core level intensities, as summarized in Figure 6.10.

6.2.2 The influence of ferroelectric poling on di-iodobenzene adsorption on Ferroelectric Films of the Copolymer 70% Vinylidene Fluoride with 30% Trifluoroethylene, P(VDF-TrFE 70:30)

The preferential adsorption and absorption of one particular isomer of di-iodobenzene on thicker *p*-benzoquinonemonoimine zwitterion molecular films at 150 K, is clearly evident from the iodine $3d_{5/2}$ core level signals, as well as combined photoemission and inverse photoemission [57]. The strong preference for the adsorption/absorption of 1,4 di-iodobenzene on P(VDF-TrFE 70:30) substrates held at 150 K, is seen here to be strongly influenced by the direction of the ferroelectric domains, as seen in Figure 6.11.

The far greater sticking coefficient evident from the I $3d_{5/2}$ intensities with 1,4-di-iodobenzene than is observed with 1, 2-di-iodobenzene exposure to P(VDF-TrFE 70:30) substrates held at 150 K, occurs with the ferroelectric poling up along the surface normal. The reverse is true when the ferroelectric polarization is reverse to down, as seen in Figure 6.12. In fact there is little difference in sticking coefficient for 1,4-di-iodobenzene adsorption on P(VDF-TrFE 70:30) substrates held at 150 K and poled up and the sticking coefficient for 1,2-di-iodobenzene adsorption on P(VDF-TrFE 70:30) substrates held at 150 K and poled down. The apparent differences in sticking coefficient are only apparent when di-iodobenzene adsorption on the P(VDF-TrFE 70:30) substrates, held at 150 K, is compared for one poling direction, as is the case in Figure 6.10.

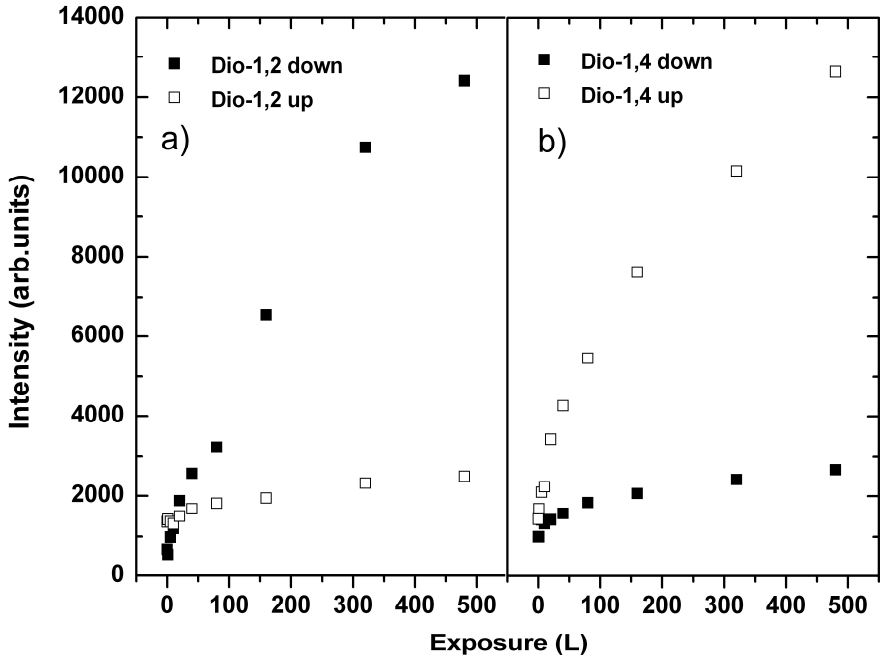

Figure 6.11 The iodine $3d_{5/2}$ core level intensities with increasing exposure of (a) 1,2-di-iodobenzene and (b) 1,4-di-iodobenzene exposures to 3 nm thick copolymer 70% vinylidene fluoride with 30% trifluoroethylene, P(VDF-TrFE 70:30) molecular films maintained at 150 K poled both up (□) and down (■). Exposures are denoted in Langmuirs (L), were 1 L=1x10^{-6}torr.sec.

As with adsorption of the various isomers of di-iodobenzene on the *p*-benzoquinonemonoimine zwitterion molecular films at 150 K [57], there is a strong dependence of the choice of isomer on the adsorption on P(VDF-TrFE 70:30) molecular films, but this isomer dependence is also strongly dependent of the direction of the ferroelectric poling. Even more important, unlike prior studies [18-20], the adsorption of the non polar 1, 4-di-iodobenzene also depends on the direction of the ferroelectric

polarization. This implicates the changes in surface chemistry that occur with reversal of the ferroelectric polarization: hydrogen-terminated when poled up and fluorine terminated when poled down. Although this is a special case as there is strong chemisorption occurring with di-iodobenzene adsorption on P(VDF-TrFE 70:30) molecular films, this means that like with adsorption on inorganic ferroelectrics [119], surface chemistry cannot be *a priori* excluded when the ferroelectric polarization is reversed.

6.2.3 Summary

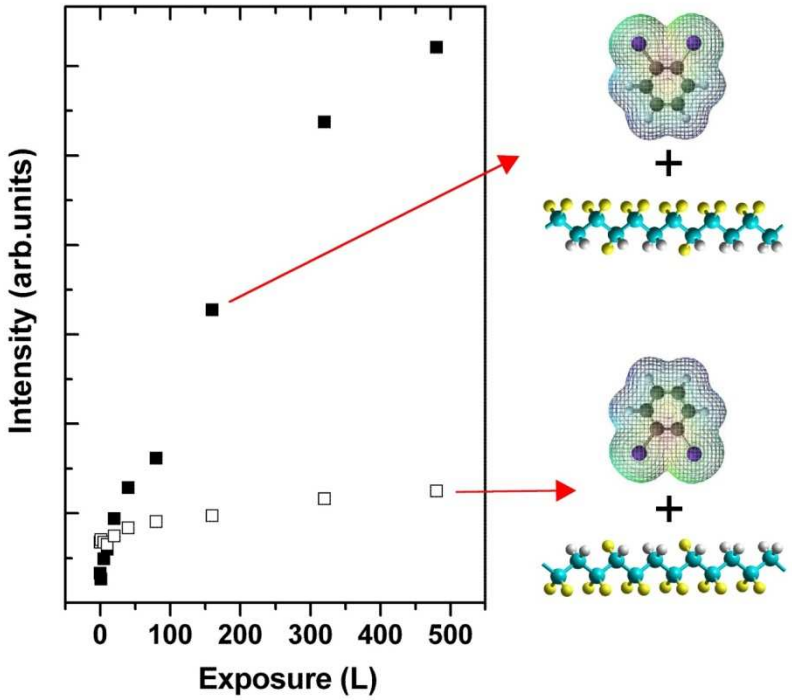

Figure 6.12 The iodine $3d_{5/2}$ core level intensities with increasing exposure of 1,2-di-iodobenzene to 3 nm thick copolymer 70% vinylidene fluoride with 30% trifluoroethylene, P(VDF-TrFE 70:30) molecular films maintained at 150 K poled both up (□) and down (■) and the schematic representation of 1, 2-di-iodobenzene absorbed on PVDF with different ferroelectric polarization. Exposures are denoted in Langmuirs (L), were 1 $L=1x10^{-6}$torr.sec.

By changing the ferroelectric polarization direction, isomer specific interfacial chemistry can be engineered. Di-idobenzene adsorption studies on P(VDF-TrFE 70:30)

molecular films, reveal that 1,2-di-iodobenzene adsorption is strongly favored when the ferroelectric polarization is down (as shown in figure 6.11 and 6.12), while 1,4-di-iodobenzene adsorption is strongly favored when the ferroelectric polarization is up. Because these experiments are isothermal, pyroelectric contributions to this selectively can be excluded. The implication is that while interface dipole orientation can strongly influence adsorption kinetics, interface chemistry can trump the influence of the interface dipole, as has been previously suggested [119]. This selective chemistry based on phenomenon related to the ferroelectric polarization orientation should therefore be understood within models going beyond simple dipolar interactions, and complements recent demonstrations that the frontier orbitals matter in adsorption and chemisorption at the molecule-molecule interface [57].

References

[1] V. S. Lvov, R. Naaman, V. Tiberkevich, Z. Vage, Chem. Phys. Lett. 381, 650–653, (2003).

[2] D. Cahen, R. Naaman, Z. Vager, Adv. Funct. Mater. 15, 1571–1578, (2005).

[3] C. G. Duan, W. N. Mei, W. G. Yin, J. J. Liu, J. R. Hardy, S. Ducharme, P. A. Dowben, Phys. Rev. B 69, 235106, (2004).

[4] M. Kuehn, H. Kliem, Phys. Status Solidi B 245, 213–223, (2008).

[5] W. Guo, S. X. Du, Y. Y. Zhang, W. A. Hofer, C. Seidel, L. F. Chi, H. Fuchs, H.-J. Gao, Surf. Sci. 603, 2815–2819, (2009).

[6] M. Feng, L. Gao, Z. Deng, W. Ji, X. Guo, S. Du, D. Shi, D. Zhang, D. Zhu, H. Gao, J. Am. Chem. Soc. 129, 2204–2205, (2007).

[7] P. A. Lewis, C. E. Inman, F. Maya, J. M. Tour, J. E. Hutchison, P. S. Weiss, J. Am. Chem. Soc. 127, 17421–17426, (2005).

[8] H. J. Gao, K. Sohlberg, Z. Q. Xue, H. Y. Chen, S. M. Hou, L. P. Ma, X. W. Fang, S. J. Pang, S. J. Pennycook, Phys. Rev. Lett. 84, 1780–1783, (2000).

[9] P. A. Dowben, L. G. Rosa, C. C. Ilie, J. Xiao, J. Electron Spectrosc.Relat. Phenom. 174, 10–21, (2009).

[10] J. Xiao, P. A. Dowben, J. Mater. Chem. 19, 2172–2178, (2009).

[11)] J. Xiao, A. Sokolov, P. A. Dowben, Appl. Phys. Lett. 90, 242907, (2007).

[12] L.G. Rosa, J. Xiao, Ya. B. Losovyj, Y. Gao, I.N. Yakovkin, X. C. Zeng, P.A. Dowben, J. Am. Chem. Soc. 127, 17261–17265, (2005).

[13] L. G. Rosa, P. A. Jacobson, P. A. Dowben, J. Phys. Chem. B 110, 7944–7950, (2006).

[14] P. A. Dowben, L. G. Rosa, C. C. Ilie, Z. Phys. Chem. 222, 755–778, (2008).

[15] N. L. Levshin, S. G. Yudin, A. P. Diankina, Moscow Univ. Phys.Bull. 52, 71–74, (1997).

[16] N. L. Levshin, S. G. Yudin, Vysokomol. Soedin., Ser. B 46, 1981 (Eng. Transl.), (2004). N. L. Levshin, S. G. Yudin, Poly. Sci., Ser. B 46, 348, (2004).

[17] N. L. Levshin, S. A. Pestova, S. G. Yudin, Colloid J. 63, 205, (2001).

[18] Y. Yun, E. I. Altman, J. Am. Chem. Soc. 129, 15684, (2007).

[19] K. Garrity, A. M. Kolpak, S. Ismail-Beigi, E. I. Altman, Adv.Mater. 22, 2969–2973, (2010).

[20] Y. Yun, L. Kampschulte, M. Li, D. Liao, E. I. Altman, J. Phys. Chem. C 111, 13951, (2007).

[21] A. L. Cabrera, G. Tarrach, P. Lagos, G. B. Cabrera, Ferroelectrics 281, 53, (2002).

[22] D. Li, M. H. Zhao, J. Garra, A. M. Kolpak, A. M. Rappe, D. A. Bonnell, J. M. Vohs, Nat. Mater. 7, 473, (2008).

[23] J. M. Vohs, M. A. Barteau, J. Phys. Chem. 95, 297–302, (1991).

[24] M. H. Zhao, D. A. Bonnell, J. M. Vohs, Surf. Sci. 603, 284, (2009).

[25] J. Garra, J. M. Vohs, D. A. Bonnell, Surf. Sci. 603, 1106, (2009).

[26] M. H. Zhao, D. A. Bonnell, J. M. Vohs, Surf. Sci. 602, 2849–2855, (2008).

[27] Z. Zhang, P. Sharma, C.N. Borca, P.A. Dowben, A. Gruverman, Appl. Phys. Lett. 97, 243702, (2010).

[28] A. Ahmadi, G. Attard, J. Feliu, A. Rodes, Langmuir 15, 2420–2424, (1999).

[29] A. J. Gellman, ACS Nano 4, 5–10, (2010).

[30] G. A. Attard, J. Phys. Chem. B 105, 3158–3167, (2001).

[31] D. S. Sholl, A. J. Gellman, AIChE J. 55, 2484–2490, (2009).

[32] G. Held, M. J. Gladys, Top. in Catal. 48, 128–136, (2008).

[33] J. N. James, D. S. Sholl, Curr. Opin. Colloid Interface Sci. 13, 60–64, (2008).

[34] T. Greber, Z. Sljivancanin, R. Schillinger, J. Wider, B. Hammer, Phys. Rev. Lett. 96, 056103, (2006).

[35] A. Kühnle, T. R. Linderoth, F. Besenbacher, J. Am. Chem. Soc. 128, 1076–1077, (2006).

[36] S. Blankenburg, W. G. Schmidt, Phys. Rev. Lett. 99, 196107, (2007).

[37] Q. Chen, N. V. Richardson, Nat. Mater. 2, 324–328, (2003).

[38] A. Kühnle, T. R. Linderoth, B. Hammer, F. Besenbacher, Nature 415, 891–893, (2002).

[39] N. M. Santagata, A. M. Lakhani, B. F. Davis, P. Luo, M. B. Nardelli, T. P. Pearl, J. Phys. Chem. C 114, 8917–8925, (2010).

[40] M. Graff, J. Bukowska, Vib. Spectrosc. 52, 103–107, (2010).

[41] M. Bieri, T. Burgi, Chem. Phys. Chem. 7, 514–523, (2006).

[42] S. De Feyter, A. Gesquiere, K. Wurst, D. B. Amabilino, J. Veciana, F. C. De Schryver, Angew. Chem., Int. Ed. 40, 3217, (2001).

[43] C. Mondelli, A. Vargas, G. Santarossa, A. Baiker, J. Phys. Chem. C 113, 15246–15259, (2009).

[44] R. Raval, Chem. Soc. Rev. 38, 707–721, (2009).

[45] S. M. Barlow, S. Louafi, D. Le Roux, J. Williams, C. Muryn, S. Haq, R. Raval, Langmuir 20, 7171–7176, (2004).

[46] S. Haq, N. Liu, V. Humblot, A. P. J. Jansen, R. Raval, Nature Chem. 1, 409–414, (2009).

[47] B. I. Kim, Langmuir 22, 9272–9280, (2006).

[48] J. M. Meyers, A. J. Gellman, Surf. Sci. 337, 40, (1995).

[49] K. Fukutani, N. Wu, P. A. Dowben, Surf. Sci. 603, 2964–2971, (2009).

[50] J. Xiao, Z.-Z. Zhang, D. Wu, L. Routaboul, P. Braunstein, B. Doudin, Ya. B. Losovyj, O. Kizilkaya, L. G. Rosa, C. N. Borca, A. Gruverman, P. A. Dowben, Phys. Chem. Chem. Phys. 12, 10329–10340, (2010).

[51] O. Siri, P. Braunstein, Chem. Commun. 208–209, (2002).

[52] P. Braunstein, O. Siri, J.-P. Taquet, M.-M. Rohmer, M. Bénard, R. Welter, J. Am. Chem. Soc. 125, 12246–12256, (2003).

[53] B. Martin, G. Vizdrik, H. Kliem, J. Applied Physics 105, 084114, (2009).

[54] L. G. Rosa, P. A. Jacobson, P. A. Dowben, J. Phys. Chem. B 110, 7944-7950, (2006).

[55] Y. Inoue, I. Yoshioka, K. Sato, J. Phys. Chem. 88, 1148-1151, (1984).

[56] Y. Inoue, Y. Watanabe, Catalysis Today 16, 487-494, (1993).

[57] Z. Zhang, J. Alvira, X. Barbosa, L. G. Rosa, L. Routaboul, P. Braunstein, B. Doudin, P.A. Dowben, J. Physical Chemistry C 115, 2812–2818, (2011).

[58] N. V. Burbure, P. A. Salvador, G. S. Rohrer, J. Am. Ceramic Soc. 89, 2943, (2006).

[59] J. L. Giocondi, G. S. Rohrer, Chem. Mater. 13, 241, (2001).

[60] J. L. Giocondi, G. S. Rohrer, J. Phys. Chem. B 105, 8275, (2001).

[61] S.V. Kalinin, D.A. Bonnell, T. Alvarez, X. Lei, Z. Hu, J.H. Ferris, Q. Zhang, S. Dunn, Nano Lett. 2, 589, (2002).

[62] J.N. Hanson, B.J. Rodriguez, R.J. Nemanich, A. Gruverman, Nanotechnology, 17, 4946, (2006).

[63] S. Dunn, P.M. Jones, D.E. Gallardo, J. Am. Chem. Soc. 129, 8724, (2007).

[64] X. Liu, K. Kitamura, K. Terabe, H. Hatano, N. Ohashi, Appl. Phys. Lett. 91, 044101, (2007).

[65] S. Dunn, D. Tiwari, Appl. Phys. Lett. 93, 092905, (2008).

[66] S. Dunn, D. Cullen, E. Abad-Garcia, C. Bertoni, R. Carter, D. Howorth, R.W. Whatmore, Appl. Phys. Lett. 85, 3537 (2004).

[67] C. Ke, X. Wang, X.P. Hu, S.N. Zhu, M. Qi, J. Appl. Phys. 101, 064107, (2007)

[68] S. Habicht, R.J. Nemanich, A. Gruverman, Nanotechnology 19, 495303, (2008).

[69] J.N. Hanson, B.J. Rodriguez, R.J. Nemanich, A. Gruverman, Nanotechnology, 17, 4946, (2006).

[70] A. Haussmann, P. Milde, C. Erler, and L. M. Eng, Nano Letters, Vol. 9, No. 2, 763-768, (2009).

[71] M. Müller, E. Soergel, K. Buse, Appl. Phys. Lett, 83, 1824, (2003).

[72] A. Mansingh, D. B. McLay, K. O. Lim, Can. J. Phys. 52, 2365–2369, (1974).

[73] H. Ishii, K. Sugiyama, E. Ito, K. Seki, Adv. Mater. 11, 605, (1999).

[74] X. Y. Zhu, Surf. Sci. Rep. 56, 1, (2004).

[75] S. Balaz, A. N. Caruso, N. P. Platt, D. I. Dimov, N. M. Boag, J. I. Brand, Ya. B. Losovyj, P. A. Dowben, J. Phys. Chem. B 111, 7009–7016, (2007).

[76] A. Natan, L. Kronik, H. Haick, R. T. Tung, Adv. Mater. 19, 4103–4117, (2007).

[77] D. Taguchi, N. Kajimoto, T. Manaka, M. Iwamoto, J. Chem.Phys. 127, 044703, (2007).

[78] A. Natan, Y. Zidon, Y. Shapira, L. Kronik, Phys. Rev. B 73, 193310, (2006).

[79] D. Deutsch, A. Natan, Y. Shapira, L. Kronik, J. Am. Chem. Soc. 129, 2989–2997, (2007).

[80] M. L. Sushko, A. L. Shluger, Adv. Funct. Mater. 18, 2228–2236, (2008).

[81] Q.-Z. Yang, O. Siri, P. Braunstein, Chem. Commun. 2660–2662, (2005).

[82] Q.-Z. Yang, O. Siri, H. Brisset, P. Braunstein, Tetrahedron Lett. 47, 5727–5731, (2006).

[83] B. Xu, J. Choi, A. N. Caruso, P. A. Dowben, Appl. Phys. Lett. 80, 4342–4344, (2002).

[84] J. Xiao, P. A. Dowben, J. Phys.: Condens. Matter 21, 052001, (2009).

[85] J. Choi, C. N. Borca, P. A. Dowben, A. Bune, M. Poulsen, S. Pebley, S. Adenwalla, S. Ducharme, L. Robertson, V. M. Fridkin, S. P. Palto, N. Petukhova, S. G. Yudin, Phys. Rev. B 61, 5760, (2000).

[86] A. Sokolov, C.-S. Yang, L. Yuan, S.-H. Liou, R. Cheng, H.-K. Jeong, T. Komesu, B. Xu, C. N. Borca, P. A. Dowben, B. Doudin, Europhys. Lett. 58, 448–454, (2002).

[87] J. Zhang, D. N. McIlroy, P. A. Dowben, H. Zeng, G. Vidali, D. Heskett, M. Onellion, J. Phys.: Condens. Matter 7, 7185–7194, (1995).

[88] D. N. McIlroy, J. Zhang, P. A. Dowben, D. Heskett, Mater. Sci. Eng., A 217/218, 64, (1996).

[89] D.-Q. Feng, D. Wisbey, Ya. B. Losovyj, Y. Tai, M. Zharnikov, P. A. Dowben, Phys. Rev. B 74, 165425, (2006).

[90] J. Xiao, L. G. Rosa, M. Poulsen, D. -Q. Feng, S. Reddy, J. M. Takacs, L. Cai, J. Zhang, S. Ducharme, P. A. Dowben, J. Phys.: Condens. Matter 18, L155, (2006).

[91] J. Choi, P. A. Dowben, S. Ducharme, V. M. Fridkin, S. P. Palto, N. Petukhova, S. G. Yudin, Phys. Lett. A 249, 505, (1998).

[92] J. R. Young, J. Vac. Sci. Technol. 10, 212, (1973).

[93] F. W. Lampe, J. L. Franklin, F. H. Field, J. Am. Chem. Soc. 79, 6129, (1957).

[94] J. E. Ortega, F. J. Himpsel, D. Li, P. A. Dowben, Solid State Commun. 91, 807, (1994).

[95] P. A. Dowben, Surf. Sci. Rep. 40, 151, (2000).

[96] N. Sato, K. Seki, H. J. Inokuchi, J. Chem. Soc., Faraday Trans. II 77, 1621, (1981).

[97] H. Fukagawa, H. Yamane, T. Kataoka, S. Kera, M. Nakamura, K. Kudo, N. Ueno, Phys. Rev. B 73, 245310, (2006).

[98] P. G. Schroeder, C. B. France, J. B. Park, B. A. Parkinson, J. Phys. Chem. B 107, 2253–2261, (2003).

[99] N. V. Smith, Prog. Surf. Sci. 51, 1227–1294, (1988).

[100] C. N. Borca, T. Komesu, P. A. Dowben, J. Electron Spectrosc. Relat. Phenom. 122, 259–273, (2002).

[101] A.V. Bune, V.M. Fridkin, S. Ducharme, L.M. Blinov, S.P. Palto, A.V. Sorokin, S.Yudin, and A. Zlatkin, Nature 391, 874, (1998).

[102] S. Ducharme, S.P. Palto, V.M. Fridkin, in: Handbook of Surfaces and Interfaces of Materials, Ferroelectric and Dielectric Films, Vol. 3, 546-592, (2002).

[103] L.M. Blinov, V.M. Fridkin, S.P. Palto, A.V. Bune, P.A. Dowben, S. Ducharme, Uspekhi Fizicheskikh Nauk [Russian edition vol.] 170, 247-262, (2000); Physics Uspekhi [English edition volume] 43, 243-257, (2000).

[104] P.A. Jacobson, L.G. Rosa, C.M. Othon, K. Kraemer, A.V. Sorokin, S. Ducharme, P. A. Dowben, Appl. Phys. Lett. 84, 88, (2004).

[105] L. G. Rosa, P. A. Jacobson, P. A. Dowben, J. Phys. Chem. B 109, 532, (2005).

[106] L. G. Rosa, I. N. Yakovkin, P. A. Dowben, J. Phys. Chem. B 109, 14189, (2005).

[107] P. A. Dowben, J. Xiao, B. Xu, A. Sokolov, B. Doudin, Appl. Surf. Sci. 254, 4238-4244, (2008).

[108] H. Qu, Wei Yao, T. Garcia, J. Zhang, A.V. Sorokin, S. Ducharme, P.A. Dowben, V.M. Fridkin, Appl. Phys. Lett. 82, 4322, (2003).

[109] L. Cai, H. Qu, C. Lu, S. Ducharme, P.A. Dowben, J. Zhang, Phys. Rev. B 70, 155411, (2004).

[110] C.N. Borca, S. Adenwalla, J. Choi, P.T. Sprunger, S. Ducharme, L. Robertson, S. P. Palto, J. Liu, M. Poulsen, V. M. Fridkin, H. You, P. A. Dowben, Phys. Rev. Lett. 83, 4562, (1999).

[111] J. Choi, P.A. Dowben, S. Pebley, A. Bune, S. Ducharme, V.M. Fridkin, S.P. Palto, N. Petukhova, Phys. Rev. Lett. 80, 1328, (1980).

[112] S. Palto, L. Blinov, E. Dubovik, V. Fridkin, N. Petukhova, A. Sorokin, K. Verkhovskaya, S. Yudin, A. Zlatkin, Europhys. Lett. 34, 465, (1996).

[113] J. Choi, S.-J. Tang, P.T. Sprunger, P.A. Dowben, V.M. Fridkin, A.V. Sorokin, S.P. Palto, N. Petukhova, S.G. Yudin, J. Phys. Cond. Matter 12, 4735, (2000).

[114] L.G. Rosa, Ya.B. Losovyj, J. Choi, P.A. Dowben, J. Phys. Chem. B 109, 7817, (2005).

[115] L. Cai, X. Wang, Y. Darici, P. A. Dowben,J. Zhang, J. Chem. Phys. 126, 124908, (2007).

[116] J. Choi, E. Morikawa, S. Ducharme, P.A. Dowben, Matt. Lett. 59, 3599, (2005).

[117] M. Qin, K. Yao, & Y. C. Liang, Appl. Phys. Lett. 93, 122904, (2008).

[118] A. Gruverman, O. Auciello and H. Tokumoto, Ann. Rev. Mat. Sci. 28, 101, (1998).

[119] Z. Zhang, P. Sharma, C. N. Borca, P. A. Dowben, A. Gruverman, Applied Physics Letters 97, 243702, (2010).

Chapter 7 Spatially Selective Deposition of Zwitterionic D-Cysteine and a *p*-benzoquinonemonoimine Molecular System on Periodically Poled Lithium Niobate

In this chapter, I will discuss our study on selective deposition of zwitterionic molecular system on periodically poled lithium niobate (PPLN). We have been able to selectively deposit folate, d-cysteine and a zwitterion compound from the class of N-alkyldiaminoresorcinones (or 4, 6-bis-dialkylaminobenzene-1, 3-diones, $C_6H_2(NHR)_2(O)_2$), compounds, where R =C_5H_{11}. All of these molecules have very strong local dipoles and appear to adopt spatial localization consistent with the ferroelectric domain structure of lithium niobate ($LiNbO_3$). We have been able to demonstrate that folate, d-cysteine and one of this class of *p*-benzoquinonemonoimine zwitterion compounds will all selectively adsorb from solution on periodically poled lithium niobate substrates using infra-red spectra-microscopy. The spatial localization of the folate, d-cysteine and the *p*-benzoquinonemonoimine zwitterionic compound on lithium niobate suggests that the ferroelectric poling of lithium niobate either alters the surface chemistry of lithium niobate or that there is some dipole-dipole interaction between the substrate and these adsorbates. The spatial zwitterion structure is consistent with the periodically poled lithium niobate structure.

One of the characteristic features of the ferroelectrics is the presence of electrically reversible polarization. In a properly oriented ferroelectric sample, the polarization can be

aligned perpendicular to the surface. In this case, the abrupt change in the normal component of the spontaneous polarization on a surface results in the appearance of a bound polarization charge, which in ambient conditions is compensated by the accumulation of ionic species or dipole molecules and through redistribution of mobile carriers in the bulk [1-12]. This screening significantly affects the surface charge distribution and the surface potential and results in band bending [13]. Similarly, charged surface states can pin the surface Fermi level resulting in a change in both the surface charge, the surface potential, and the molecular band offsets [14]. It has been recently shown that these electrically switchable properties of the ferroelectrics can be used to tailor surface reactivity. Several examples illustrating the effect of polarization on the photoreduction rate of Ag+ ions, the sticking coefficients and interaction energies of alcohol and water molecules can be found in literature [15-21], including the selective deposition of virus particles [22]. This effect opens a possibility of controlled assembling of complex organic/ inorganic nanostructures for hybrid electronic devices [23].

In spite of sizeable amount of experimental evidence on the effect of polarization on surface reactivity, the physicochemical mechanism of adsorption on the polar surfaces is not well understood. Band bending and induced redistribution of polarization screening charges was invoked as a mechanism for photoinduced adsorption of metals on ferroelectric surfaces [15, 24]. On the other hand, the photoinduced reduction of silver can occur on domains of both polarities under sufficiently high dose of irradiation. Different physisorption energies and chemisorption modes of CO_2 molecules (dissociative versus associative adsorption) have been reported for opposite domains in barium titanate [25]. The strong effect of the $LiNbO_3$ polarity on the thermal desorption of polar acetic acid

molecules but not the nonpolar dodecane molecules was explained by electrostatic interactions of polar molecules with uncompensated surface charges arising due to pyroelectric effect [17]. Nonetheless, polarizationdependent surface chemistry was not excluded in prior studies of molecular adsorption on $LiNbO_3$ (Refs. [17], [18], and [25]) and thus must be considered as another possible mechanism affecting molecular adsorption and desorption. An investigation of the electronic structure of molecules on ferroelectric surfaces can provide additional information regarding the polarization effect on molecular adsorption.

7.1 Selective Deposition of the *P*-benzoquinonemonoimine Zwitterion on Periodically Poled Lithium Niobate

Molecules of the *p*-benzoquinonemonoimine zwitterion compound (6Z)-4-(butylamino)-6-(butyliminio)-3-oxocyclohexa-1,4-dien-1-olate $C_6H_2(\underline{\cdots}NHR)_2(\underline{\cdots}O)_2$ where R = *n*-C_4H_9 (see Figure 4.1) selectively adsorb from solution on periodically poled lithium niobate ($LiNbO_3$) substrates as illustrated in the infra-red spectra-microscopy mapping of this compound on lithium niobate (Figure 7.1). The image shows the distribution of the molecules, using the molecular vibrational mode at 1730 cm^{-1} (see the arrow in figure 7.2 e) as a marker of the molecular localization. No vibrational modes specific to $LiNbO_3$ substrate exist in this region of the IR spectrum and $LiNbO_3$ contributions can be excluded.

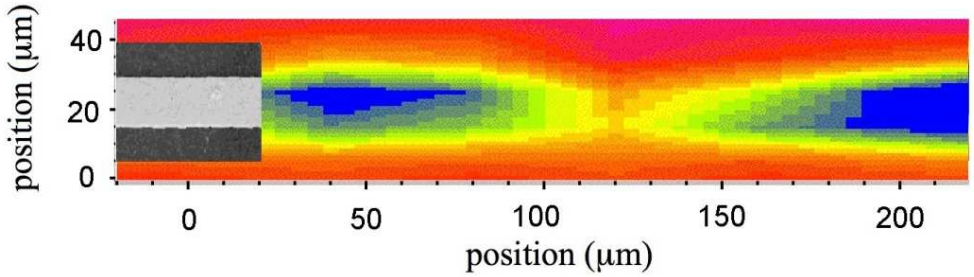

Figure 7.1 The spatial localization of the *p*-benzoquinonemonoimine zwitterion compound using infra-red spectra-microscopy at room temperature. The resolution in the y-axis (vertical) direction is limited to several microns. The resolution in the x-axis (horizontal) direction is 10-15 microns. The inset at left shows the piezoresponse force microscopy phase image of a portion of the periodically poled lithium niobate stripe domains. The IR spatial map was taken using the 1730 cm^{-1} absorption indicated by the arrow in Figure 7.2 e, and is in no way characteristic of the lithium niobate substrate. The less red and more blue seen in the above image, the greater the IR absorption associated with the vibrational mode associated with the *p*-benzoquinonemonoimine zwitterion core to nitrogen group asymmetric stretch at 1730 cm^{-1} (1609 cm^{-1} as calculated).

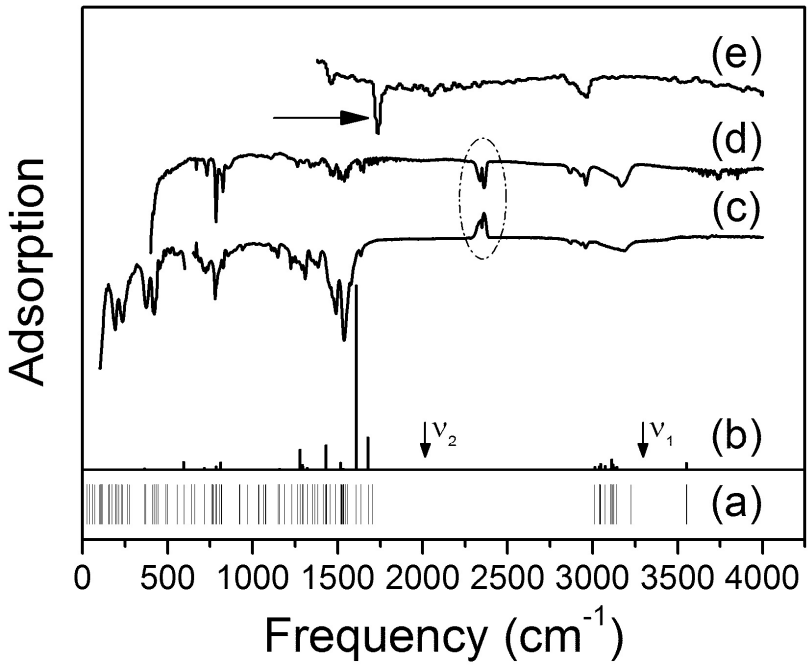

Figure 7.2 The infrared absorption spectra of the *p*-benzoquinonemonoimine zwitterion, compared with the vibrational eigen-values (a) and the calculated IR active modes (b). The experimental IR spectra include the *p*-benzoquinonemonoimine zwitterion in the solid state (c), adsorbed on Au (d), and adsorbed on lithium niobate (e). The modes indicated in the spectra by the oval are from CO_2. The placement of the modes, obtained from photoemission vibronic fine structure, are also indicated, by ν_1 and ν_2 and the IR imaging was undertaken using the absorption line indicated with the larger arrow (see text).

This selective deposition is not a result of the change in bulk composition. Spatially resolved X-ray adsorption near edge spectroscopy (XANES) at the Nb K-shell edge shows no change in the absorption fine structure on the scale of a micron, i.e. at dimensions much smaller than the dimensions of the poled ferroelectric strip domains (see Supplementary

Material). The selective deposition (Figure 7.1) of this *p*-benzoquinonemonoimine zwitterion compound thus results from a surface interaction effect on the surface of poled lithium niobate. The failure of the IR microscopy image to localize the *p*-benzoquinonemonoimine zwitterion molecules precisely to the ferroelectric stripe domains is likely a resolution issue associated with the limitations of the IR microscopy and infrared synchrotron beamline. The resolution in the y-axis direction of figure 7.1 is limited to 2-3 microns, while the resolution in the x-axis direction is 10-15 microns.

The general spatial localization of this *p*-benzoquinonemonoimine zwitterion molecule (Figure 7.1) suggests that the ferroelectric poling of $LiNbO_3$ either alters the surface chemistry or that there is some dipole-dipole interaction between the zwitterion and ferroelectric domains of the substrate surface. Dipole interactions alone would likely have the zwitterion decorate both "up" and "down" domains of the ferroelectric, so some surface chemistry is certainly implicated in the interation of $LiNbO_3$.

The prior surface characterization of $LiNbO_3$ could be interpreted as indicating some changes in either the surface defect density or the terminal layer surface composition accompany the reversal of polarization [1]. The direction of the ferroelectric dipole has been seen to alter the adsorption and desorption chemistry of a number of organic molecules on the surface of several inorganic ferroelectrics [2-8], including changes in surface chemistry of lithium niobate [2, 6-8]. Thus the selective deposition of our *p*-benzoquinonemonoimine zwitterion molecule from solution (Figure 7.1) is not entirely unexpected. The zwitterion adheres better to the lithium niobate surface with one dipole orientation surface than the other and is not so easily removed by an ethanol wash (used to

remove excess molecules). It should be re-iterated that presently, alterations in surface chemistry resulting in spatial chemical localization issues cannot be excluded.

Because our studies are isothermal, we can exclude the preferential adsorption and desorption as being caused by a surface pyroelectric charge. Such a temperature dependent surface charge could influence thermal desorption of polar molecules from $LiNbO_3$ and was not ruled out in prior studies [2, 6-8]. As is the case here, changes in thermal desorption and chemical reactivity reported previously [2, 5-8] could be explained by changes in the surface chemistry that may occur with polarization reversal. There was no proof offered that the surface composition, stoichiometry and surface structure was not altered with reversal of the ferroelectric dipole direction [2, 5-7]. The *p*-benzoquinonemonoimine zwitterion spatial selectivity on $LiNbO_3$(001) nevertheless further confirms that there are ferroelectric domain specific chemistries, as previously noted [4, 6].

The infra-red absorption modes of this zwitterionic compound seen on $LiNbO_3$ (Figure 7.2 e) resemble those seen in the photoemission vibronic fine structure (Figure 4.6). The infra-red absorption spectra are dominated by two absorption lines indicative of very selective selection rules: the *p*-benzoquinonemonoimine zwitterion core plane must be aligned preferentially with the surface normal thus placing the zwitterion dipole parallel to the lithium niobate dipole direction (along the surface normal), possibly again adopting the orientation schematically illustrated in Figure 4.4. Obtaining IR adsorption spectra of molecular adsorbates on transparent wide band gap oxides is widely recognized to be very difficult [9, 10] particularly for reflection IR, as is the case here. Molecular adsorbate IR vibrational modes absorption intensities on oxide surfaces tend to be about an order of magnitude weaker than observed for the same adsorbate on a metal substrate. The strong

dipole of the *p*-benzoquinonemonoimine zwitterion is an advantage, as the IR cross-section is much improved for the strong dipole active modes, hence the differences in the IR spectra of Figure 7.2.

The dipole active modes predicted to be located at energies of 3126 cm^{-1} and 3227 cm^{-1}, associated with the core molecular stretching modes (schematically shown as (a) and (b) in figure 4.6) are in good agreement with the observed infrared absorption in the region of 2800 to 2900 cm^{-1} (Figure 7.2 e) of the *p*-benzoquinonemonoimine zwitterion compound when selectively adsorbed on the $LiNbO_3$ (001) surface. This agreement and the paucity of IR absorption bands make a compelling case for a molecular orientation where the plane of the zwitterion core is again aligned preferentially close to the surface normal. The observed infrared absorption at *ca.* 1730 cm^{-1} (Figure 7.2 e) for the zwitterion, when selectively adsorbed on the $LiNbO_3$(001) surface should be assigned to one of the strong dipole active modes schematically shown as (c) and (d) in Figure 4.6. The strong dipole field at the interface, and absence of image dipole (the substrate is a dielectric) will contribute further to symmetry restrictions in the IR absorption spectroscopy, leaving only a few modes to contribute to the IR absorption spectra in the specular geometry, as is observed. Many such modes will appear slightly shifted towards higher energies because of the strong dipole field, resulting from the substrate interactions. Because the local fields are not as strong as the transient electric field created in photoemission, an increase in the vibrational mode energies should not be and is not as large as is observed in the vibronic photoemission fine structure.

Adsorption studies have shown that strong interactions develop between the zwitterionic *p*-benzoquinonemonoimine compound $(C_6H_2(\underline{\cdots}NHR)_2(\underline{\cdots}O)_2$ where R = *n*-

C_4H_9) and a ferroelectric insulating substrate (lithium niobate). The core of the zwitterion tends to align preferentially along the surface normal, likely because of the image charge and/or the substrate dipole.

The static dipole field, in the mean field approximation either in the initial state (as seen with molecular adsorption on the $LiNbO_3$ ferroelectric substrate) or in the photoemission final state (as seen in the vibrational fine structure contributions to the valence band photoemission), perturbs the adsorbate vibrational states. Strong local dipole fields created owing to the photo-hole in the photoemission final state [11], or through adsorption on a ferroelectric substrate, can lead to vibrational mode stiffening of the dipole active modes associated with the nitrogen groups of the zwitterion. This is reflected in the change of energy of the asymmetric vibrational mode linking the core of the zwitterion molecule to the nitrogen, increasing from 1500 ± 50 cm^{-1} (Au substrate) to 1730 ± 30 cm^{-1} ($LiNbO_3$ substrate) and 2016 ± 110 cm^{-1} (photoemisson final state). This expected perturbation of the adsorbate vibrational states can finally be observed because these adsorbed zwitterion molecules adopt a preferential orientation leading to very restrictive selection rules, simplifying the otherwise complex vibrational mode spectra.

The selective deposition of molecules onto specific ferroelectric domains has also been demonstrated for a spatially periodically poled ferroelectric surface. This represents an attractive approach to pattern molecular deposition on optically transparent planar substrates through electrostatic dipolar interactions, although some surface chemical interactions must be invoked since the entire surface of $LiNbO_3$ is NOT covered. The results presented here, on ferroelectric domain selective adsorption, exclude preferential

molecular adsorption due to a surface charge resulting from the pyroelectric effect, which could not be excluded in some prior studies.

7.2 Selective Deposition of Zwitterionic D-Cysteine on Periodically Poled Lithium Niobate

We investigate the polarization effect on adsorption of d-cysteine molecules [a chiral isomer of *l*-cysteine (chemical formula $C_3H_7NO_2S$)] on ferroelectric substrates using a combination of infrared spectramicroscopy and spatially resolved x-ray absorption near edge spectroscopy (XANES). (It is worth mentioning that there is a rich literature of cysteine adsorption chemistry [26-30] and the characteristics of cysteine adsorption molecules on polar surfaces could be of interest for differentiating amino acid molecules.) We have shown that although experiments were performed in the absence of any external electronic excitation (optical or thermal), the adsorption was still affected by polarization with preferential deposition occurring on the positive domains. This observation allows us to exclude selective molecular adsorption due to the surface charge resulting from, for example, the pyroelectric effect, restricting the possible surface interactions to polarization-dependent surface chemistry and dipole-dipole interaction.

Periodically poled lithium niobate (PPLN) substrates of congruent composition, which are similar to the ones used in Ref. [24], were used as the ferroelectric substrates, as described in Chapter 2.

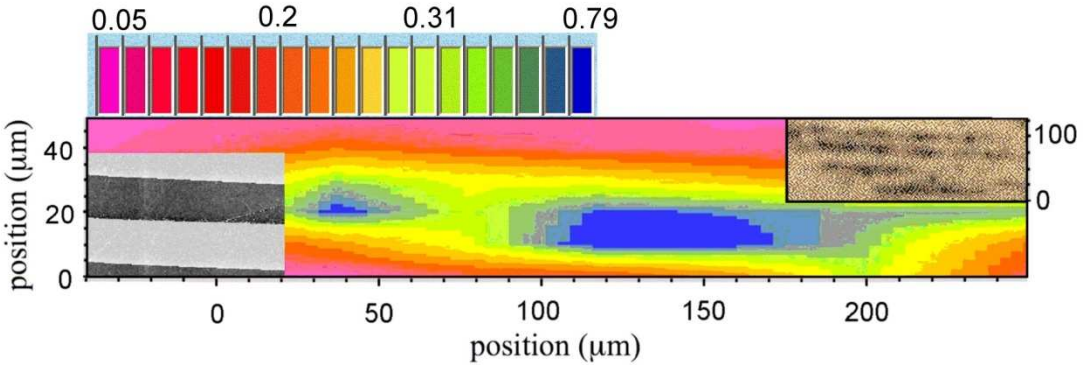

Figure 7.3 (Color) The spatial localization of the d-cysteine molecules on a periodically poled lithium niobate detected using an infrared spectramicroscopy with a blue contrast.

Deposition of d-cysteine molecules on PPLN has been carried out by immersing the PPLN substrate in aqueous 1*M* d-cysteine solution for 24 h. Following immersion, the samples were washed in a weak 1*M* NaOH alcohol-water solution to remove excess molecules followed by rinsing in ethanol using the previously described cleaning process [22] and dried. Deposition was carried out in isothermal conditions at room temperature without illumination. Spatially resolved chemical mapping has been performed using infrared spectramicroscopy to determine the domain-specific localization of d-cysteine molecules by means of the IR reflection mode of Thermo Nicolet continuum microscope at the synchrotron of the Center for Advanced Microstructures and Devices at Louisiana State University [32, 33]. With the synchrotron as a light source, the infrared incident light is highly planepolarized and s-polarized in the geometry of the experiment.

Figure 7.3 shows IR spatial microscopy images of the d-cysteine coverage of the PPLN surface. Blue contrast in Figure 7.3 and darker contrast in the right inset correspond to regions covered with d-cysteine molecules. Comparison of the stripe shape of these

regions with the periodical domain structure revealed by PFM indicates that d-cysteine adsorption closely follows the polarization pattern. Combined AFM/PFM inspection of the PPLN surface after deposition showed larger accumulation of substance on the positive ends of domains.

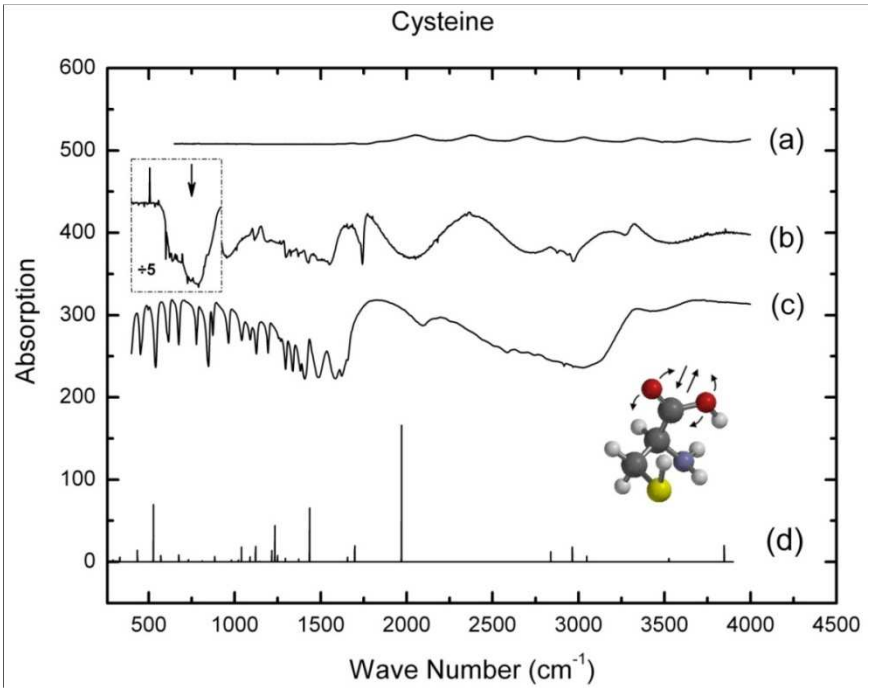

Figure 7.4 (Color) (a) IR spectrum on PPLN surface before d-cysteine deposition. [(b) and (c)] Spectrum of d-cysteine molecules on PPLN (b) as compared to reference IR spectra of solid d-cysteine (c). (d) The calculated vibrational modes of d-cysteine from density functional theory. Note that in the absence of d-cystseine, $LiNbO_3$ shows little IR absorption in the reflection geometry, as expected. The molecular scissor mode experimentally determined to be at 775 cm^{-1} and calculated to be at 753 cm^{-1} is schematically shown as an inset. This mode (see arrow) occurs in a region where there is no absorption from $LiNbO_3$ undecorated by d-cysteine, and was used to construct the IR spatial absorption map of Figure 7.3.

The change in the infrared spectra associated with adsorption of d-cysteine on lithium niobate is shown in Figure 7.4. In the absence of d-cysteine, absorption on the $LiNbO_3$ (001) surface is weak [Fig. 7.4(a)]. The characteristic IR absorption lines of d-cysteine are clearly evident in the IR spectra of d-cysteine deposited on $LiNbO_3$ [Fig. 7.4(b)], but the huge increase in the relative absorbance of the dipolar molecular scissor mode is a strong indication of d-cysteine aligned with the long molecular axis normal to the surface. The suppression of the other modes of a different symmetry is also consistent with this interpretation. There is some shift of the dipole modes to higher vibrational energies, as has been seen with other dipolar molecules on ferroelectric substrates [34]. Obtaining the IR absorption spectra of molecular adsorbates on transparent wide band gap oxides is widely recognized to be very difficult and intensity of IR vibrational modes of molecular adsorbates on oxide surfaces tend to be about an order of magnitude weaker than observed for the same adsorbate on a metal substrate [35-37]. Beyond the obvious surface localization, ascertaining the surface density of d-cysteine molecules is difficult from the data available here.

In prior deposition experiments, employing the particles in solution [21, 38], it has been assumed that the interaction between the deposited ions or charged particles and the ferroelectric surface is electrostatic in nature and results from the fact that the ferroelectric holds a bound surface charge arising from its spontaneous polarization. However, in an aqueous solution, the formation of an electric double layer due to the adsorption of water dipoles or different ionic species should lead to essentially complete screening of the polarization charges. (For lithium niobate, this is the dominant screening mechanism [24].) Only generation of uncompensated surface charges via band gap illumination or

temperature change resulted in polarization-specific adsorption. In present experiment, adsorption of the d-cysteine molecules occurs in the isothermal conditions and without optical excitation. Hence, it cannot be attributed to the effect of pyroelectric or photoinduced charge. The data suggest that polarization-dependent surface chemistry can be implicated in the selective adsorption of d-cysteine. Nonetheless, the indications of a preferential alignment of adsorbed d-cysteine molecules along the surface normal, while not completely inconsistent with a polarization-dependent surface chemistry do suggest that interface dipole-dipole interaction should play a role as well. The d-cysteine molecules largely contain a nonpolar thiol group (-0.1 excess charge on S), a polar amine group (-0.75 excess charge on N), and a polar carboxilate group (-0.45 and -0.56 excess charge on each oxygen, respectively), as derived from density functional theory (the standard B3LYP function). The latter two groups possibly participate in the dipoledipole interaction with the polar lithium niobate surface and thus cause polarization-dependent adsorption. Polarization-dependent surface reconstructions and surface relaxations are indicated by the apparent variations of Li/Nb concentration ratios at the lithium niobate surface determined from temperature dependent Auger electron spectroscopy, while the possibility of defects at the surface mediated by the polarization are suggested by the changes in the O/Nb ratio [39, 40]. Nonuniformity of surface composition can also explain considerable variations in d-cysteine concentration along the domain stripes.

In summary, the polarization-specific adsorption of d-cysteine on periodically poled lithium niobate during isothermal deposition from solution has been studied by means of infrared spectramicroscopy and XANES spectroscopy. The reported effect is attributed to dipole-dipole interaction between polar d-cysteine molecules and ferroelectric polarization

dipoles. Surface chemistry related to polarizationdependent variations in Li/Nb concentration is also implicated as a contributing factor in the domain-specific adsorption of d-cysteine.

This work could be widely applicable in other fields outside physics. In recent years, there is a rich literature of cysteine adsorption chemistry and the characteristics of cysteine adsorption molecules on polar surfaces could be of interest in differentiating amino acid molecules. More complex polar molecules, such as folate acid, and fibroblast cell have also been investigated on ferroelectric substrates. It can be seen that folate acid also has a selective deposition on PPLN (as shown in figure 7.5 (c)). Carried out as a complement to this work by the group of Dr. Axel Rosenhahn, Christof Christofis, and Prof. M. Grunze, University of Heidelberg, a similar study of fibroblast adhesion on periodically poled $LiTaO_3$ (as shown in figure 7.6, 7.7) shows that for initial cell adhesion, cells adhere passively on the periodically poled substrate and do not show actively respond or choose of a preferred adhesion site. And for long time cell incubation, cells do spread and elongate on all substrates uniformly and occur in random orientation.

In conclusion, although those experiments were performed in the absence of any external electronic excitation (optical or thermal), the adsorption was still affected by polarization with preferential deposition occurring on the ferroelectric domains.

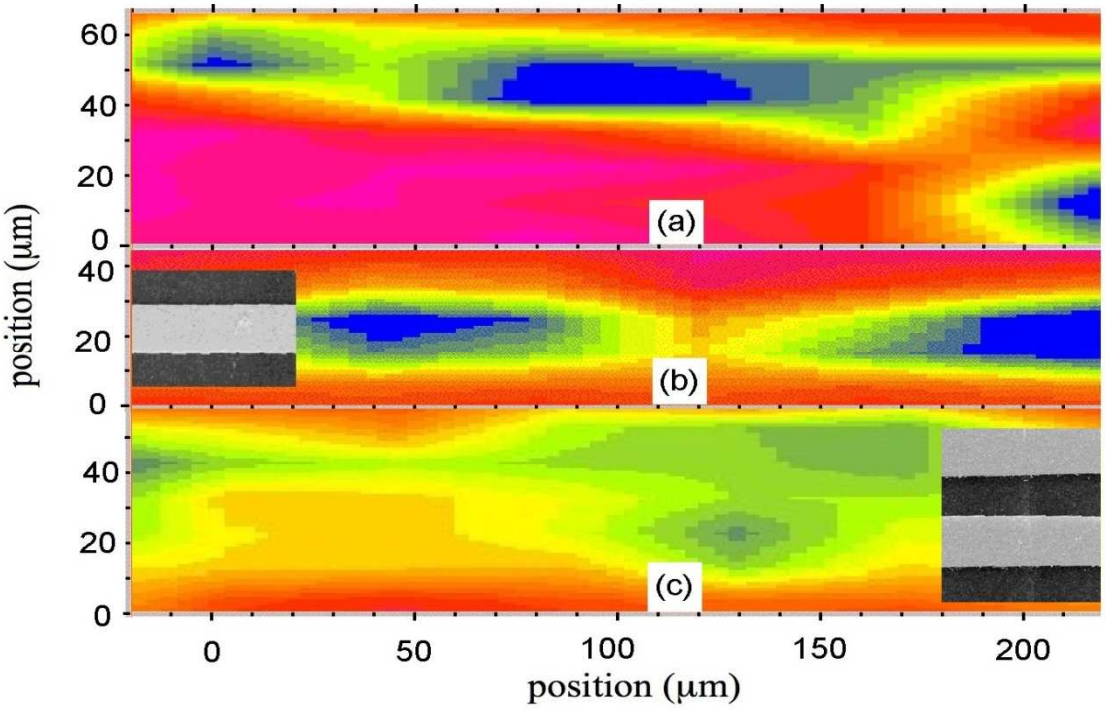

Figure 7.5 (Color) Infra-red color map comparison of (a) D-cysteine (b) Zwitterion **2** (c) folate acid on periodically poled lithium niobate. The spatial localization of the molecules on a periodically poled lithium niobate detected using an infrared spectramicroscopy with a blue contrast indicating a higher degree of adsorption. The insets at the (b) left or at the (c) right show a PFM phase image of domains (at the same magnification as the infrared microscopy image). Positive domains appear with dark PFM contrast.

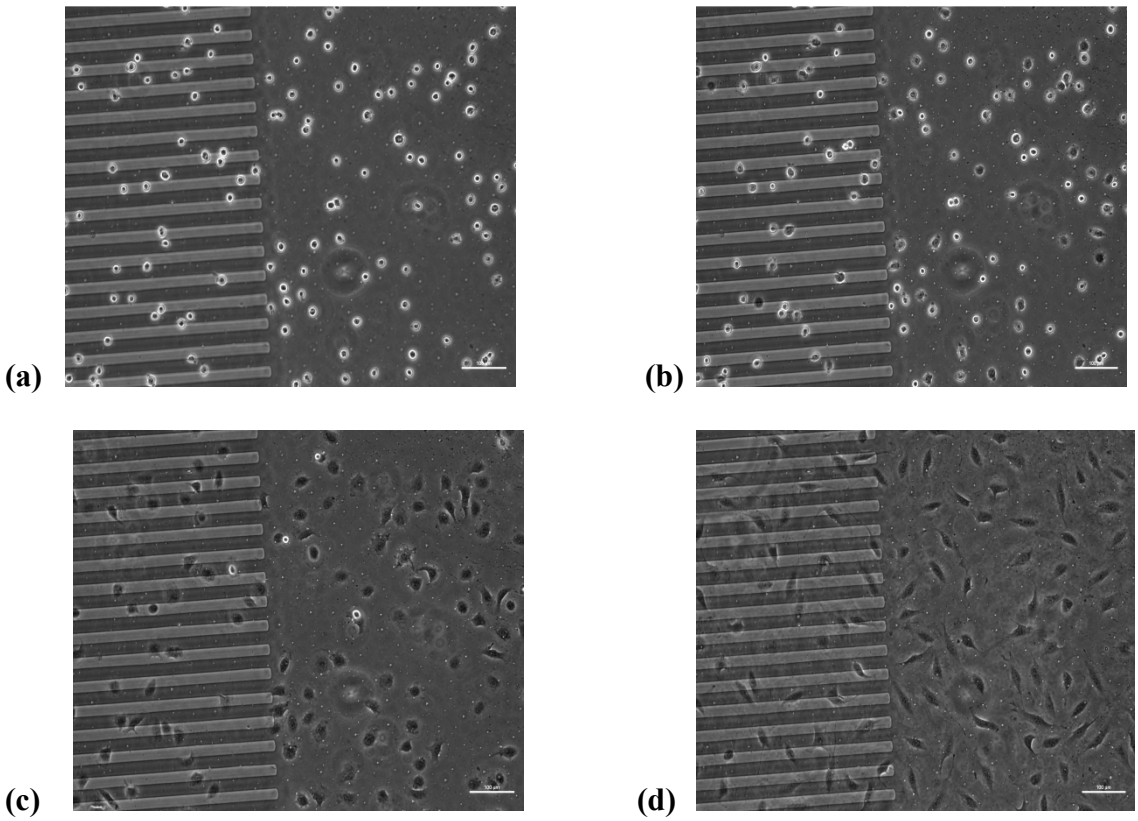

Figure 7.6 Fibroblast adhesion on periodically poled $LiTaO_3$ (40μm period). Initial adhesion and long time incubation of mammalian fibroblasts on periodically poled $LiTaO_3$ substrates: (a) 0 min; (b) 10 min; (c) 1h; (d) 18h.

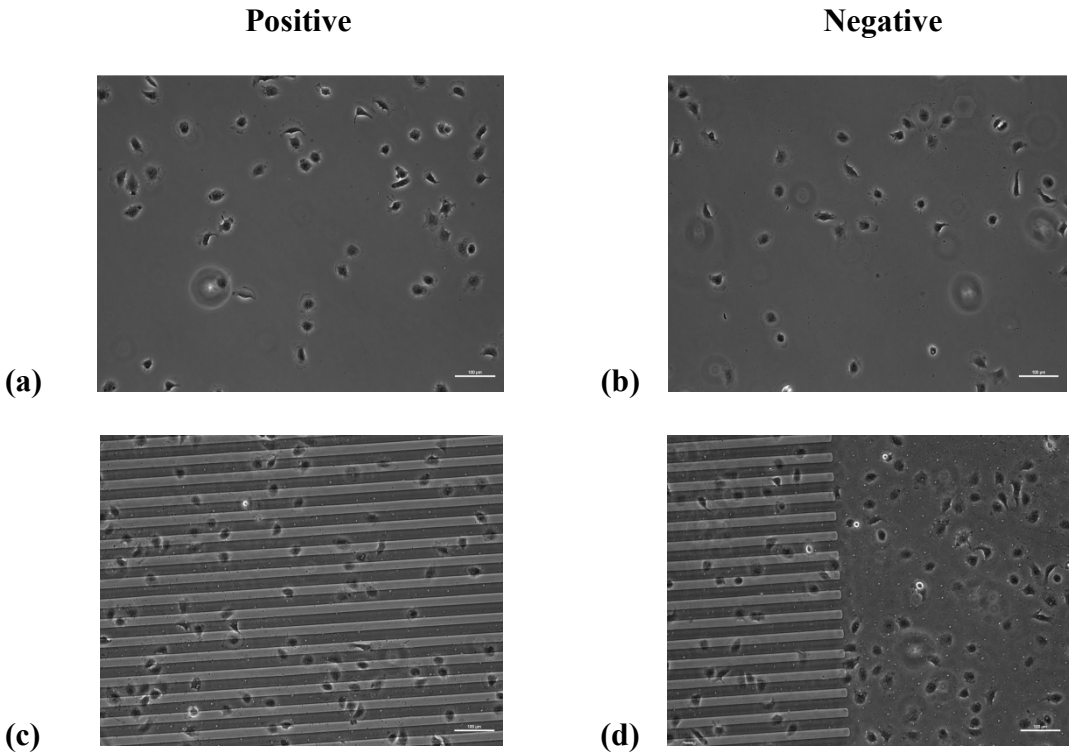

Figure 7.7 Fibroblast adhesion on (a) positive and (b) negative poled $LiTaO_3$ after 1h. (c) and (d) are fibroblast adhesion on periodically poled $LiTaO_3$ (40μm period) after 1h.

References

[1] A. Ye. Lushkin, V. B. Nazarenko, K. N. Pilipchack, V. F. Shnyukov and A. G. Naumovets, J. Phys. D: Appl. Phys., 32, 22, (1999).

[2] Y. Yun and E. I. Altman, J. Am. Chem. Soc., 129, 15684, (2007).

[3] A. L. Cabrera, G. Tarrach, P. Lagos and G. B. Cabrera, Ferroelectrics, 281, 53, (2002).

[4] J. L. Giocondi and G. S. Rohrer, Chem. Mater., 13, 241, (2001).

[5] M. H. Zhao, D. A. Bonnell and J. M. Vohs, Surf. Sci., 603, 284, (2009).

[6] D. Li, M. H. Zhao, J. Garra, A. M. Kolpak, A. M. Rappe, D. A. Bonnell and J. M. Vohs, Nat. Mater., 7, 473, (2008).

[7] Y. Yun, L. Kampschulte, M. Li, D. Liao and E. I. Altman, J. Phys. Chem. C, 111, 13951, (2007).

[8] J. Garra, J. M. Vohs and D. A. Bonnell, Surf. Sci., 603, 1106, (2009).

[9] J. Kattner and H. Hoffmann, in Handbook of Vibrational Spectroscopy, ed. J. M. Chalmers and P. R. Griffiths, Wiley, Chichester, pp. 1–19, (2002).

[10] Y. Wang, A. Glenz, M. Muhler and Ch. Wöll, Rev. Sci. Instrum., 80, 113108, (2009);

Ch. Rohmann, Y. Wang, M. Muhler, J. Metson, H. Indriss and Ch. Wö ll, Chem. Phys. Lett., 460, 10, (2008).

[11] J. E. Ortega, F. J. Himpsel, D. Li and P. A. Dowben, Solid State Commun., 91, 807. 10340, (1994).

[12] V. M. Fridkin, Ferroelectric Semiconductors (Consultants Bureau, New York, 1980).

[13] W.-C. Yang, B. J. Rodriguez, A. Gruverman, and R. J. Nemanich, Appl. Phys. Lett. 85, 2316, (2004).

[14] J. Xiao, A. Sokolov, and P. A. Dowben, Appl. Phys. Lett. 90, 242907, (2007).

[15] J. L. Giocondi and G. S. Rohrer, Chem. Mater. 13, 241, (2001).

[16] G. Parravano, J. Chem. Phys. 20, 342, (1952).

[17] Y. Yun and E. I. Altman, J. Am. Chem. Soc. 129, 15684, (2007).

[18] J. Garra, J. M. Vohs, and D. A. Bonnell, Surf. Sci. 603, 1106, (2009).

[19] D. Li and D. A. Bonnell, Ceram. Int. 34, 157, (2008).

[20] M. H. Zhao, D. A. Bonnell, and J. M. Vohs, Surf. Sci. 603, 284, (2009).

[21] S. Habicht, R. J. Nemanich, and A. Gruverman, Nanotechnology 19, 495303, (2008).

[22] S. Dunn, D. Cullen, E. Abad-Garcia, C. Bertoni, R. Carter, D. Howorth, and R. W. Whatmore, Appl. Phys. Lett. 85, 3537, (2004).

[23] S. V. Kalinin, D. A. Bonnell, T. Alvarez, X. Lei, Z. Hu, and J. H. Ferris, Nano Lett. 2, 589, (2002).

[24] J. N. Hanson, B. J. Rodriguez, R. J. Nemanich, and A. Gruverman, Nanotechnology 17, 4946, (2006).

[25] D. Li, M. H. Zhao, J. Garra, A. M. Kolpak, A. M. Rappe, D. A. Bonnell, and J. M. Vohs, Nature Mater. 7, 473, (2008).

[26] A. Kühnle, T. R. Linderoth, M. Schunack, and F. Besenbacher, J. Am. Chem. Soc. 128, 1076, (2006).

[27] R. Otero, M. Schöck, L. M. Molina, E. Lægsgaard, I. Stensgaard, B. Hammer, and F. Besenbacher, Angew. Chem. 44, 2270, (2005).

[28] A. Kühnle, T. R. Linderoth, and F. Besenbacher, J. Am. Chem. Soc. 125, 14680, (2003).

[29] A. Kühnle, T. R. Linderoth, B. Hammer, and F. Besenbacher, Nature (London) 415, 891, (2002).

[30] Y. Zubavichus, A. Shaporenko, M. Grunze, and M. Zharnikov, J. Phys. Chem. 111, 11866, (2007); 111, 9803, (2007); 110, 3420, (2006).

[31] A. Gruverman and S. V. Kalinin, J. Mater. Sci. 41, 107, (2006).

[32] O. Kizilkaya, J. D. Scott, E. Morikawa, J. D. Garber, and R. S. Perkins, Rev. Sci. Instrum. 76, 013703, (2005).

[33] O. Kizilkaya, A. Prange, U. Steiner, E. C. Oerke, J. D. Scott, E.Morikawa, and J. Hormes, Nucl. Instrum. Methods Phys. Res. A 582, 274, (2007).

[34] J. Xiao, Z. Zhang, D. Wu, L. Routaboul, P. Braunstein, B. Doudin, Y. B. Losovyj, O. Kizilkaya, L. G. Rosa, C. N. Borca, A. Gruverman, and P. A. Dowben, Phys. Chem. Chem. Phys. 12, 10329, (2010).

[35] J. Kattner and H. Hoffmann, in Handbook of Vibrational Spectroscopy, edited by J. M. Chalmers and P. R. Griffiths (Wiley, New York, 2002), pp. 1–19.

[36] Y. Wang, A. Glenz, M. Muhler, and C. Woll, Rev. Sci. Instrum. 80, 113108, (2009).

[37] C. Rohmann, Y. M. Wang, M. Muhler, J. Metson, H. Indriss, and C. Woll, Chem. Phys. Lett. 10, 460, (2008).

[38] G. I. Distler, V. P. Konstantinova, V. M. Gerasimov, and G. A. Tolmacheva, Nature 218, 762, (1968).

[39] A. Y. Lushkin, V. B. Nazarenko, K. N. Pilipchak, V. F. Shnyukov, and A. G. Naumovets, J. Phys. D 32, 9, (1999).

[40] A. M. Prokhorov and Yu. S. Kuz'minov, Physics and Chemistry of Lithium Niobate (Hilger, Bristol, 1990).

Chapter 8 Applications

Organic materials are commonly regarded as electrical insulator with a large range of application in electronics, biomedical and pharmaceutical purposes. This is largely true even today when we observed man made organic materials in our surroundings. However, electrical conduction on organic materials began to draw attention of scientists. Even today questions such as underlying mechanism of electron mobility, synthesis of materials with determine conductivity properties, which electronic state promotes conduction, are current subject of research for scientist in materials and nanotechnology research. The field of organic semiconductors has developed from a fundamental laboratory discovery into a manufacturing technological material for a large range of thin- film electronics applications[1-3], which benefits from the compatibility of organic materials with large area, low-cost, room temperature solution processing and direct-write printing. Since their discovery of organic semiconductor applications today include emissive light emitting diodes, flat panel displays, and low cost thin film transistor circuits on flexible substrates[i].

One of the general issues in molecular electronics is the transport through organic molecules. The hybridization of molecular orbitals to form band structure has been studied for nearly three decades [2-6], and is a fairly well established phenomenon. With larger molecular species, intramolecular band structure is far more likely and commonly observed [2-4]. Such intramolecular band dispersion has been found in self-assembled monolayers [11, 12], including polyphenyl species [12]. In contrast, because of the very small effective Brillouin zone (requiring exceptionally good wave vector resolution) and the generally very

small intermolecular interactions, band structure resulting from intermolecular interactions is generally not observed for ordered assemblies of large molecules, with only a few exceptions [5-13].

.The study of the details of transport mechanisms in organic systems has demonstrated that, not only do interface dipoles and valence band electronic structure symmetry play a role, but that there is a strong dependence on molecular vibrations [14-20] that couple to the transport properties through electronic structure. In this chapter, we will discuss the corresponding applications in molecule electronics based on our investigation on charge transport properties on metal-organic interfaces and the doping of semiconducting polymers.

8.1 The Electrical Transport Properties of Ultra-thin Films of Zwitterions

In Chapter 3, we have investigated surface electronic spectroscopic properties of $C_6H_2(\cdots NHR)_2(\cdots O)_2$, where R = H, *n*-$C_4H_9$, C_3H_6-S-CH_3, C_3H_6-O-CH_3, CH_2-C_6H_5, adsorbed on Au. Direct measurement of the electrical transport properties of these ultra-thin films is challenging, especially when considering that these zwitterion species do not all absorb on insulating substrates. For example, we identified a preferential adsorption of the molecule **3** on Au, identified by IR spectroscopy (Figure 8.1), suggesting that adsorption on oxides surfaces is unreliable, or varies with oxide surface. Although this conclusion is also true of molecule **2** as discussed elsewhere [21], we found that molecule **2** was the best candidate for adsorption on Au and SiO_2 substrate, for the purpose of lateral device measurements.

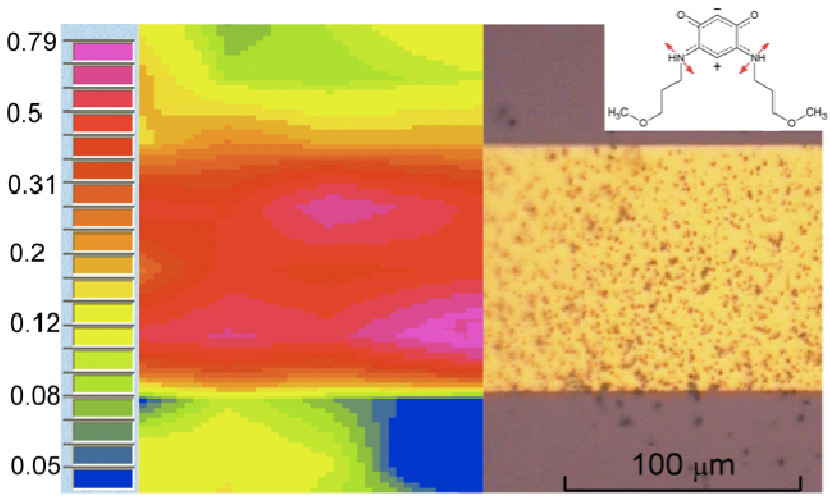

Figure 8.1 The localization of molecule **3** on a gold stripe over a native oxide silicon surface. At right is the image of the gold stripe, and at left is the IR map based on vibrational mode absorption at 3130 cm^{-1}. This energy is characteristic of the symmetric wagging mode of the *p*-benzoquinonemonoimine zwitterions, as indicated in the inset at right. The color scale on the left indicates the absorption strength.

We fabricated electrodes nanogaps structures, with nanometer distance separating two Au contacts on a microfluidic-equipped chip allowing chemical exposure and cleaning of the nanogaps [22]. Figure 8.2 shows that significant current flow can be established in junctions made of a few molecules, especially when compared to dodecanedithiols, used as benchmark of molecular transport [23]. Measurements are performed on samples that were immersed overnight in solutions containing the zwitterions, and washed in a microfluidic channel. We found that the solvent flow should not exceed 0.01 m/s, in order to maintain

electrical interconnects. We conclude that the electrical transport through molecule **2** is robust and significantly larger than current in alkane thiol molecules.

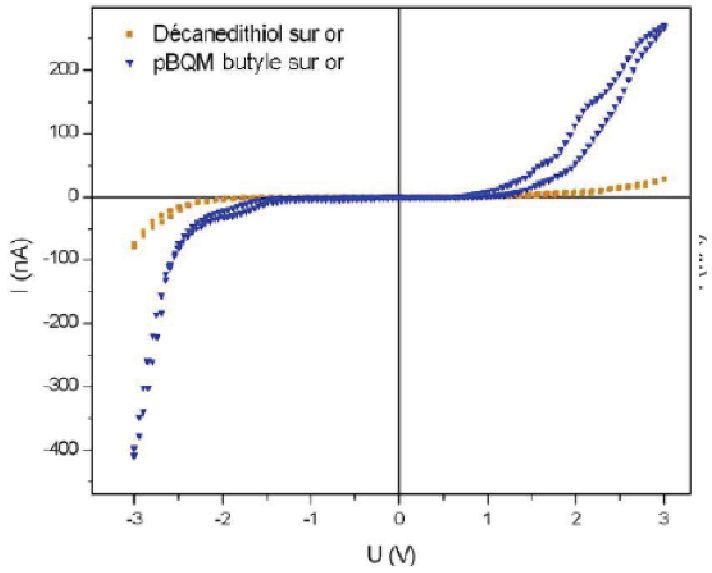

Figure 8.2 Current/voltage curve of molecule **2**, compared with decanedithiol molecules trapped between Au electrodes separated by 1-3 nm distance. A gain of nearly one order of magnitude is found (with the hysteresis in the IV curve likely related to charge trapping by the SiO_2 substrate).

In Chapter 3, we have shown that crystalline ordering of the *p*-benzoquinonemonoimine molecules was possible. Here we find that the related π-stacking promotes conductivity in the thin films that was mostly evidenced by the occurrence of molecular density of states at the substrate Fermi level and significant intrinsic conductivity of this type of molecules. The interface molecular films can therefore play an important role

for organic electronics devices, creating ideally a highly conductive interface with metallic electrodes, promoting efficient carrier injection in an organic film.

8.2 Doping Poly[2-methoxy-5-(2'-ethylhexyloxy)-1,4-phenylenevinylene] with PbSe nanoparticles or PCBM fullerenes

The doping of semiconducting polymers is a hugely active area of interest [24–28]. However, it is not clear whether nanoparticles dope a polymer in the conventional sense of acting as charge donors or acceptors, or merely act as particulates in a polymer matrix with a high surface area to volume ratio. In the latter case, doping can still occur due to the dipole layer at the nanoparticle interface [29]. Two such dopants command attention: lead selenide (PbSe) quantum dots and the fullerene based molecule [(6)]-1-(3-(methoxycarbonyl)propyl)-[(5)]-1-phenyl-[5,6]-C61, known as PCBM. Polymer photodetectors based on poly[2-methoxy-5-(2'-ethylhexyloxy)-1,4-phenylenevinylene] (MEH-PPV) and related PPV polymers, doped with lead selenide (PbSe) [30–32], lead sulfide (PbS) [33, 34], and cadmium selenide (CdSe) [35, 36] nanocrystal quantum dots have shown significant increases in quantum efficiencies. PCBM has also been used to dope MEH-PPV, with promising results [28, 37–39]. Fullerene derivatives have been used to dope other semiconducting polymers [24, 27, 40–50], sometimes in combination with other nanoparticle systems [51]. Certainly doping polymers with semiconducting nanoparticles or fullerene molecules is seen as a route to improving polymer solar cell performance [24, 27, 32, 52–55]. Recently Zhao *et al* reported that a composite of blue light emitting conjugated polymer polyfluorene, red light emitting dye, and a large-*Z* atom (*Z* is the atomic number) 1,3-diiodobenzene shows promising γ radiation detecting properties

[56]. They confirmed the fluorescence resonance energy transfer between the polymer and the dye. The photoluminescence intensities respond linearly to γ-ray dosage. Campbell and Crone presented scintillation results of CdSe–ZnSe core–shell quantum dots and MEH-PPV composite for radiation-detection application [57]. They demonstrated the Forster excitation transfer from the quantum dots to the polymer and thus potential for gamma-ray, neutron, and charged-particle detection while having benefits of a low cost, easy processability, and large-area applications.

Both PbSe and PCBM accept excited electrons from MEH-PPV at extremely high charge transfer rates (time in picoseconds), aiding charge separation: but do they act as charge acceptors in the ground state? If not uniformly dispersed, there is also the issue of when nanoclusters cease to dope with increasing concentrations. The latter issue is of importance if PbSe, or like nanocrystal quantum dots, are added to the MEH-PPV matrix to make a composite suitable for gamma radiation detection; both to add a large-*Z* material to the polymer, thus increasing the cross-section, as well as to improve quantum efficiencies. Here we explore both questions.

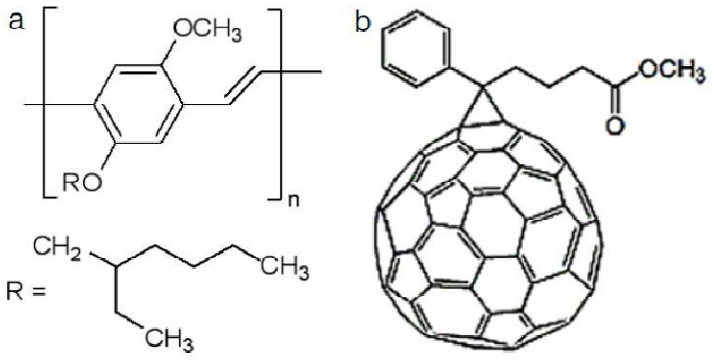

Figure 8.3 Schematics of (a) poly[2-methoxy-5-(2'-ethylhexyloxy)-1,4-phenylenevinylene] (MEH-PPV) and (b) [(6)]-1-(3-(methoxycarbonyl)propyl)-[(5)]-1-phenyl-[5,6]-C61, known as PCBM.

The chemical structures of the MEH-PPV and PCBM are shown in figure 8.3. In Chapter 2, Section 2.7.6., we have described the doping procedure of PbSe nanocrystals and PCBM fullerenes into MEH-PPV. We use angle-resolved photoemission to study the electronic structure of MEH-PPV with dopped PbSe and PCBM.

While the electronic structure of MEH-PPV and PCBM have many similarities, as a composite, the electronic structure does change as expected from that predicted for MEH-PPV to that predicted for PCBM, as seen in figure 8.4. After a shift of the calculated orbital energies by about 4.4 eV (roughly the expected work function), the experiment is seen to be in qualitative agreement with very simplistic calculated representation of the density of states based on the ground state molecular orbitals (NDO-PM3 or neglect of differential diatomic overlap, parametric model number 3) [61] for a single PCBM complex or a short

chain of MEH-PPV, with a 1 eV width Gaussian envelope applied to each molecular orbital, without correcting for the substrate, final state or matrix element effects, as has been done elsewhere [62, 63]. Some changes are evident in the photoemission spectra as the composite concentration changes (figure 8.4). In the shape of the photoemission spectra, these changes are even more clear when PbSe nanocrystals are dispersed in MEH-PPV host (figure 8.5).

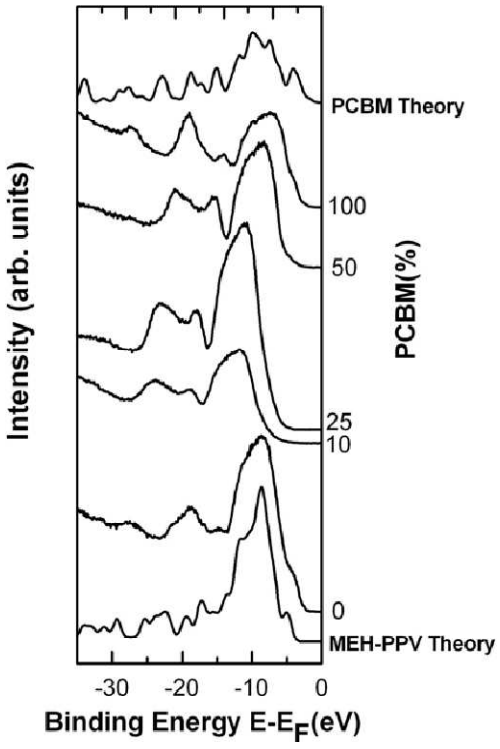

Figure 8.4 The occupied electronic structure of MEH-PPV polymer with increasing amounts of PCBM, as characterized by photoemission. The photoemission spectrum of pure MEH-PPV compared with model expectations (bottom curve) and the photoemission spectrum of pure PCBM films compared with model expectations (top curve). There is qualitative agreement with the calculated ground state molecular orbitals following a summation and using a 1 eV Gaussian applied to each molecular orbital. The photoemission spectra were taken at a photon energy of 62 eV with a light incidence angle of 45^0 relative to the surface normal with normal emission.

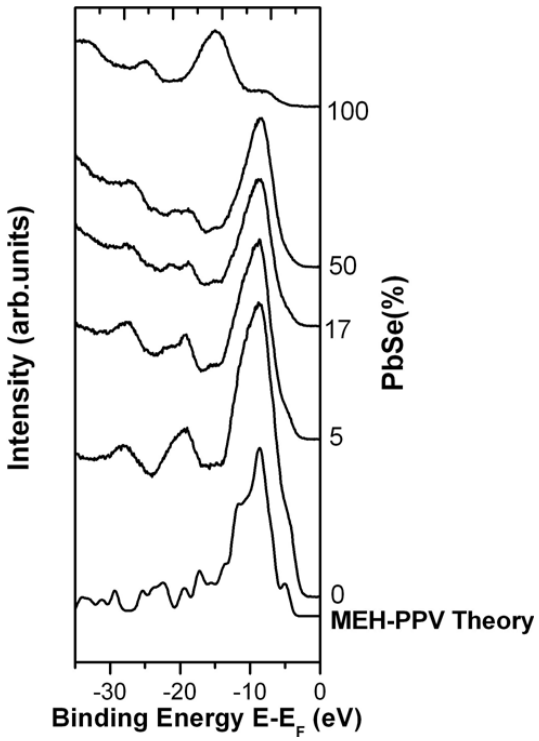

Figure 8.5 The occupied electronic structure of MEH-PPV polymer with increasing amounts of PbSe nanocrystals, as characterized by photoemission. The photoemission spectrum of pure MEH-PPV compared with model expectations (bottom curve). The photoemission spectra were taken at a photon energy of 66 eV with a light incidence angle of 45^0 relative to the surface normal with normal emission.

With increased PCBM doping, to about 10%, PCBM does not act much like an electron acceptor, but more like an electron donor. In the picture of band filling, the introduction of extra electrons to the MEH-PPV system fills any empty states near the Fermi level E_F and increases the binding energies of all the molecular orbitals [63]. The subtraction of electrons from the MEH-PPV system should lead to a decrease in binding energy of all the bands. To a concentration of about 10%, PCBM (figure 8.4), and to a

lesser extent PbSe (figure 8.5), appear to act as electron donor, when added to the MEH-PPV system. This is because the addition of these nanocluster components leads to greater binding energies of the occupied molecular orbitals valence bands and the valence band maximum (relative to the Fermi level) and a decrease in density of states near E_F as seen in similar doped polymer systems [63].

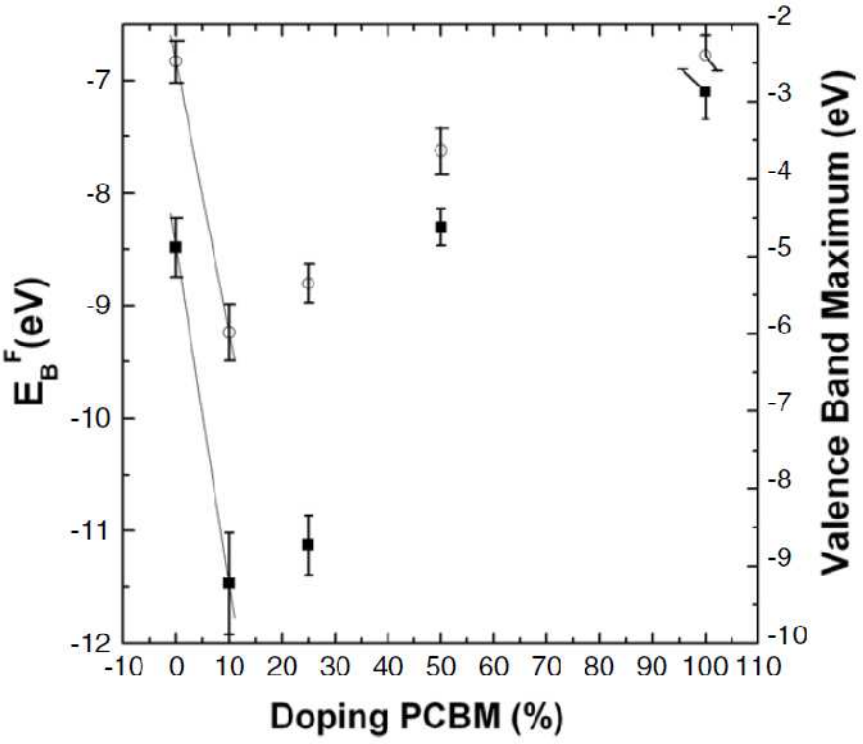

Figure 8.6 The binding energy of the main photoemission feature (■) and the binding energy of the valence band maximum (○) of MEH-PPV with increasing amounts of PCBM as characterized by photoemission.

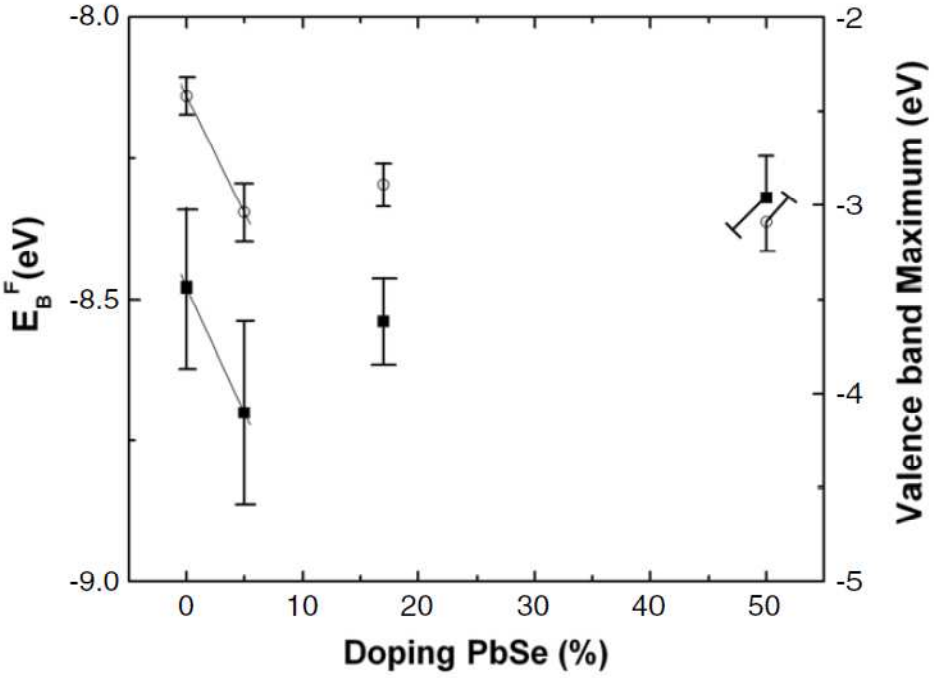

Figure 8.7 The binding energy of the main photoemission feature (■) and the binding energy of the valence band maximum (□) of MEH-PPV with increasing amounts of PbSe nanocrystals, as characterized by photoemission.

This influence of increasing concentrations of PCBM, resulting in a decrease in the density of states at the Fermi level and an increase in binding energies of the features due to the occupied molecular orbitals, is not as evident with increasing concentrations of PbSe nanocrystals, and does not extend to the very high doping concentrations. We have plotted the binding energies of the valence band maximum and the most prominent photoemission for both composites with PCBM (figure 8.6) and PbSe (figure 8.7). These increases in binding energies occur either because of band filling, that occurs in the case of PCBM, or due to charging. To a far lesser extent this also seems true for composites with PbSe nanoclusters. This means that the doped MEH-PPV material likely remains a good

dielectric for loading concentrations of 10–25%. This is valuable because it provides a route for high loading values of PbSe, while retaining properties that make the material a good gamma-ray scintillation detector.

For PCBM concentrations above 10%, the valence band maximum and density of states is restored, and to a far lesser extent with PbSe nanocluster inclusion. This restoration of the valence band maximum closer to the Fermi level tends to indicate that, at the higher concentrations, neither PbSe nor PCBM effectively dope MEH-PPV, but rather cluster or agglomerate, so that doping occurs only at the interface between the two mixed components. Clearly some structural studies are needed to establish whether the composites are phase separated or component materials separated.

In conclusion, the positions of the molecular orbitals of the semiconducting polymer MEH-PPV, relative to the Fermi level, shift with the doping of MEH-PPV by either PbSe nanocrystal quantum dots, or fullerene based molecule PCBM. The effect is more dramatic with PCBM than with PbSe and results in a decrease in density of states near Fermi level and shifts to greater binding energies of the occupied molecular orbitals and the valence band edge as probed by photoemission. Phase or component segregation seems likely for dopant concentrations greater than 10%. The composite of MEH-PPV and a large-Z material such as PbSe nanocrystal quantum dots is a potential gamma-detection material.

References

[1] R. Friend, “Polymers show they’re metal”, Nature, 44, 37, (2006).

[2] V.I. Roldughin and V.V. Vysotskii, “Percolation properties of metal-filled polymer films, structure and mechanisms of conductivity”, Progress in Organic Coatings, 39, 81, (2000).

[3] T. Ohta, A. Bostwick, T. Seyller, K. Horn and E. Rotenberg, “Controlling the electronic structure of bilayer graphene”, Nature, 313, 951, (2006).

[4] G. Gustafsson, Y. Cao, G. M. Treacy, F. Klavetter, N. Colaneri and A. J. Heeger, “Flexible light-emitting diodes made from soluble conducting polymers”, Nature, 357, 477, (1992).

[5] P. A. Dowben, B. Xu, J. Choi, & E. Morikawa. Band Structure and orientation of molecules adsorbates on surfaces by angle resolved electron spectroscopies. In: Handbook of Thin Film Materials, vol. 2, Characterization and Spectroscopy of thin Films, Hari Singh Nalwa (Ed.), Academic Press: A division of Harcourt, Inc. 61–113, (2002).

[6] E. W. Plummer, & W. Eberhardt, Adv. Chem. Phys., 49, 533, (1982).

[7] H.-P. Steinrück, Vacuum, 45, 715, (1994).

[8] F. Zwick, D. Jérome, G. Margaritondo, M. Onellion, J. Voit, and M. Grioni, Physical Review Letters, 81, 2974, (1998).

[9] C. Rojas, J. Caro, M. Grioni and J. Fraxedas, Surface Science, 482-485, 546, (2001).

[10] J. Choi, C. N. Borca, P. A. Dowben, A. Bune, M. Poulsen, S. Pebley, S. Adenwalla, S. Ducharme, L. Robertson, V. M. Fridkin, S. P. Palto, N. Petukhova,& S. G. Yudin, Phys. Rev. B, 61, 5760, (2000).

[11] D. Yoshimura, H. Ishii, Y. Ouchi, E. Ito, T. Miyamae, S. Hasegawa, K.K. Okudaira, N. Ueno, & K. Seki, Phys. Rev. B, 60, 9046, (1999).

[12] S. Narioka, H. Ishii, K. Edamatsu, K. Kamiya, S. Hasegawa, T. Ohta, N. Ueno, & K. Seki, Phys. Rev. B, 52, 2362, (1995).

[13] A. N. Caruso, R. Rajesekaran, G. Gallup, J. Redepenning, & P. A. Dowben, J. Phys. Cond. Matt., 16, 845 (2004).

[14] M. Galperin, A. Nitzan, M. Ratner, Inelastic effects in molecular junctions in the Coulomb and Kondo regimes: Nonequilibrium equationof- motion approach. Phys. ReV. 76 (035301), 1–10, (2007).

[15] H. Yamane, S. Nagamatsu, H. Fukagawa, S. Kera, R. Friedlein, K. K. Okudaira, N. Ueno, Hole-vibration coupling of the highest occupied state in pentacene thin films. Phys. ReV. B 72 (15), 153412, (2005).

[16] J. S. Seldenthuis, H. S. J. van der Zant, M. A. Ratner, J. M. Thijssen, Vibrational excitations in weakly coupled single-molecule junctions: A computational analysis. ACS Nano 2 (7), 1445–1451, (2008).

[17] A. Troisi, M. A. Ratner, Molecular signatures in the transport properties of molecular wire junctions: What makes a junction “molecular”? Small 2, 172-181, (2006).

[18] V. Mujica, M. Kemp, M. A. Ratner, Electron conduction in molecular wires. II. Application to scanning tunneling microscopy. J. Chem Phys. 101, 6856–6864, (1994).

[19] M. Galperin, A. Nitzan, M. Ratner, Inelastic effects in molecular junctions in the Coulomb and Kondo regimes: Nonequilibrium equationof- motion approach. Phys. ReV. B 76, 035301, (2007).

[20] V. Mujica, M. Kemp, M. Ratner, Electron conduction in molecular wires I. A scattering formalism. J. Chem. Phys. 101, 6849–6855, (1994).

[21] J. Xiao, Z. Zhang, D. Wu, L. Routaboul, P. Braunstein, B. Doudin, Y. B. Losovyj, O. Kizilkaya, L. G. Rosa, C. N. Borca, A. Gruverman, P. A. Dowben, Phys. Chem. Chem. Phys., 12, 10329 – 10340, (2010).

[22] H. Ma, H.-L. Yip, F. Huang, A. K.-Y. Jen, Adv. Funct. Mater. 20, 1371–1388, (2010).

[23] I. G. Hill, A. Rajagopal, A. Kahn, Y. Hu, Appl. Phys. Lett., 73, 662-664, (1998).

[24] G. Dennler, C. Lungenschmied, H. Neugebauer, N. S. Sariciftci and A. Labouret J. Mater. Res. 20, 3224, (2005).

[25] G. Dennler and N. S. Sariciftci, Proc. IEEE 93, 1429, (2005).

[26] S. Gunes and N. S. Sariciftci, Inorg. Chim. Acta 361, 581, (2008).

[27] H. Hoppe and N. S. Sariciftci, J. Mater. Res. 19, 1924, (2004).

[28] N. S. Sariciftci, L. Smilowitz, A. J. Heeger andF. Wudl, Science 258, 1474, (1992).

[29] L. Bozano, S. E. Tuttle, S. A. Carter and P. J. Brock Appl. Phys. Lett. 73, 3911, (1998).

[30] D. Qi, M. Fischbein, M. Drndic and S. Selmic Appl. Phys. Lett. 86, 093103, (2005).

[31] N. Tessler, V. Medvedev, M. Kazes, S. Kan and U. Banin Science 295, 1506, (2002).

[32] D. Cui, X. Jian, X. Sheng-Yong, G. Paradee, B. A. Lewis and M. D. Gerhold, IEEE Trans. Nanotechnol. 5, 362, (2006).

[33] L. Bakueva, S. Musikhin, M. A. Hines, T. W. F. Chang, M. Tzolov, G. D. Scholes and E. H. Sargent Appl. Phys. Lett. 82, 2895, (2003).

[34] T. W. F. Chang, S. Musikhin, L. Bakueva, L. Levina, M. A. Hines, P. W. Cyr and E. H. Sargent Appl. Phys. Lett. 84, 4295, (2004).

[35] L. Han, Q. Donghuan, X. Jiang, Y. Liu, L. Wang, J. Chen and Y. Cao Nanotechnology 17, 4736, (2006).

[36] B. Sun, E. Marx and N. C. Greenham, Nano Lett. 3, 961, (2003).

[37] C. H. Lee, G. Yu, D. Moses, K. Pakbaz, C. Zhang, N. S. Sariciftci, A. J. Heeger and F. Wudl Phys. Rev. B 48, 15425, (1993).

[38] C. H. Lee, G. Yu, K. Pakbaz, D. Moses, N. S. Sariciftci, F. Wudl and A. J. Heeger Synth. Met. 70, 1353, (1995).

[39] N. S. Sariciftci, D. Braun, C. Zhang, V. I. Srdanov, A. J. Heeger, G. Stucky and F. Wudl, Appl. Phys. Lett. 62, 585, (1993).

[40] C. Arndt, U. Zhokhavets, G. Gobsch, C. Winder, C. Lungenschmied and N. S. Sariciftci, Thin Solid Films 451, 60, (2004).

[41] C. J. Brabec, A. Cravino, G. Zerza, N. S. Sariciftci, R. Kiebooms, D. Vanderzande and J. C. Hummelen, J. Phys. Chem. B 105, 1528, (2001).

[42] C. J. Brabec, N. S. Sariciftci and J. C. Hummelen, Adv. Funct. Mater. 11, 15, (2001).

[43] C. J. Brabec, S. E. Shaheen, T. Fromherz, F. Padinger, J. C. Hummelen, A. Dhanabalan, R. A. J. Janssen and N. S. Sariciftci, Synth. Met. 121, 1517, (2001).

[44] M. Drees, H. Hoppe, C. Winder, H. Neugebauer, N. S. Sariciftci, W. Schwinger, F. Schaffler, C. Topf, M. C. Scharber and Z. Zhu, J. Mater. Chem. 15, 5158, (2005).

[45] R. A. Janssen, J. C. Hummelen, K. Lee, K. Pakbaz, N. S. Sariciftci, A. J. Heeger and F. Wudl, Chem. Phys. 103 788, (1995).

[46] T. Munters, T. Martens, L. Goris, V. Vrindts, J. Manca, L. Lutsen, W. De Ceuninck, D. Vanderzande, L. De Schepper and J. Gelan, Thin Solid Films, 403, 247, (2002).

[47] J. Parisi, V. Dyakonov, M. Pientka, I. Riedel, C. Deibel, C. J. Brabec, N. S. Sariciftci and J. C. Hummelen, Z. Naturf. a 57, 995, (2002).

[48] M. T. Rispens, A. Meetsma, R. Rittberger, C. J. Brabec, N. S. Sariciftci and J. C. Hummelen, Chem. Commun. 2003, 2116, (2003).

[49] G. Sliauzys, G. Juska, K. Arlauskas, A. Pivrikas, R. Osterbacka, M. Scharber, A. Mozer and N. S. Sariciftci, Thin Solid Films 511, 224, (2006).

[50] Y. Liang, S. Xiao, D. Feng and L. Lu, J. Phys. Chem. C 112, 7866, (2008).

[51] B. V. K. Naidu, J. S. Park, S. C. Kim, S. M. Park, E. J. Lee, K. J. Yoon, S. J. Lee, J. W. Lee, Y. S. Gal and S. H. Jin, Sol. Energy Mater. Sol. Cells 92, 397, (2008).

[52] E. Arici, N. S. Sariciftci and D. Meissner, Adv. Funct. Mater. 13, 165, (2003).

[53] L. E. Greene, M. Law, B. D. Yuhas and P. Yang, J. Phys. Chem. C 111, 18451, (2007).

[54] S. Gunes, K. P. Fritz, H. Neugebauer, N. S. Sariciftci, S. Kumar and G. D. Scholes, Sol. Energy Mater. Sol. Cells 91, 420, (2007).

[55] D. Cui, X. Jian, Z. Ting, G. Paradee, S. Ashok and M. Gerhold, Appl. Phys. Lett. 88, 183111, (2006).

[56] Y. S. Zhao, H. Zhong and Q. Pei, Phys. Chem. Chem. Phys. 10, 1848, (2008).

[57] I. Campbell and B. Crone, Adv. Mater. 18, 77, (2006).

[58] P. A. Dowben, D. LaGraffe and M. Onellion, J. Phys.: Condens. Matter 1, 6571, (1989).

[59] Y. Losovyj, I. Ketsman, E. Morikawa, Z. Wang, J. Tang and P. Dowben, Nucl. Instrum. Methods Phys. Res. A 582, 264, (2007).

[60] J. Hormes, J. D. Scott and V. P. Suller, Synchrotron Radiat. News 19, 27, (2006).

[61] J. J. P. Stewart, Encyclopedia of Computational Chemistry ed P R Schleyer (New York: Wiley) p 2759, (1998).

[62] D. K. Chambers, S. Karanam, D. Qi, S. Selmic, Y. B. Losovyj, L. G. Rosa and P. A. Dowben, Appl. Phys. A 80, 483, (2005).

[63] B. Xu, J. Choi, A. N. Caruso and P. A. Dowben, Appl. Phys. Lett. 80, 4342, (2002).

This Thesis is based on the following works:

1) David Keith Chambers, Zhengzheng Zhang, Fauzia Khatkhatay, Srikanth Karanam, Orhan Kizilkaya, Yaroslav B. Losovyj, and Sandra Zivanovic Selmic, "Doping Poly[2-methoxy-5-(2'-ethylhexyloxy)-1,4-phenylenevinylene] (MEH-PPV) with PbSe nanoparticles or fullerenes", *J. Phys.: Condens. Matter* 20, 382202, (2008).

2) Zhengzheng Zhang, David Keith Chambers, Leon Rohan Pinto, Orhan Kizilkaya, Sandra Zivanovic Selmic, "Doping Poly[2-methoxy-5-(2'-ethylhexyloxy)-1,4-phenylenevinylene] (MEH-PPV) with LiF micro/nanoparticles", Physics and Technology of Organic Semiconductor Devices, edited by Marc Baldo, Antoine Kahn, Paul W.M. Blom, and Peter Peumans, MRS Symposium Proceedings 1115, HO5-01, (2009).

3) Jie Xiao, Zhengzheng Zhang, Dong Wu, Lucie Routaboul, Pierre Braunstein, Bernard Doudin, Yaroslav B. Losovyj, Orhan Kizilkaya, Luis G. Rosa, Camelia N. Borca, Alexei Gruverman, and Peter A. Dowben, "The interface bonding and orientation of a quinonoid zwitterion", *Physical Chemistry Chemical Physics* 12, 10329 - 10340, (2010). DOI: 10.1039/C003996A

4) Zhengzheng Zhang, Camelia N. Borca, D. Wu, Alexei Gruverman, Orhan Kizilkaya, Jie Xiao and Peter A. Dowben, "Preparation and Characterization of Periodically Poled Ferroelectric Lithium Niobate ($LiNbO_3$)", Structure-Function Relations at Perovskite Surfaces and Interfaces, Ed.: Arthur Baddorf, MRS Symposium Proceedings (2010), in press.

5) Zhengzheng Zhang, P. Sharma, C.N. Borca, P.A. Dowben, and A. Gruverman, "Polarization-specific adsorption of organic molecules on ferroelectric $LiNbO_3$ surfaces", *Applied Physics Letters* 97, 243702, 1-3, (2010).

6) Lingmei Kong, Cameron Bjelkevig, Sneha Gaddam, Mi Zhou, Young Hee Lee, Gang Hee Han, Hae Kyung Jeong, Ning Wu, Zhengzheng Zhang, Jie Xiao, P. A. Dowben, and Jeffry A. Kelber, "Graphene/Substrate Charge Transfer Characterized by Inverse Photoelectron Spectroscopy", *Journal of Physical Chemistry C* 114, 21618-21624, (2010).

7) Zhengzheng Zhang, Jose Alvira, Xenia Barbosa, Luis G. Rosa, Lucie Routaboul, Pierre Braunstein, Bernard Doudin, and Peter A. Dowben, "Lock and Key Adsorption Chemistry: Preferential Absorption of an Isomer of Di-iodobenzene on Molecular Films of Quinonoid Zwitterions", *Journal of Physical Chemistry C* 115, 2812-2818, (2011).

8) Lucie Routaboul, Pierre Braunstein, Jie Xiao, Zhengzheng Zhang, Peter A. Dowben, Guillaume Dalmas, Victor DaCosta, Olivier Félix, Gero Decher, Luis G. Rosa, and Bernard Doudin, "Altering the static dipole on surfaces though chemistry: Molecular Films of p-benzoquinonemonoimine Zwitterionic Compounds", *Journal of the American Chemical Society* , manuscript in preparation, (2011).

9) Zhengzheng Zhang, Rosette González, Gerson Díaz, Luis G. Rosa, Ihor Ketsman, Xin Zhang, Pankaj Sharma, Alexei Gruverman, and Peter A. Dowben, "Dipole Orientation Mediated Chemistry at Polymer Surfaces", submitted to *Journal of the American Chemical Society*, (2011).

10) Luis G. Rosa, Julian Velev, Zhengzheng Zhang, Jose Alvira, Omar Vega, Gerson Diaz, Lucie Routaboul, Pierre Braunstein, Bernard Doudin, Ya. B. Losovyj, and Peter A Dowben, "Approaching an Organic Semi-metal: Band Mapping and Electron Pockets at the

Fermi Level for *p*-benzoquinonemonoimine Zwitterion", *Journal of the American Chemical Society*, manuscript in preparation, (2011).